THE DECAY OF KRYPTON-90

THE DECAY OF KRYPTON-90

AND

ENERGY LEVELS IN RUBIDIUM-90

By

RONALD HALBERT GOODMAN, B.A.

A Thesis

Submitted to the Faculty of Graduate Studies

in Partial Fulfilment of the Requirements

for the Degree

Doctor of Philosophy

McMaster University

May 1964

DOCTOR OF PHILOSOPHY (1964)
(Physics)

McMASTER UNIVERSITY
Hamilton, Ontario.

TITLE: The Decay of Krypton-90 and Energy Levels in Rubidium-90

AUTHOR: Ronald Halbert Goodman, B.A. (University of Saskatchewan)

SUPERVISOR: Professor M.W. Johns

NUMBER OF PAGES: viii, 113

SCOPE AND CONTENTS:

This work describes a study of the gamma rays and beta particles emitted during the decay of the 33-second fission product Krypton-90. Procedures for the analysis of gamma, gamma-gamma coincidence, beta and beta-gamma coincidence experiments are discussed. The application of these analyses to the short-lived Krypton-90 activity yields the prominent features of this decay. The total energy release of this decay was found to be 4.56 ± 0.02 MeV, in agreement with beta systematics. A level scheme for the daughter, Rubidium-90, is proposed.

ACKNOWLEDGEMENTS

I would like to acknowledge the help and encouragement of my research director, Dr. M. W. Johns, without whose unfailing guidance and kind patience, this work would not have been completed. The meetings with my supervisory committee (Drs. C.F. Mate, T.J. Kennett, J.S. Kirkkaldy and M.W. Johns) were of much assistance in the planning of this research.

To all members of the McMaster Beta- and Gamma-Ray Spectroscopy group, who have by numerous discussions and helpful advice contributed to this work, I give my thanks. Particular mention should be made of the work of Mr. A. Groen, who spent many a long evening, in constructing the electronics used for these experiments. Mr. Jim Kitching's help in performing some of the experiments is gratefully acknowledged.

The drawings in this thesis are the work of Mr. Paul Schmoor of McMaster University and Mr. C.A. Josling of the Department of Mines and Technical Surveys, Ottawa. Any credit for the neatness of these rests with these people, while any errors are those of the author.

I would like to thank my wife, Tine, for her encouragement during the course of this work and for her proofreading of the final draft of the thesis.

The typing of this thesis has been most ably performed by Mrs. Della Varette, to whom due credit must be given for the addition of a significant number of punctuation marks.

TABLE OF CONTENTS

LIST OF FIGURES

LIST OF TABLES

INTRODUCTION

Ever since the discovery of radioactivity in 1895, advances in the study of nuclear decay modes have been closely linked with technological advances in related areas. Within the past 20 years, many nuclear reactors have been built, advances have been made in the field of nuclear particle detection and extensive improvements in electronic circuitry have been made. The intense sources, produced by nuclear-reactor-generated neutrons, and studied with precision magnetic beta-ray spectrometers and crystal grating spectrographs, have resulted in the precise measurements of many beta- and gamma-ray transitions. Internal conversion measurements have revealed much detail concerning complex decay modes and have given information on the spin and parities of nuclear levels. This increase in the wealth of experimental information has been complemented by theoretical studies of nuclear properties. In the absence of any secure knowledge of the nature of nuclear forces, particular emphasis has been placed on the role of models as a means of understanding and systematizing experimental data.

The beta- and gamma-ray spectroscopy group at McMaster has been interested for a number of years in those neutron induced activities whose half-lives are greater than a few hours. Particular effort has been devoted

to the platinum metals. The study of nuclides with a short half-life has recently been made possible by the acquisition of a nuclear reactor by the university (Fleming 1962). The purchase of a multi-channel analyser, with which it is possible to accumulate a large amount of data rapidly, has greatly facilitated the work on short-lived isotopes.

Ockenden and Tomlinson (1962) of the Chemistry Department at McMaster devised a beam port apparatus with which they were able to separate the xenon and krypton rare-gas fission products by means of gas chromatography. They studied the gamma spectrum, using a single sodium iodide crystal, of both the 3.2-min Kr^{89} and the 33-sec Kr^{90}. These results are essentially in agreement with other workers (Kofoed-Hansen and Nielsen 1951; Wahlgren 1961). In order to further investigate these decay schemes, electronic apparatus was built by the author especially for the study of short-lived nuclides. The simplicity of the single crystal gamma spectrum of Kr^{90} indicated that detailed studies of this isotope would be profitable. This work is a description of the techniques employed and the results obtained concerning the decay of 33-sec Kr^{90}.

The even-even nucleus Kr^{90} decays by beta emission to levels in the odd-odd nuclide Rb^{90}. There is some current interest in the study of the complex level structure of odd-odd nuclei and a systematic study of the level schemes of many such nuclides is required to provide sufficient data for the testing of nuclear models.

In the first section of this thesis the relevant theoretical concepts, which are needed to understand the purpose and method of interpretation

of the experimental measurements, will be discussed. The next section will describe the experimental apparatus and techniques employed in the study of Kr^{90}, while in the third part, the experimental results and their interpretation in terms of a level scheme of Rb^{90} will be presented.

CHAPTER I

THEORETICAL CONCEPTS

The experimental data of nuclear physics is interpreted in terms of the fundamental properties of the nucleus. These, in turn, are described by a quantum-mechanical formulation which was originally developed for atomic systems. Following a brief presentation of the terminology used in quantum mechanics, this chapter deals with some of the basic ideas concerning radioactive decay, and two of the nuclear models, which have been used to explain the low-energy properties of nuclei. This chapter contains those concepts which are of particular import to the problem at hand; for a more complete and detailed description, the reader should consult the many excellent reference texts available (Siegbahn 1955; Ajzenberg-Selove 1960; Preston 1962).

A) Terminology

The application of Newtonian mechanics to physical problems involves the setting up of differential equations containing the space coordinates of all the particles of that system, their first and second time derivatives and the boundary conditions appropriate to the problem. The solution of these second-order differential equations led to precise predictions of the positions and velocities of the components of the system at any desired time. However, it became clear during the first two decades of the 20th century that this

approach failed to account for the behaviour of systems of atomic dimensions. The period from 1913-1933 led to the development of a new type of mechanics, the so-called quantum mechanics. A basic tenet of this quantum theory is that there is an inherent limitation on the precision with which a pair of canonically conjugate variables (for example, energy and time; a position coordinate and its associated momentum) can simultaneously be measured. This uncertainty is summarized by Heisenberg's principle that

$$\Delta X \Delta Y \geq h \qquad (1\text{-}1)$$

In this expression, ΔX and ΔY are the uncertainties in X and Y and h is Planck's constant, 6.55×10^{-27} erg-sec. For macroscopic systems, this limitation is only of academic interest since the experimental errors in physical measurements in these situations are much greater than the value of h. However, for atomic or nuclear systems, the Heisenberg limitation completely dominates the description of the problem. As a consequence of this, it is no longer possible to precisely describe the position of the particle of a system as a function of time. Instead, one replaces quantities such as position, momentum, energy and angular momentum, of the classical system, by a series of differential operators O. These operators correspond to the classical concepts in the limit of macroscopic systems, and operate on wave functions, symbolized by $|>$, which are well behaved algebraic functions of the space variable of the problem. The properties of a system

are described by an equation of the form

$$O|> = \alpha|> \qquad (1-2)$$

The experimentally measured values are the eigenvalues (α) of the system. The square of the wavefunction of a system describes its probability density, which is generally normalized to unity over all of space. The eigenvalues of the system may be used as labels to describe the system, and the definition of some of these will be given.

1) ENERGY

The energy eigenvalues of a system are defined by the operator equation

$$H|> = E|> \qquad (1-3)$$

where H is the Hamiltonian or energy operator of the system. These energy eigenvalues are usually measured with respect to the most stable state of the system (the ground state). The unit of energy commonly used by experimental nuclear physicists is the million-electron volt, abbreviated as MeV, the value of which is 1.6×10^{-6} ergs.

For relativistic particles, such as electrons, the total energy is often more meaningful than the kinetic energy E, of the particle. For electrons, whose rest mass is equivalent to 0.511 MeV, one can write the total energy, W, in units of the electron mass as

$$W = \frac{E\,(MeV)}{0.511} + 1 \qquad (1-4)$$

The momentum, p, in the same units, is related to this total energy by

the expression

$$p = (W^2 - 1)^{\frac{1}{2}} \qquad (1\text{-}5)$$

These relativistic units will be used in the discussion of beta decay, which is presented later in this chapter.

2) SPIN

The spin or total angular momentum denoted by the symbol J, and measured in units of $h/2\pi$ or $\hbar$, is the eigenvalue of the angular momentum operator. Both J^2 and J_z are simultaneously observable and are defined by the equations

$$J^2 \left| JM> = J(J + 1) \right| JM> \qquad (1\text{-}6)$$

and

$$J_z \left| JM> = m \right| JM> \qquad (1\text{-}7)$$

The values of J, characteristic of nuclei of even-mass, are all integral, while those of odd-mass are half-integral. These values simply reflect the fact that both neutrons and protons (collectively nucleons) have a spin of $\frac{1}{2}\hbar$. The electron and neutrino (both leptons) also have a spin of $\frac{1}{2}\hbar$. All these particles obey Fermi-Dirac statistics, that is, no two particles of the same type may have the same eigenvalues (quantum numbers). This restriction imposes limitations on the possible configurations of a system of particles and accounts for many of the observed properties of both nuclear and atomic systems.

3) PARITY

The parity, π, of a state refers to the behaviour of the wave function, describing the state, under the operation of a mirror reflection. A wave function with positive parity remains unchanged, whereas, one of negative parity changes sign. Symbolically, if P is the parity operator, then

$$P|> = \pm 1|> \qquad (1-8)$$

depending on whether $|>$ has even or odd parity. The eigenvalues of the parity operator are ± 1. Experimentally only changes in the parity of a system can be measured. Thus a transition will be characterized by its parity change (yes or no). It is customary to assume that the parity of the ground state of even-even nuclei is positive. The angular-momentum component of a wave function has a positive parity for even values of ℓ and a negative parity for odd values of ℓ, where ℓ is the orbital angular momentum.

B) Beta Decay

1) SIMPLE THEORY

The emission in nuclear decay of a beta particle (electron) was discovered early in the study of radioactivity (Becquerel 1896). Since the emitted electrons were found to have a continuous energy distribution, while the two states involved in the beta transition possessed discrete energies, it was necessary either to abandon the principle of conservation of energy, or assume that another unobserved particle was emitted in the decay. The neutrino was postulated by Pauli (1933) to solve this problem. Fermi (1934) proposed a theory of beta decay based on the conservation of energy and

momentum and the statistical sharing of phase space between the electron and neutrino. Fermi's calculations showed that the number of electrons. Decaying per unit time, in the energy interval dW, N (W) dW, is given by

$$N(W)dW = KF(Z, W)pW(W_o - W)^2 dW \qquad (1-9)$$

where W is the total electron energy, p its momentum, and W_o is the total decay energy. The expression F(Z, W) describes the influence of the Coulomb field of the extra-nuclear electrons on the emitted charged particle. The constant K contains the nuclear matrix elements and is independent of W for allowed transitions.

The total decay rate, λ, is the integral of N(W)dW over all values of W from 1 to W_o. That is

$$\lambda = \int_1^{W_o} N(W)dW = K \int_1^{W_o} F(Z, W)pW(W_o - W)^2 dW = Kf(Z, W_o) \qquad (1-10)$$

where $f(Z, W_o) = \int_1^{W_o} F(Z, W)pW(W_o - W)^2 dW$. This integral is readily evaluated for low Z materials where F(Z, W) is essentially constant. For heavier elements, the values of $f(Z, W_o)$ are more difficult to calculate. Tabulationsof $f(Z, W_o)$ for all Z have been given by Feenberg and Trigg (1950).

Using the fact that $\lambda = \frac{0.693}{t_{\frac{1}{2}}}$, where $t_{\frac{1}{2}}$ is the half-life of the decay, equation 1-10 may be written as

$$\frac{\ell n 2}{K} = ft \qquad (1-11)$$

Thus the product f t characterizes the nuclear aspects of the decay. The experimentally observed values of f t span many orders of magnitude and therefore it is usual to quote $\log_{10} ft$ rather than f t itself.

The determination of selection rules and the calculation of the matrix elements for beta decay require a greater knowledge of the details

of the theory than has been so far presented. The general formula for the transition probability between any two quantum states is (Schiff 1955)

$$T = \frac{2\pi}{\hbar} \left| \langle i \left| O \right| f \rangle \right|^2 \rho(E) \qquad (1\text{-}12)$$

where $\langle i \left| O \right| f \rangle$ is the matrix element between the initial and final states of the system, and describes the amount of over-lap of the two states as well as the strength of the interaction between them. The operator O is the beta transition operator and $\rho(E)$ is the density of the final states of the system. In the case of beta decay, $\rho(E)$ is given by equation 1-9, and the constant K in this equation thus represents the effects of the nuclear matrix elements. Both the operator O and the wave functions of the leptons may be expanded in a power series, the successive terms of which have less and less importance. The lowest order approximation assumes that the motion of the nucleons is slow, compared to that of the electrons, and hence terms of the order v/c in the nucleon motion may be ignored. Also it is assumed that the wave function of the lepton system does not change across the nuclear diameter, which is equivalent to saying that no orbital angular momentum is carried away by the leptons. These assumptions lead to two possible decay modes; the leptons may either be in a singlet (spins opposed) or triplet (spins adding) state. The former is known as the Fermi interaction while the latter is the Gamow-Teller interaction. The selection rules for these are:

$$\begin{aligned} &\text{Fermi } \triangle J = 0 && \text{(no parity change)} \\ &\text{Gamow-Teller } \triangle J = 0 \pm 1, && 0 \text{ to } 0 \text{ forbidden} \\ & && \text{(no parity change)} \end{aligned} \qquad (1\text{-}13)$$

When the spins and parities of the initial and final states prohibit such transitions, a higher order of approximation must be used. The resulting first forbidden transitions are all characterized by a change in parity between the initial and final states and a more complex set of selection rules, which are given by

$$\triangle J = \pm 2, \pm 1, \quad 0 \text{ (parity change)} \qquad (1\text{-}14)$$

Certain exclusions to these are given by Preston (1962).

If neither allowed nor first forbidden transitions are permitted by the properties of the initial and final states, higher order terms in the expansion of the lepton function will still lead to transitions of lower probability (longer life-time). This subject is discussed in Siegbahn (1955).

A knowledge of the transition rate, and hence the $\log_{10} ft$ values, allows one to estimate the degree of forbiddeness of the beta decay and thus to obtain some insight into the spins and parity of the parent and daughter states. Unfortunately, detailed features of the wave functions of these states may either enhance or retard the transitions to such an extent that there is no exact one-to-one correspondence between $\log_{10} ft$ and the degree of forbiddeness. However, one may observe general trends, and in the region of mass 90, the values of $\log_{10} ft$ for the various transitions are found to be between 4 and 6 for allowed, 6 and 8 for first forbidden and greater than 8 for second forbidden.

2) FERMI PLOTS

A beta spectrum is characterized by its end-point energy E_o. A plot of energy versus counting rate for a beta spectrum does not allow the end point to be accurately determined, since the counting rate approaches zero asymptotically as E approaches E_o. Thus a special method of analysis is used to give a better measure of the beta end-point energy. If the analysing system accepts a constant energy channel width, dW, then one may rewrite equation 1-9 as

$$\left[\frac{N(W)\,dW}{F(Z,W)pW\,dW}\right]^{\frac{1}{2}} = K(W_o - W) \qquad (1\text{-}15)$$

In this equation N(W)dW is the observed counting rate for energies between W and W + dW. A plot of $\left[\frac{N(W)\,dW}{F(Z,W)pW\,dW}\right]^{\frac{1}{2}}$ versus W will yield a straight line "Fermi plot" for allowed and most first forbidden transitions, with intercept W_o. Values of F(Z, W)pW or related functions have been tabulated by Rose et al. (1955a). For the $\Delta I = 2$ yes (first forbidden unique) transitions and other transitions which have a high degree of forbiddeness, a shape factor, S, must be included in 1-15 to account for the energy dependence of the matrix elements of equation 1-12. Thus a plot of $\left[\frac{N(W)\,dW}{F(Z,W)S\,pW\,dW}\right]^{\frac{1}{2}}$ vs W will yield a straight line. Values of S have been tabulated by Rose (1955b) for all cases of interest.

3) RECENT EXPERIMENTS

Over the last twenty years, much effort has been expended in the search for the correct operators responsible for beta decay. The discovery of parity non-conservation in beta decay by Wu et al. (1957) and the flurry

of experimental work which followed has clarified the situation materially. It is now clear (Lauritsen et al. 1958; Barnes et al. 1958; Lauterjung et al. 1958), that the vector (Fermi) interaction and the axial vector (Gamow-Teller) interaction are the only two operators necessary to account for all the experimental data. Other details of the beta-decay process, such as the polarization of the emitted electrons and the helicity of the neutrino, have been measured, but since these experiments in no way influence the measurements to be described, they will not be further discussed.

C) Gamma Emission

The emission of a photon in radioactive decay (gamma emission) is an electromagnetic process, similar to that encountered in atomic systems. The wavelength of the gamma ray is much greater than the nuclear diameter, and variations of the electromagnetic field across the nuclear volume may normally be neglected. The field producing the gamma radiation may be classified according to its multipolarity (λ-value) and its character (σ), which may be either electric or magnetic in origin. Thus transitions are labelled as E 1, M 1, E 2, ... ($\sigma\lambda$) etc. The parity change of an electric transition is $(-1)^{\lambda}$ while that of a magnetic transition is $-(-1)^{\lambda}$. The angular momentum carried away by a gamma ray may only have integral values greater than zero. The conservation of angular momentum requires the

following selection rules for gamma emission:

$$J_i + J_f \geq \lambda \geq |J_i - J_f| \qquad (1\text{-}16)$$

where J_i and J_f are the angular momenta of the initial and final states of the decay. Since the nuclear radius R is much smaller than the gamma wavelength, the transition probability is proportional to $(kR)^{\lambda}$ where k is the wave number (the reciprocal of the wavelength). Thus only the radiation of the lowest multipole order, which can occur between the two nuclear states involved, will in general contribute appreciably to the transition. The one important exception to this is the competition of E 2 with M 1 transitions found in certain deformed nuclei.

The general expression for the transition probability for gamma emission is (Preston 1962)

$$T(\sigma\lambda) = \frac{8\pi(\lambda + 1)}{\lambda\left[(2\lambda + 1)!!\right]^2}\left(\frac{k}{\hbar}\right)^{2\lambda + 1} B(\sigma\lambda) \qquad (1\text{-}17)$$

where $B(\sigma\lambda)$ is the reduced matrix element of the transition, and is defined in terms of the initial and final states of the system, and the multipole operator responsible for the transition. It is the nuclear contribution to the decay. In order to estimate the value of $B(\sigma\lambda)$, calculations have been made by Weisskopf (1951) in which a single proton is held responsible for the emission of the radiation. These calculations lead to the so-called Weisskopf single-particle estimates for magnetic and electric transitions. Although the details of nuclear structure are ignored, these predictions are widely used as standards of reference for the interpretation of measured transition probabilities. The Weisskopf single-particle reduced

transition probabilities have the form

$$B_W(E_\lambda) = \frac{e^2}{4\pi}\left(\frac{3}{\lambda+3}\right)^2 R^{2\lambda} \qquad (1\text{-}18)$$

for the electric case and

$$B_W(M_\lambda) = \frac{e^2}{4\pi}\left(\frac{3}{\lambda+3}\right)^2 R^{2\lambda}\, 10\left(\frac{\hbar}{M_c R}\right)^2 \qquad (1\text{-}19)$$

for magnetic transitions where M is the nuclear mass and R is the nuclear radius. According to these expressions, the magnetic transition rate is about $0.3A^{-2/3}$ of the electric transition rate of the same multipole order. For A = 90, this factor is about 1.5×10^{-2}. The total transition rate between two nuclear levels is the gamma transition rate plus the decay due to internal conversion.

D) Internal Conversion

The direct interaction of the nuclear electromagnetic field with the atomic electrons results in the ejection of electrons of discrete energies, a process known as internal conversion. This process is in direct competition with gamma emission in the decay of an excited nuclear state. The internal conversion coefficient is defined as

$$\alpha = \frac{N_e}{N_\gamma} \qquad (1\text{-}20)$$

where N_e and N_γ are the number of electrons and photons respectively emitted in the transition. The total transition rate N is thus

$$N = N_\gamma (1 + \alpha) \qquad (1\text{-}21)$$

Since conversion electrons may be ejected from any of the occupied atomic shells, α is the sum

$$\alpha = \alpha_K + \alpha_{L_I} + \alpha_{L_{II}} \ldots\ldots \qquad (1\text{-}22)$$

where $\alpha_K, \alpha_{L_I} \ldots\ldots$ are the conversion coefficients for a given shell or sub-shell. The rate of internal conversion is a measure of the strength of the nuclear electromagnetic field at the electron orbit, and thus is sensitive to the multipolarity of the transition. The value of the internal conversion coefficient is also strongly dependent on the transition energy and the atomic number of the nucleus. Extensive tabulations of internal conversion coefficients have been published by Rose (1955c) and Sliv (1957). K-shell internal conversion coefficients for rubidium are given below:

Energy/Character MeV	E1	E2	E3	E4	M1	M2	M3	M4
0.076	1.66 (-1)	1.97 (0)	1.92 (1)	1.79 (2)	2.12 (-1)	2.74 (0)	3.01 (1)	3.66 (3)
0.102	7.03 (-2)	6.97 (-1)	5.65 (0)	4.44 (1)	9.56 (-2)	9.48 (-1)	8.65 (0)	7.74 (1)
0.255	4.80 (-3)	2.47 (-2)	1.09 (-1)	4.59 (-1)	8.63 (-3)	4.26 (-2)	1.93 (-1)	8.34 (-1)
0.511	7.56 (-4)	2.46 (-3)	7.12 (-3)	1.97 (-2)	1.64 (-3)	5.20 (-3)	1.52 (-2)	4.37 (-2)
1.022	1.68 (-4)	3.87 (-4)	7.98 (-4)	1.59 (-3)	3.54 (-4)	8.24 (-4)	1.70 (-3)	3.42 (-3)

where $m(r) = mx10^r$. Thus it is evident that internal conversion will only contribute significantly to transitions of low energy and high multipolarity.

The calculation of the transition probability of a decay, and the level order within a nucleus, requires the use of some nuclear model. Certain of these models will now be discussed.

E) Nuclear Structure

The theoretical interpretation of the available data concerning the nucleus has followed two main courses. The more basic of these considers that the nucleus is made up of nucleons which interact with each other through the nuclear force field. The nature of this force has been measured by various scattering experiments. This approach for determining nuclear properties has been very limited in its application, because of the great difficulties associated with calculations involving more than two mutually interacting particles. The recent developments in high speed computers make this approach more promising in that detailed iterative processes are now feasible. A variant of this approach treats the nucleus as a many-particle system and uses the techniques of statistical mechanics for the prediction of the gross features of nuclear matter. This is also only partially successful, since there are not enough particles involved to establish a proper statistical average.

The other course, which the theoretical study of nuclei has followed, involves the use of models for the prediction of nuclear properties. These models use ideas generally borrowed from atomic systems, which are modified to conform to the experimentally observed properties of the nucleus. Two such models will be discussed: the nuclear shell model which is directly

related to the theory of atomic shells, and the collective model which has been developed using concepts first introduced in molecular spectroscopy.

1) THE SHELL MODEL

The suggestion of a shell model for the nucleus was advanced by Bethe and Bacher (1936) but other early workers discounted this view since it was believed that nucleons could not enter into free motion within the nucleus. Further studies showed the existence of magic numbers, the evidence for which is primarily from the number of nucleons occurring in the naturally existing or stable isotopes. The tightly bound structure of ${}_{2}He_{2}^{4}$ and ${}_{8}O_{8}^{16}$ gives evidence of the special strength of 2 and 8 nucleon systems. Also, for a given value of neutron number N, there are in general three or four naturally occurring species, but for N = 20 there are five, N = 50 has six and N = 82 has seven stable isotopes. Similarly, for proton number Z, there are ten tin (Z = 50) isotopes found in nature. The heaviest even-even stable nuclide ${}_{82}Pb_{126}^{208}$ is very tightly bound, which indicates that N = 126 has special properties. In order to explain these observed magic numbers at 2, 8, 20, 50, 82 and 126, Mayer (1949) and Haxel, Jensen and Suess (1949) independently proposed the shell model for the nucleus. The predictions of this model have to a large extent been confirmed by experiment, which is surprising considering its relatively simple nature.

The basic tenet of the shell model is that many of the properties of the nucleus are due to the motion of one, or possibly a few nucleons, moving in a potential created by the other nucleons. The choice of this

potential is arbitrary, but it is impossible to obtain the experimentally observed shells for any purely central potential, which has a simple shape. The inclusion of a spin-orbit coupling term in the potential, allows one to obtain the magic numbers in a natural fashion. The shell model potential has the form

$$V = V(r) \left\{1 + \alpha \vec{\ell} \cdot \vec{s}\right\} \qquad (1\text{-}23)$$

with the sign of α chosen such that higher angular momenta have a lower energy. The value of α is adjusted, so that the levels are in agreement with experiment. V(r) may be a square well, or a simple harmonic oscillator well, or almost any form between these. The effect of the spin orbit force is to pull the high spin states from one oscillator shell into the next lower shell, thus bringing states of different parity close together.

In applying the model to the prediction of spins, one must establish certain other criteria:

a) the neutrons and protons separately fill shells.

b) two nucleons in the same shell, pair and couple their spins to zero angular momentum. Thus the ground state spin of all even-even nuclei should be zero.

c) the spin of an odd-A nuclide is determined by the spin of the one unpaired nucleon. (In a few cases three nucleons may couple to form the observed spin).

d) the spin of the ground state of an odd-odd nuclide can be estimated by considering the coupling of the unpaired neutron and proton. Nordheim's rules (1950), as modified by Brennan and Bernstein (1960), give the preferred coupling between these nucleons. If N is defined as

$$N = (J_p - \ell_p) + (J_n - \ell_n) \qquad (1\text{-}24)$$

then Nordheim's strong rule states that for N = O, the ground state spin is $|J_n - J_p|$ while the weak rule states that for $N = \pm 1$, J is either $|J_n - J_p|$ or $J_n + J_p$ with the larger spin being the more probable.

The ground state spins, experimentally determined, are in general agreement with the shell theory, with the exception of those cases discussed below. The shell model predicts high spin ground states, which are however not observed. States with these predicted spins are found as low lying isomeric states, while the ground states of these nuclei have a lower spin. This effect may be explained if one assumes a pairing energy, whose magnitude is a function of the value of the angular momentum of the system. The incorporation of such a term will mean that a configuration $(s_{\frac{1}{2}})^1 (g\ 9/2)^2$ has a lower energy than the configuration $(s_{\frac{1}{2}})^2 (g\ 9/2)^1$ and hence the ground state would have a spin of $\frac{1}{2}$, and a low lying isomer would have a spin of $9/2$.

In the region of the lanthanides and actinides, the shell model is in poor agreement with the empirically observed characteristics of these nuclides. These nuclei are known to be deformed and this case will be dealt with later.

The above description of the nucleus, known as the single particle model, has been elaborated into a model which considers all those nucleons which are outside a closed shell, as contributing to the observed nuclear structure. These nucleons interact with each other and with the core or closed shell nucleons. Thus the individual levels are no longer pure particle states, but each has been altered by the configuration mixing of nearby states. The magnitude of the intermixing has been measured by Cohen and Price (1960), by stripping reactions, and is consistent with the theoretical work of Kisslinger and Sorenson (1960).

The application of the shell model to the prediction of the level order in nuclei, using a coupling of two nucleons, has been applied to levels in Zr^{90} (Ford 1955), and also to the levels in Pb^{206} (True and Ford 1958), a nucleus with two nucleons missing from a closed shell. The agreement between theory and experiment is very good for these cases.

The shell model has treated the nuclear properties as being determined by one, or at most a few nucleons, and has ignored the presence of all the other nucleons, except as they contribute to the central potential. The shape of this potential has been assumed to be spherical. However, the very nature of the shell structure implies that a spherical shape may not always be the most stable. The properties of non-spherical nuclei (deformed nuclei) may be explained as the collective motion of many nucleons.

2) COLLECTIVE MODEL

The equilibrium shape of the nucleus is determined by the competition between the deforming power of the individual nucleons and the effect of pairing forces. In the region of the closed shells, the pairing forces predominate and the nuclei are spherical. As particles are added outside the closed shell, the nucleus experiences non-spherical forces and eventually it will become deformed into an ellipsoidal shape. The early study of the process of fission employed a hydrodynamical model of a deformed nucleus to explain the splitting of heavy nuclei. The possible collective motions of such a deformed nucleus may be separated into two modes: the rotational and vibrational modes, the former corresponding to a change in orientation without a change in shape and the latter to an oscillation about an equilibrium shape. Both these modes are also found in the treatment of the spectra of diatomic molecules, and much of the notation used in the nuclear situation has been borrowed from this source.

i) Vibrational Spectra

The oscillation of the nuclear core may be treated as an expansion, in a power series of the coordinate along the deformation axis, about an equilibrium position. The first term of the expansion corresponds to a translation, and the second term to a motion of a simple harmonic oscillator. If these motions are treated in spherical coordinates, the second term corresponds to an oscillation with angular momentum of two. Thus the level order of such a system will have equally spaced levels with energy

differences of $\hbar\omega$, where ω is the characteristic frequency of the vibration as shown in the accompanying sketch. The quadrupole nature of the deformation results in a large overlap with an electromagnetic quadrupole operator and thus E 2 transitions rates are much greater than predicted from the single particle estimates. This enhancement may be up to two or three orders of magnitude. The transition probability between adjacent states of an harmonic oscillator is much greater than between non-adjacent levels and thus one would expect a suppression of cross-over transitions.

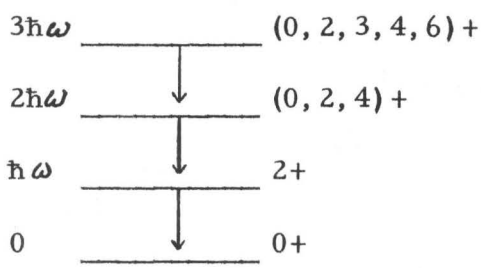

Non-harmonic terms will in general complicate this simple picture, and will give rise to cross-over transitions and unequal energy differences. However, level structures which correspond in appearance to the prediction of this model are found in the slightly deformed nuclei near closed shells. As the nucleus becomes more seriously deformed, the pattern alters and reveals the rotational-vibrational structure discussed below.

ii) Rotational Spectra

The study of rotational spectra was first applied to the rotation of diatomic molecules. Spectra of similar character have also been observed for the nuclear case. The energy eigenvalues of a rigid rotator are given by

$$E_{rot} = \frac{\hbar^2}{2\mathcal{I}} J(J+1) \qquad (1\text{-}25)$$

where J is the spin of the state and $\mathcal{I}$ is the effective moment of inertia. In the case of deformed nuclei, the rotation may be thought of as an irrotational movement of the non-spherical portion of the nucleus about a stationary fixed spherical core. Alternatively, one might consider that the motion is a rotation of the total nucleus about an axis perpendicular to the symmetry axis (rigid rotation). The experimentally observed moments of inertia have values intermediate between those, calculated by assuming either irrotational or rigid motions.

The spins of the rotational levels, based on a level of intrinsic spin of zero, are J = 0, 2, 4, ..., the odd J values being forbidden by symmetry arguments. The rotational levels based on a level of spin K, ($K \neq 0$) have spins J = K, K + 1, K + 2, ...

The quantum number K is the projection of J along the nuclear symmetry axis, as shown in the figure on the right; J is the total angular momentum, and M is the projection of J along a space fixed axis.

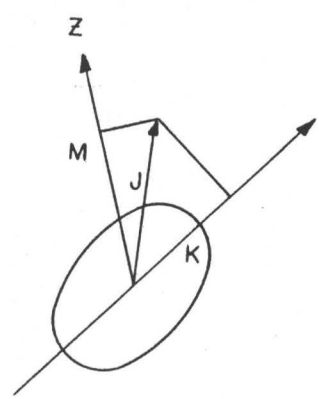

The case of $K = \frac{1}{2}$ requires special attention because of the possibility that the intrinsic spin of the last nucleon, due to the exclusion principle, may not be able to follow the rotation. For example, consider a $s_{\frac{1}{2}}$ state coupled to a core with K = 0. The $s_{\frac{1}{2}}$ state is spherically symmetric, and hence

the total energy of the system must be independent of the manner of the coupling between the nucleon angular momentum and the rotation of the core. Thus for $K = \frac{1}{2}$, the energy of a rotator has an added term and is given by

$$E_{rot}(K = \tfrac{1}{2}) = \frac{\hbar^2}{2\mathcal{I}} \left\{ J(J+1) + a(-1)^{J+\frac{1}{2}} (J + \tfrac{1}{2}) \right\} \qquad (1\text{-}26)$$

where a is a decoupling parameter and is a function of the intrinsic structure of the system. For the $s_{\frac{1}{2}}$ state above, a = 1.

For the lanthanides and actinides, rotational spectra with the characteristics described above account for many of the low-lying levels. The transitions exhibit an enhancement of the E2 transition probability, up to a factor of 100 above the single particle estimate. Interactions between rotational and vibrational modes will complicate the picture considerably, but the general features of these collective motions are still clearly in evidence.

iii) Intrinsic Spectra

The shell model assumes a spherically symmetric potential, but as has been discussed above, many nuclei are strongly deformed. Nilsson (1955) studied the motion of a nucleon in such a deformed potential using the concepts of the shell model. He assumed a Hamiltonian of the form

$$H = H_o + C\,\vec{\ell} \cdot \vec{s} + D\ell^2$$

where

$$H_o = \frac{\hbar^2}{2M} \nabla'^2 + \frac{M}{2} \left(\omega_x^2 x'^2 + \omega_y^2 y'^2 + \omega_z^2 z'^2 \right) \qquad (1\text{-}27)$$

where the characteristic frequencies ω_x, ω_y and ω_z, refer to motions along the nuclear coordinates x′, y′ and z′. The term H_o is simply an

energy operator of a central deformed potential. The term $\vec{\ell} \cdot \vec{s}$ represents a spin-orbit coupling as in the shell model. The term ℓ^2 depresses the energy of higher angular momentum states and gives the observed spectra for non-deformed (spherical) nuclei.

The angular momentum of the nucleons is no longer a constant of motion of the system, but its component along the nuclear symmetry axis is a good quantum number (Ω). The spins of the ground states of deformed nuclei are obtained by replacing the role of J in the shell model by Ω, and using the rules previously discussed.

In this chapter the various parameters characterizing the nuclear system have been assumed known and measurable to a high degree of accuracy. In practice, this may be far from true and in the next chapter some of the techniques and instrumentation used in nuclear physics will be discussed.

CHAPTER II

EXPERIMENTAL TECHNIQUES AND INSTRUMENTATION

The early experiments in radioactivity employed simple radiation sensitive devices such as zinc sulphide screens, photographic emulsions, Geiger counters and cloud chambers. For many years, the measurement of the magnetic rigidity of electrons by various field combinations has been used to determine the energies of nuclear transitions. Much effort has been devoted to improving the resolution, transmission and luminosity of magnetic instruments and present day magnetic beta-ray spectrometers are capable of measuring electron energies with high precision; indirectly, gamma-ray energies may be obtained with the same instrument, by measuring the energies of the photoelectrons, ejected from thin foils of high Z materials. While these magnetic instruments give high accuracy, they are generally limited to point by point measurement, and thus the time required to accumulate a significant amount of data makes it difficult to use such instruments for short-lived activities.

Because of its versatility and high sensitivity, the thallium activated sodium iodide crystal and photomultiplier combination has become very widely used as a gamma-ray scintillation spectrometer, particularly when

studying short half-lives. Their usefulness has been greatly enhanced by the availability of multi-channel pulse height analysers (kicksorters), which now make it possible to record the entire gamma-ray spectrum at the same time. Plastic and anthracene scintillators can be used in the same way for the detection of electrons, although the energy resolution of these detectors is inferior to that of the gamma scintillators, and vastly poorer than the magnetic spectrometer. Recently, semiconductors suitable for electron detection have become available, and although at present their use is limited, they show much promise for the future.

In this chapter only the NaI(Tl) and plastic (NE102) scintillation detectors, used for the experiments involving Kr^{90}, will be discussed. The description of their mode of operation will be followed by a discussion of coincidence techniques.

A) The Gamma-Ray Scintillation Spectrometer

1) METHOD OF OPERATION

The use of large crystals of NaI(Tl) for gamma spectrometers has become standard in recent years. The detection of a gamma-ray photon, by a scintillation detector, involves a rather complex chain of events, which results in an electrical pulse with a height (voltage) proportional to the incident photon energy. The interaction of the gamma-ray with the crystal transfers some or all of its energy to an electron which, in turn, optically excites the NaI(Tl) to produce a cascade of photons, some of which have wavelengths to which the photosensitive surface of the photomultiplier is sensitive. The photoelectrons created at this surface are then multiplied

by an assembly of secondary emission dynodes to give a usable electrical pulse of brief duration.

The interaction of the gamma ray with the scintillator involves three principle mechanisms: the photoelectric effect, the Compton effect and pair production. Although all these may be involved in the detection of a single photon, they are discussed separately in the following paragraphs.

The photoelectric interaction between a gamma ray and an atomic electron results in the complete transfer of the photon energy to the electron and the recoiling atom. The kinetic energy given to these two bodies is the total energy of the gamma photon less the atomic binding energy of the electron. The cross-section for the photoelectric process varies in a complex manner with the photon energy and the atomic number of the target, but it is roughly proportional to Z^5 and $(1/E)^{7/2}$. This process is thus very important for the interaction of low energy gamma rays with high Z materials.

When a photon is inelastically scattered by an atomic electron, the energy (E') of the photon, scattered at an angle θ, is given by

$$E' = \frac{E}{1 + \frac{E}{m_o c^2}(1-\cos\theta)} \qquad (2\text{-}1)$$

where E is the incident gamma energy and $m_o c^2$ is the rest energy of an electron (0.511 MeV). This type of scattering is known as Compton scattering. It has a cross-section which is proportional only to the number of atomic electrons in the material, since the scattering is an electronic phenomenon. Inasmuch as the number of electrons per gram of matter is

nearly the same for all substances, the Compton cross-section per unit mass is nearly independent of Z or A. The probability of Compton scattering is only slightly dependent on energy, changing by a factor of 2 between 0.1 and 1 MeV. The energy of the recoil electron has a continuous distribution from zero when $\theta = 0$, to $E\left\{\frac{2\alpha}{1 + 2\alpha}\right\}$ when $\theta = \pi$, ($\alpha = E/m_o c^2$). As E approaches infinity, the maximum electron energy approaches asymptotically to $(E - \frac{1}{2}m_o c^2)$. For the energy region from 0.5 MeV to 5 MeV, the Compton effect is the dominant form of the interaction of gamma-rays with matter.

The production of a positron and an electron, by a gamma ray of energy greater than 1.022 MeV ($2m_o c^2$), is known as pair production. The subsequent annihilation of the positron with an atomic electron produces two 0.511 MeV photons. The cross-section for pair production varies as Z^2, and becomes very important for incident photon energies above 2 MeV.

The observed response of a detector to gamma radiation can be accounted for on the basis of multiple interactions of these three types. In the photoelectric effect all the photon energy is transferred to charged particles in a one stage process. In the other two processes, only a portion of the energy is so transferred, but the scattered radiation is reduced in energy, and therefore it is more probable that it will interact with another atom of the crystal by a photoelectric effect. The result of such multiple scattering events for an infinitely large crystal is to transfer all the original photon energy to ionizing particles, while for a finite size crystal there is the possibility that some of the scattered radiation will escape undetected.

The probability of such multiple processes is obviously enhanced by increasing the dimensions of the detector and by choosing a material of high density. The material which best meets these requirements is NaI(Tl), which can be grown as large crystals of high density and which scintillates efficiently.

The effect of detector size is shown in Fig. 1, where the response of a 2" x 2" NaI(Tl) and a 3" x 3" NaI(Tl) crystal are compared for incident gamma rays of energies 0.661 MeV and 2.76 MeV. The accentuation of the photoelectric peak in the response of the three inch crystal is very marked, particularly at higher energies. The effect of the geometry on the spectral response may be divided into two parts: the effect of source-crystal distance and the effect of any absorbers between the source and detector. A smaller source to crystal distance slightly enhances the Compton effect because the scattered radiation more readily escapes from the crystal. The effect of absorber is shown in Fig. 2. The filling in of the valley between the photopeak and the Compton distribution is due to small angle (Compton) scattering in the absorber.

The total energy peak or photopeak is Gaussian in shape, and is characterized by its resolution, that is the ratio (in per cent) of its width, at half height, to its position. The resolution is dependent on the characteristics of the crystal and the coupling between the crystal and photomultiplier; it is reasonably well expressed by the empirical formula

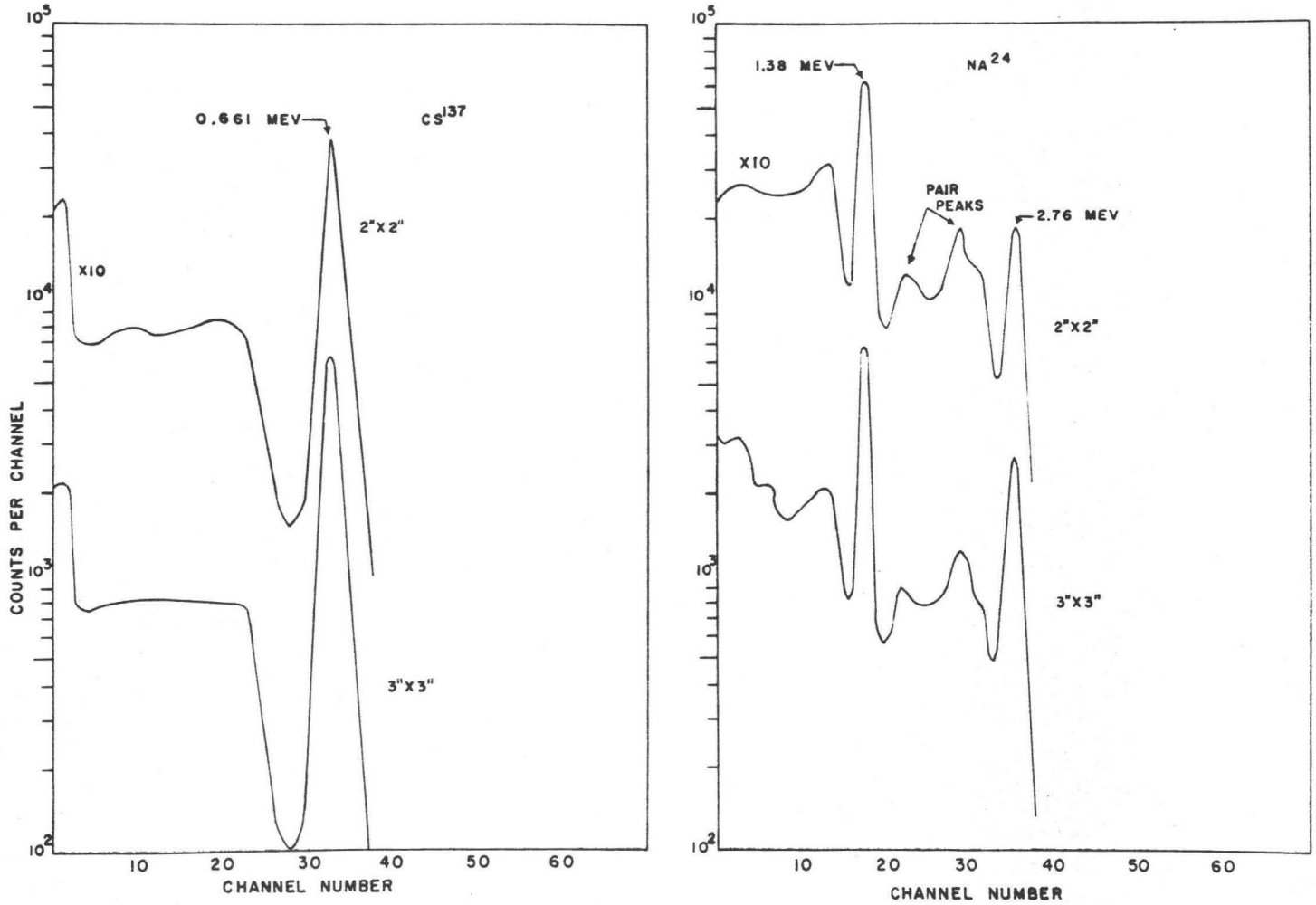
COUNTS PER CHANNEL
CHANNEL NUMBER
0.661 MEV
Cs137
2"x2"
X10
3"x3"
1.38 MEV
Na24
PAIR PEAKS
2.76 MEV
X10
2"x2"
3"x3"
CHANNEL NUMBER

Figure 1

Figure 2

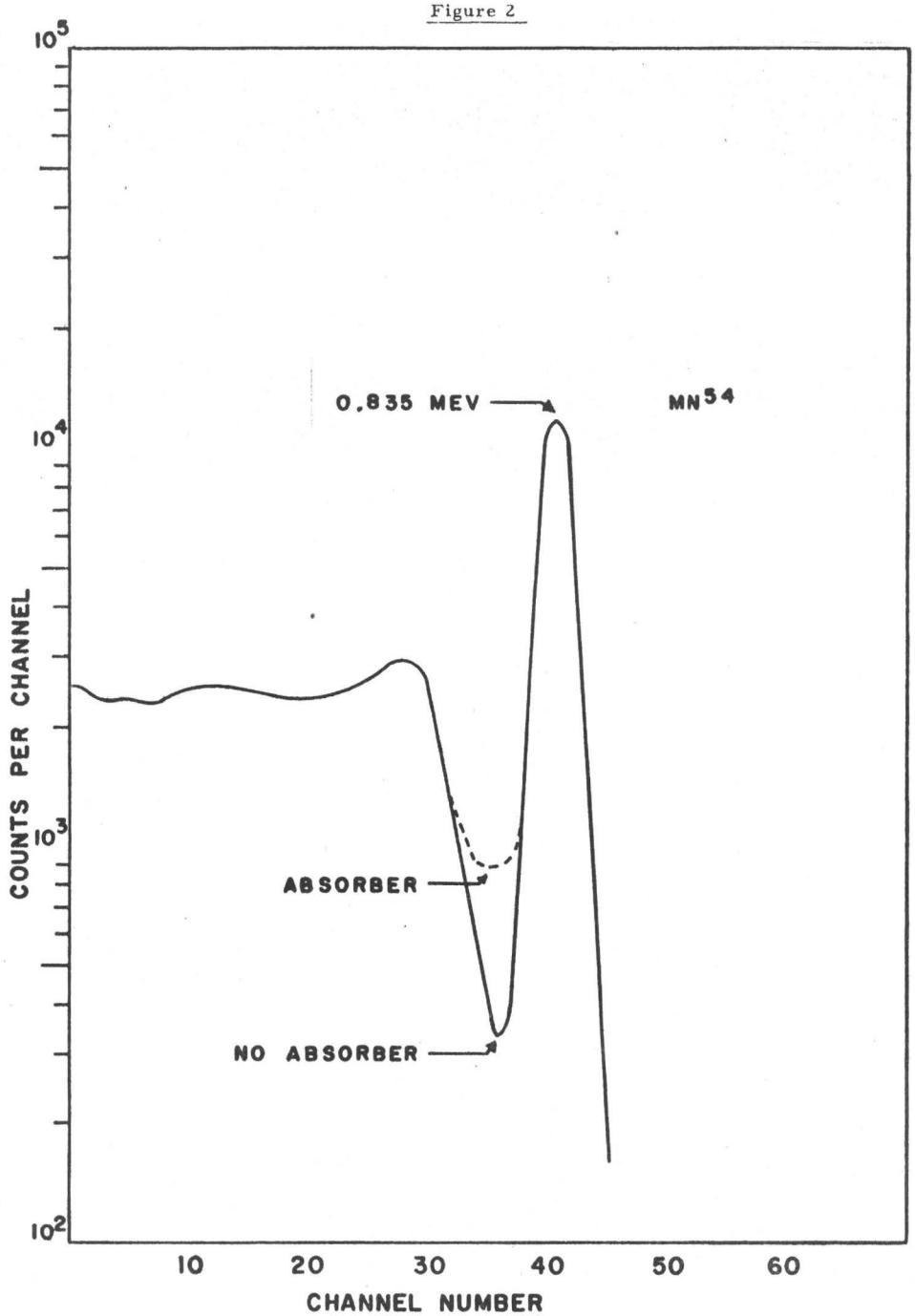
10^5
10^4
10^3
10^2
COUNTS PER CHANNEL
0.835 MEV
MN^{54}
ABSORBER
NO ABSORBER
10
20
30
40
50
60
CHANNEL NUMBER

$R = A + B/\sqrt{E}$ in which the second term is dominant. For a selected 3" crystal-photomultiplier combination, the value of R for the 0.661 MeV Cs^{137} gamma ray is in the range of 7 to 8%.

2) THE EFFICIENCY OF A GAMMA DETECTOR

The efficiency of a sodium iodide detector varies rapidly with energy, as does the shape of the response curve. This efficiency may be considered as the product of two parts: the total probability of the gamma ray interacting with the crystal, Y(E), and the probability that this interaction will lead to full absorption, P(E). The product of these two functions is called the photoefficiency, and is denoted by $P_e(E) = Y(E).P(E)$. In order to evaluate P(E) empirically, it is necessary to measure the ratio of the areas of the full-energy peak to the total response function, for a series of gamma rays of different energies. In Figs. 3a and 3b, values of P(E), for the crystals used in this work, are given as a function of energy. Alternatively, calculations of P(E) have been made using Monte Carlo methods (Berger and Dogget, 1956). Such calculations cannot of course reflect all the idiosyncrasies of an experimental apparatus, and were used only as a guide to interpolation. Y(E) may also be evaluated either experimentally or theoretically. The experimental observation of the total number of counts, from a source of known strength, is of course, the best method, but the difficulty of calibrating source strengths accurately, leads one to rely on calculations. Values of Y(E) have been calculated using the absorption coefficients for NaI, and evaluating the total probability of an interaction for a given source-crystal geometry, (Stanford and Rivers, 1958;

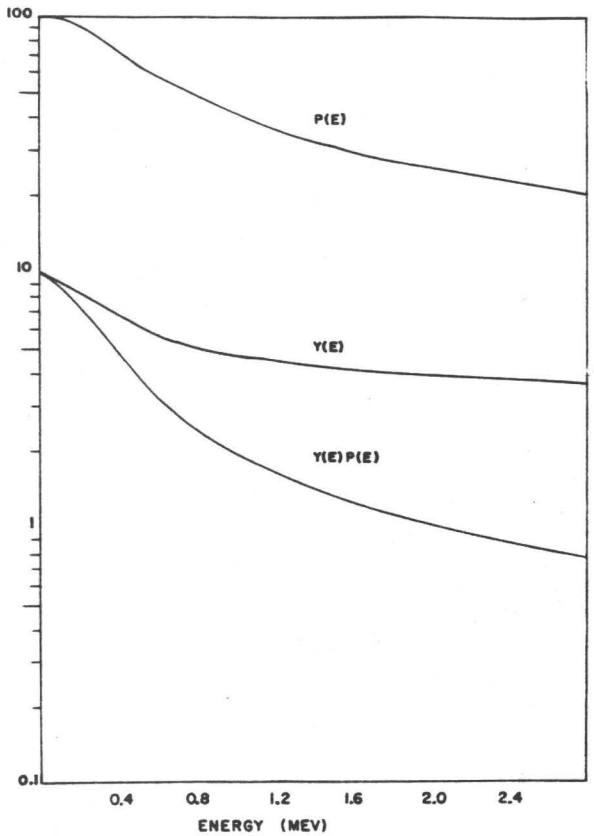

EFFICIENCY FACTORS FOR THE 3" x 3"
NaI(Tl) detector

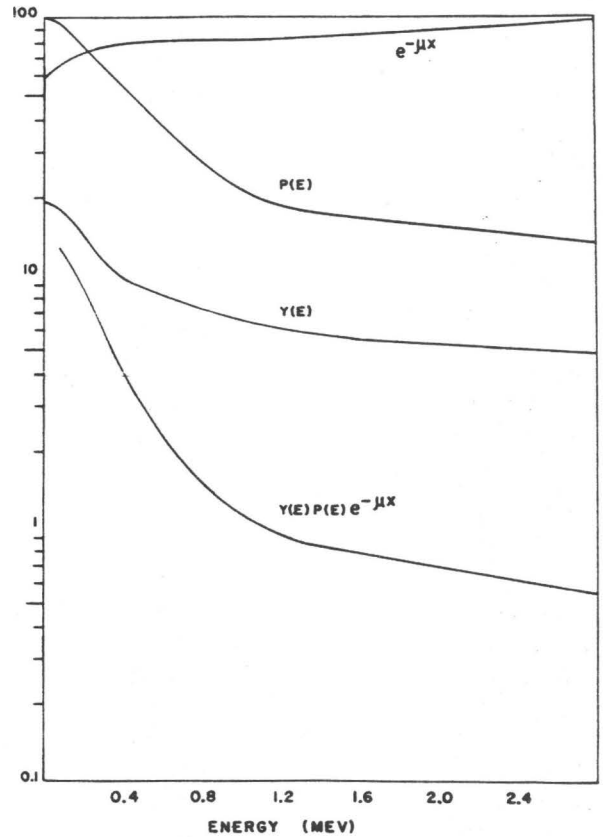

EFFICIENCY FACTORS FOR THE 2" x 2"
NaI(Tl) detector

Figures 3a and 3b

Heath, 1957). In Figs. 3a and 3b, the values of Y(E), from Heath, for the geometry and crystals used are plotted as a function of energy. The product Y(E).P(E) is also shown on these graphs. The only other efficiency factor that is required in order to compare the intensities of gamma rays of different energies is the effect of the beta stopper, which was placed between the source and the detector. This absorption correction was obtained from the tables of Davisson (1955). The total detection efficiency, given in Figs. 3a and 3b, will be used in Chapter 3 for the calculation of the intensities of the gamma rays resulting in the decay of Kr^{90}.

3) THE STRIPPING OF A COMPLEX GAMMA SPECTRUM

The lack of a simple response of a gamma spectrometer to monoergic photons imposes severe problems on the analysis of a complex gamma spectrum. The resolving or stripping of such a spectrum requires a detailed knowledge of the nature of the response of the spectrometer as a function of energy. It is not practical to generate such a function theoretically, and therefore the spectra of various sources, known to emit monoergic gamma rays over a wide range of energies, must be obtained using the same geometry and absorbers as used with the unknown spectrum. Such a library has been established for both 2" and 3" crystals using the spectra of In^{114} (0.191 MeV), Au^{198} (0.412 MeV), Cu^{64} (0.511 MeV), Cs^{137} (0.661 MeV), Mn^{54} (0.836 MeV), Na^{22} (1.28 MeV), Al^{28} (1.78 MeV), and Na^{24} (1.38 and 2.76 MeV). Certain of these spectra for the 2"crystal are shown in Fig. 4; those for the 3" crystal were similar to the ones given by Heath (1957).

These line shapes were used in the following manner to analyse the relatively complex gamma spectrum of the decay of Kr^{90}. First all the spectra were plotted on semi-log paper to facilitate the analysis. An examination of an unknown spectrum, containing N gamma rays will reveal a number of peaks. There will be a photopeak corresponding to the highest energy gamma ray in the decay, and the response curve for a gamma ray of this energy may be obtained from the library of standard responses. The normalized response curve is subtracted from the data, point by point, leaving a residual spectrum containing N - 1 gamma rays. The process is repeated until the original spectrum has been reduced to N response curves from which the energies and intensities of all N gamma rays may be calculated. While this method would appear to be quite subjective, the consistency between analyses, carried out by different persons, is rather remarkable. The analysis of the gamma spectrum of Kr^{90} was performed in this manner and is discussed in Chapter 3.

B) The Beta-Ray Scintillation Spectrometer

1) CHARACTERISTICS OF A PLASTIC SCINTILLATOR

The use of a scintillation spectrometer, for studying the characteristics of a beta spectrum, is complicated by the complex response function of the scintillator for electrons. In principle, one would expect a simple Gaussian pulse distribution from a beam of monoergic electrons, but in fact, the presence of large-scale multiple scattering of the electrons results in many leaving the detector without losing all their energy. The response curve is therefore a Gaussian peak with a continuous low energy distribution somewhat

Figure 4

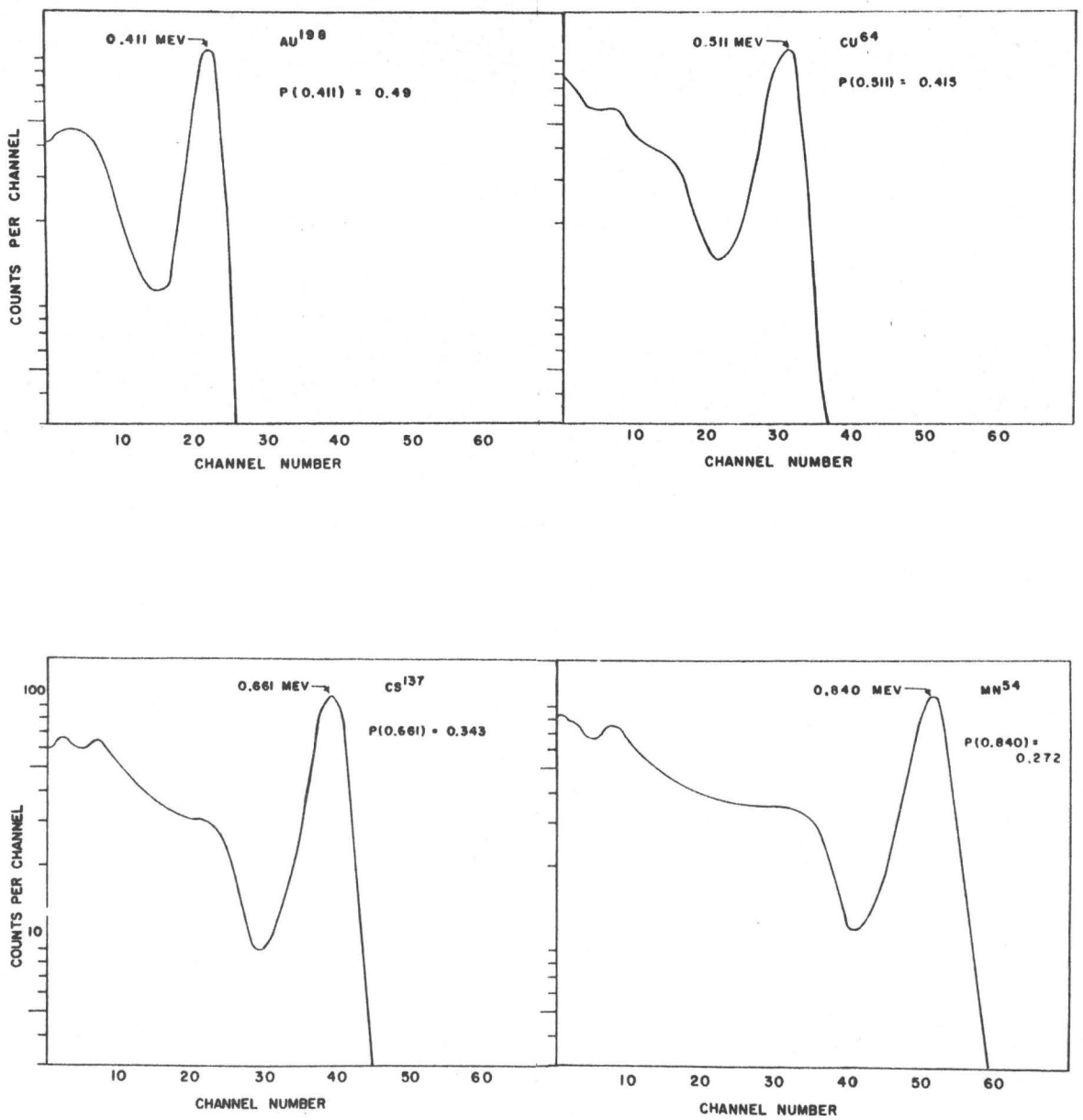
0.411 MEV
AU198
P(0.411) = 0.49
0.511 MEV
CU64
P(0.511) = 0.415
COUNTS PER CHANNEL
CHANNEL NUMBER
10
20
30
40
50
60
100
0.661 MEV
CS137
P(0.661) = 0.343
0.840 MEV
MN54
P(0.840) = 0.272

similar to that of a gamma scintillation spectrum. The use of a detector made of low Z material minimizes both the scattering and the sensitivity of the device to gamma rays. Plastic scintillators (Eichholz 1954) are widely used for beta scintillation counters, although the use of a magnetic spectrometer is generally preferred where practical. As outlined in Chapter 1, beta spectra are presented as Fermi plots in which $\sqrt{\frac{N'}{pWf}}$ is plotted against energy. Such plots should yield a straight line for allowed transitions. As shown by Ketelle (1950), a scintillation counter produces a straight-line Fermi plot only when the source is counted in 4π geometry. When a source external to the detector is used, the presence of the multiple scattering always produces an apparent excess of low-energy electrons. The experiments on Kr^{90} required the use of a large volume source, which necessarily was placed external to the detector. In order to account for the effect of the electrons being scattered out of the detector, a guard detector was placed around the main detector, and only those events producing an interaction in the inner detector and not in the outer were accepted. A diagram of the detector is shown in Fig.5. By using the anti-coincidence guard, about 60% of the electrons, detected by the inner scintillator, had to be rejected. Freedman et al. (1956) have shown that in an organic scintillator, a monoergic electron beam produces a pulse distribution of the form shown below, and that the ratio of a/b is

Figure 5

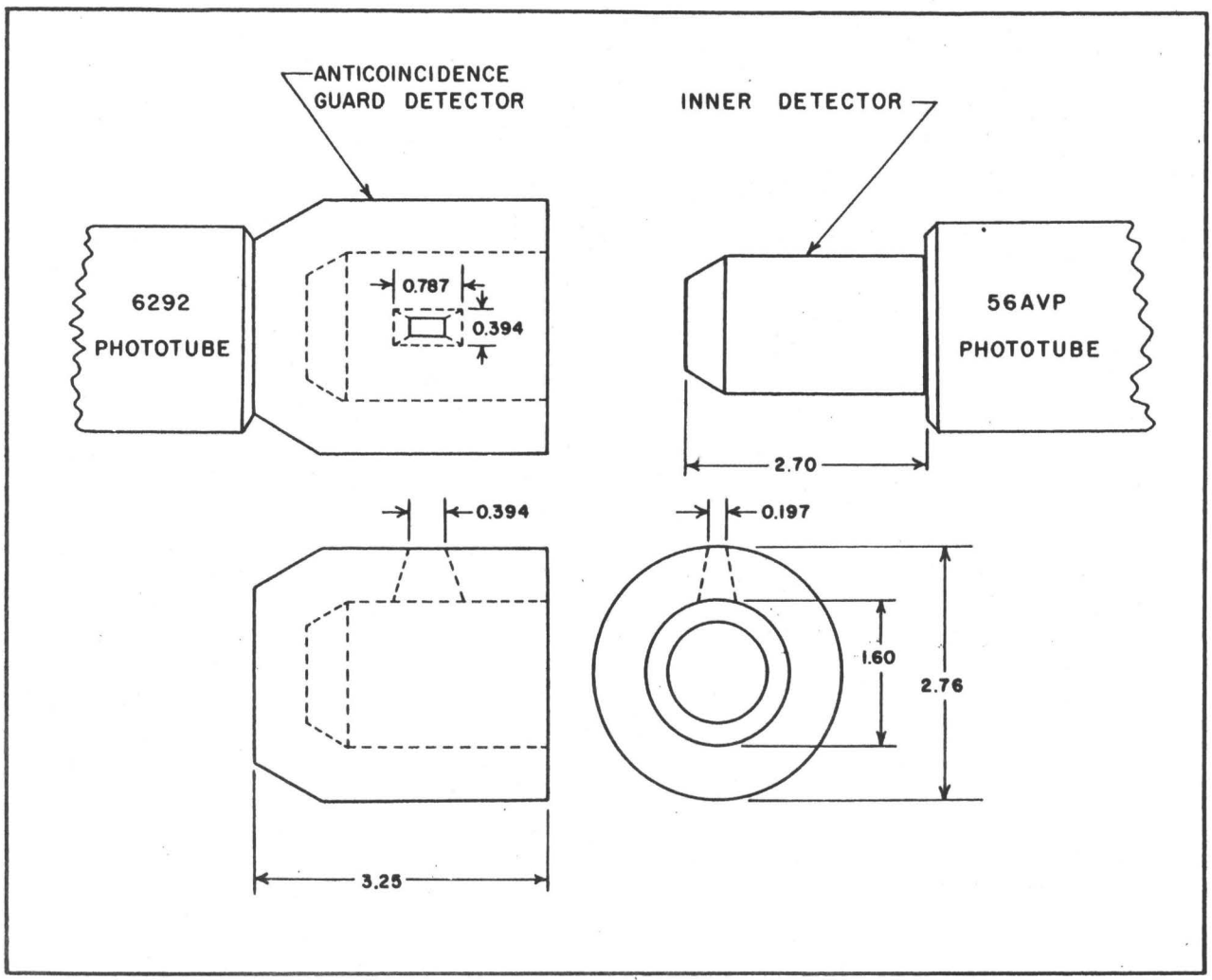
ANTICOINCIDENCE
GUARD DETECTOR
INNER DETECTOR
6292
PHOTOTUBE
0.787
0.394
56AVP
PHOTOTUBE
2.70
0.394
0.197
1.60
2.76
3.25

nearly independent of energy. Since the anti-coincidence shield rejects all those electrons which suffer only partial energy loss, the efficiency ϵ of the detector is given by

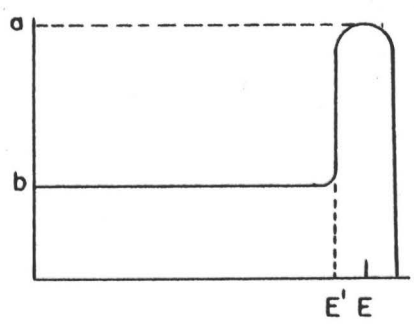

$$\epsilon = \frac{A}{A + B} \qquad (2\text{-}2)$$

where A is the area of the photopeak and B is the area of the tail. From the experience with gamma scintillation spectrometers, one expects A to be a function of energy of the form:

$$A = c + \frac{d}{\sqrt{E}} \qquad (2\text{-}3)$$

and the area of the tail is given by $B = b E'$ (2-4)

Hence by knowing the values of a/b, c and d, it is possible to evaluate ϵ. The evaluation of these constants is difficult and the validity of equations 2-3 and 2-4 is probably only approximate. Thus an empirical determination of ϵ as a function of energy was made. Beta spectra with allowed shapes were obtained with the scintillation spectrometer; a Fermi plot of such spectra typically showed a linear high energy portion which extrapolated to cut the energy axis at the end-point, and a lower energy portion which curved steadily upward. The departure of the experimental curve from the expected linear Fermi plot was interpreted as due to the variation of ϵ with energy, and was used to establish this variation. By using spectra with different end-points, it was possible to obtain an experimental curve of ϵ versus E. The standard beta sources most commonly used for

calibration were In^{114} with a 2 MeV end-point, Al^{28} with an end-point at 2.88 MeV and Rh^{106} with a 3.53 MeV end-point. The Al^{28} beta spectrum is complicated by the presence of a 1.79 MeV gamma ray, which is also detected by the detector: however, the use of beta-gamma coincidence data resulted in a simple beta spectrum. The Rh^{106} spectrum was complicated by the presence of an 8% 3.00 MeV group and several weak lower energy beta groups. This spectrum was fabricated using the branching ratios established from published magnetic spectrometer measurements, and then applied to the plastic scintillation data to obtain ε. The variation of ε with energy is shown in Fig. 6. This experimentally determined efficiency curve changes somewhat more rapidly at low energies than predicted from equations 2-3 and 2-4, but the disagreement is not serious above 0.8 MeV. This suggests that the electrons, being scattered out of the inner cylinder, were losing so much energy in the light seal between the inner and the outer detectors as to be ineffective in operating the anti-coincidence circuit. The value of ε was normalized to unity at 0.5 MeV, since only relative efficiencies are used in the analysis of beta spectra. It was gratifying that the same efficiency curve could be used for all data, even though the detector had been dismantled and reassembled between experiments. Sources, with beta end-point energies close to those of Kr^{90}, were used for calibration.

2) APPROXIMATIONS USED FOR FERMI PLOTS

The analysis of the data obtained from a high-resolution beta-ray spectrometer, in terms of a Fermi plot, is a well established procedure. Since the data involved is in general of high accuracy, the method of treating the data must include corrections to a high order of approximation. These second-order corrections are unnecessary for the analysis of the beta spectra obtained from a scintillation counter, since the detector has a rather poor resolution and its response function is poorly determined. As discussed in Chapter 1, a Fermi plot is a plot of $\sqrt{\frac{N}{pWF}}$ vs W; the quantity under the root sign may be written as $\frac{1}{W}\sqrt{\frac{N}{G}}$ where G is the tabulated function $G = \frac{Pf}{W}$ (Rose 1955a). The total energy W is the kinetic energy plus the rest mass energy of an electron, where the kinetic energy of the electron detected by a scintillation spectrometer is proportional to the channel number (Ch) in which it is recorded. Thus a plot of $\frac{\sqrt{N/G}}{Ch + Ch_o}$ vs Ch, where Ch_o is the channel equivalent to 0.511 MeV, is also a Fermi plot. However, for Z = 37, the value of G is almost independent of energy, varying from 0.27 at zero energy to 0.283 at 3 MeV. Thus the data can be analysed by plotting $\frac{\sqrt{N}}{(Ch + Ch_o)\sqrt{\epsilon}}$ vs Ch where ϵ is the efficiency factor previously discussed. An approximate correction for the energy dependence of G is also made, due to the manner in which the efficiency function is determined. Ch_o was evaluated from the calibration beta spectra obtained with each Kr^{90} experiment.

Figure 6

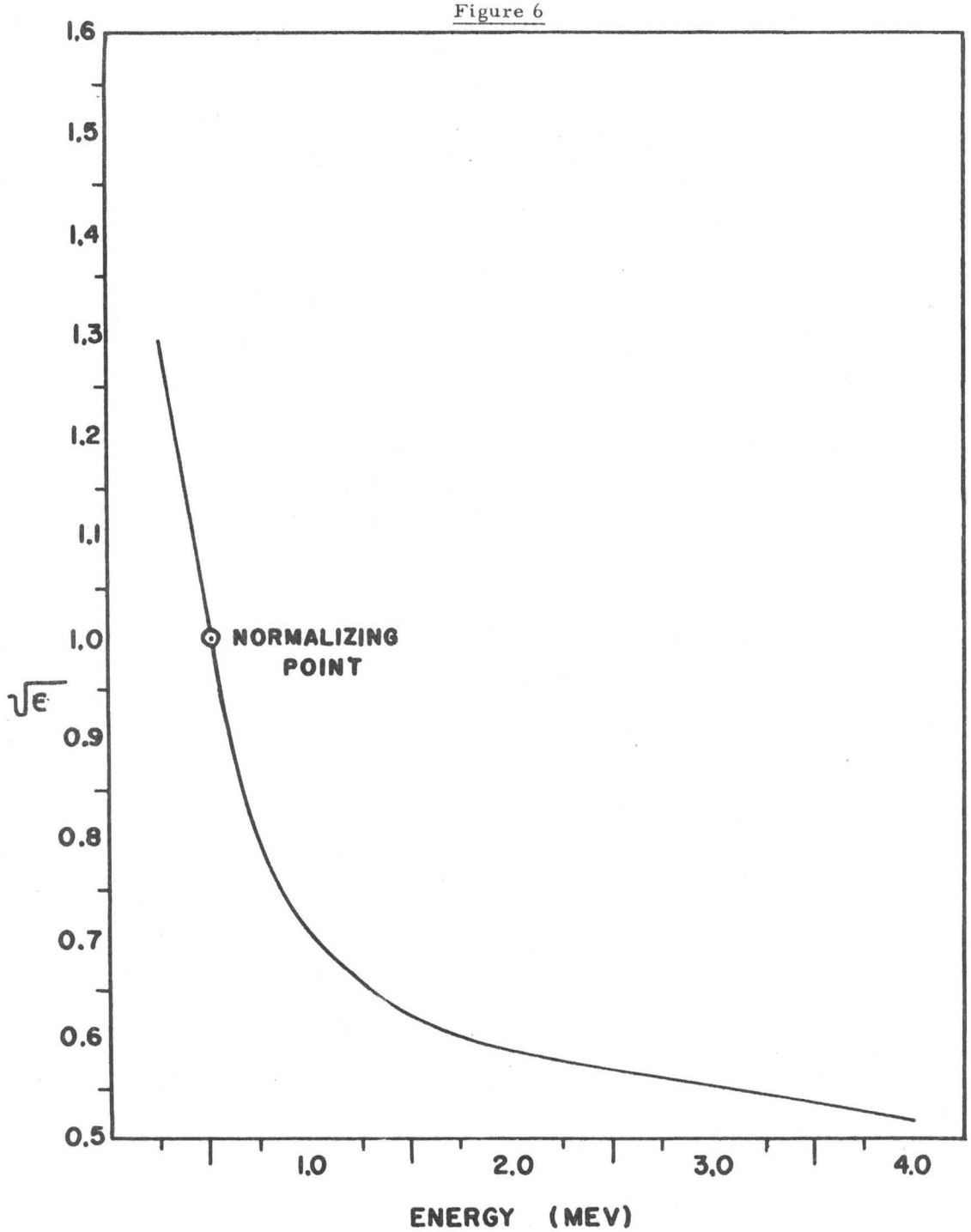
1.6
1.5
1.4
1.3
1.2
1.1
1.0
0.9
0.8
0.7
0.6
0.5
√ε
NORMALIZING POINT
1.0
2.0
3.0
4.0
ENERGY (MEV)

The poor resolution of the beta spectrometer also proved to be troublesome in that it contributed to a high energy tail on the Fermi plots. It was not possible to obtain sufficient information on the resolution of the detector to correct this effect. However, the number of counts represented by this high energy spectrum is quite small. A few such counts, at high energy, are made to appear more prominent by the nature of the Fermi plot. While beta spectra obtained with a scintillation spectrometer are not as definitive as those obtained from magnetic spectrometers, their interpretation gives useful information on the nature of the decay. The intensity of the various beta groups is in general not well determined, and the analysis of the gamma spectra will be of greater importance to the intensity balancing considerations required in formulating a decay scheme.

C) Coincidence Counting

A powerful technique for the study of decay schemes is offered by the use of beta-gamma and gamma-gamma coincidence counting. The simultaneous arrival of two events in different detectors indicates that these events are in cascade. This information is very useful when establishing a decay scheme.

The coincidence counting rate N_{12} between two gamma rays, 1 and 2, may be written as

$$N_{12} = N f_{12} e_{12} (YP)_1 (YP)_2 \qquad (2\text{-}5)$$

where $(YP)_1$ and $(YP)_2$ are the photoefficiences of the two radiations, e_{12} is the coincidence efficiency of the circuit, N is the source strength, and

f_{12} is the probability of the gamma 1-gamma 2 coincidence occurring in the decay. The determination of $(YP)_1$ and $(YP)_2$ has already been discussed and these factors may be considered known. The determination of e_{12} will be discussed later. The important point to realize here is that the ratio

$$\frac{N_{12}}{e_{12}(YP)_1(YP)_2} \tag{2-6}$$

is proportional to the factors f_{12}, which yield information concerning the decay pattern.

All coincidence counting rates must be corrected for chance coincidences which are recorded when two unrelated events occur within the resolving time of the circuit. The rate of random coincidences is

$$N_r = 2\tau N_1 N_2 e_{12} \tag{2-7}$$

where τ is the resolving time of the circuit and N_1 and N_2 are the single channel counting rates. The signal to chance ratio is given by

$$N_{12}/N_r = f_{12}/2\tau N \tag{2-8}$$

A reduction in τ is seen to result in a corresponding increase in usable source strength for a given value of signal to chance ratio. To avoid the necessity of making large corrections for random events, this ratio should be kept large. For the experiments on Kr^{90} to be discussed, the ratio of the true to the random rates was about 1000 for the stronger cascades and about 50 for the weaker ones.

The analytical expressions, given above, assume that the energy selection process is unique, and that only one gamma ray is being detected by each detector. The response curves of NaI(Tl) detectors are such that this assumption is far from realistic and corrections for the underlying background must be made. Using the spectrum stripping techniques previously discussed, it is possible to determine the composition of the gating spectrum. However, the errors involved in this may be rather large and limit the accuracy of f_{12} values determined from coincidence measurements.

The setting up of a decay scheme involves the measurement of beta-ray and gamma-ray energies and intensities and the determination of the coincidence relationships existing between them. As we have seen, for short lived isotopes, the necessity of rapid data collection make it necessary to use scintillation spectrometers and accept the difficulties imposed by their complex response functions. The experiments carried out on Kr^{90} using these techniques will be discussed in the next chapter.

CHAPTER III

THE DECAY OF Kr^{90}

The production of radioactive isotopes with thermal neutrons may either be direct (eg. n, γ reaction), or may be the result of fission. These fission products are neutron rich and therefore decay by beta minus emission. The radiations emitted in the decay of some of the short-lived fission products are of high energy, and many levels in the daughter nucleus are excited. Their decay scheme is usually complicated. It is the study of the decay of one such fission product (33-sec Kr^{90}) which will now be described.

The first measurement of the half-lives of rare-gas fission products was made by Dillard et al. (1951), who found the half-life of Kr^{90} to be 33 sec. In their experiments, radioactive inert fission-product gases were passed at a steady rate along a charged wire, and the distribution of the daughter products, thus collected, was analysed using a mass spectrometer.

Experiments using an electromagnetic isotope separator (Kofoed-Hansen and Nielsen, 1951) also showed that Kr^{90} has a half-life of 33 seconds, and that it decays with a 3.2 MeV beta group. This beta measurement was obtained using aluminum absorbers and Geiger counters. No study of the gamma spectrum was reported.

A study of the gamma spectrum of Kr^{90} was made by Wahlgren and Meinke (1961) using a sodium iodide scintillation technqiue. They identified gamma rays of energies 0.12, 0.24, 0.54, 1.12, 1.54 and 1.77 MeV as

belonging to the decay of Kr^{90}. Ockenden and Tomlinson (1962) also studied the gamma spectrum of several rare-gas fission products and their data on Kr^{90} is in agreement with that of Wahlgren and Meinke. To date, no decay scheme of Kr^{90} has been published. The present work was undertaken to establish a decay scheme for this nuclide.

A) Source Preparation

The sources, used for these experiments, were obtained by using the apparatus described by Ockenden and Tomlinson (1962). A diagram of part of this equipment is shown in Fig. 7. U^{235}, in the form of uranyl stearate, was melted onto both surfaces of the production chamber. This coating contained about 500 mg. of U^{235} and was about 20 mg/cm^2 thick. The cadmium shutter was used to control the neutron flux impinging upon the target. The inert gas fission products were swept out of the production chamber by a flow of helium gas initiated by opening valves A, B, E of the system shown in Fig. 8. The mixture of radioactive krypton and xenon was trapped in the hold-up volume between valves C and D where it was allowed to decay for 10 seconds to reduce the amount of 10-sec.Kr^{91} in the source. By opening valves C, D, G, G′, the sample was pushed through the gas chromatograph, which separated the krypton and xenon activities. The lighter krypton component came through first, 10 seconds after the gas had been swept out of the hold-up volume. As soon as this activity was in the counting chamber, it was trapped by closing GG′ and opening F. The xenon activity was passed directly into the cold trap through valve F.

Figure 7

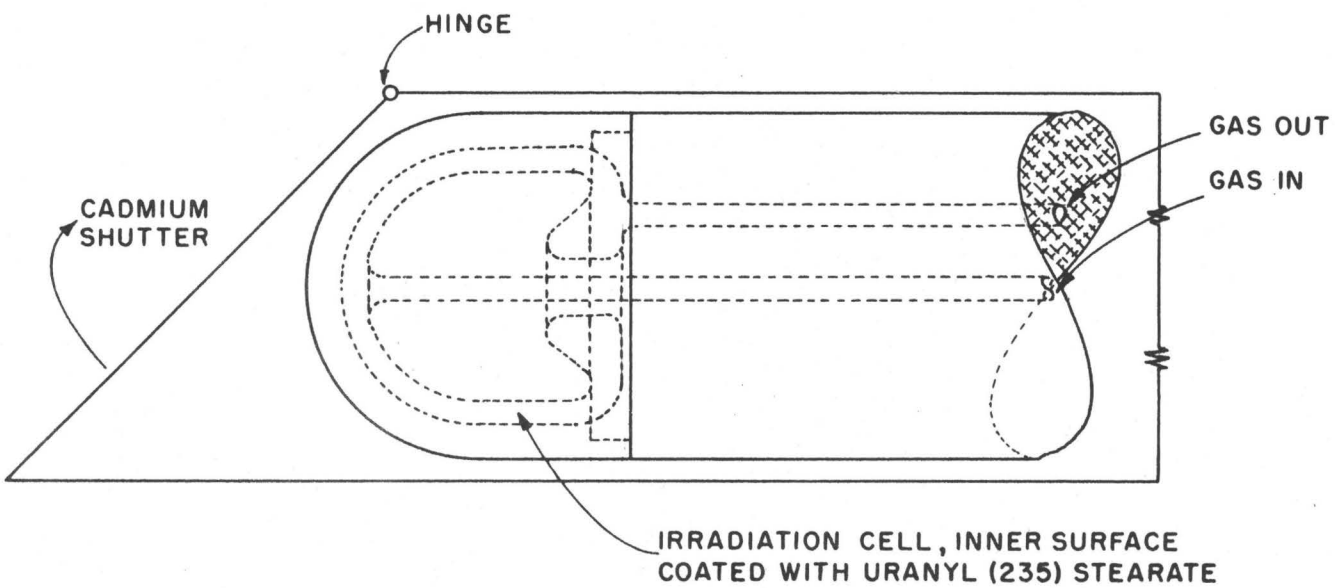

MATERIAL - IS ALUMINUM

Figure 8

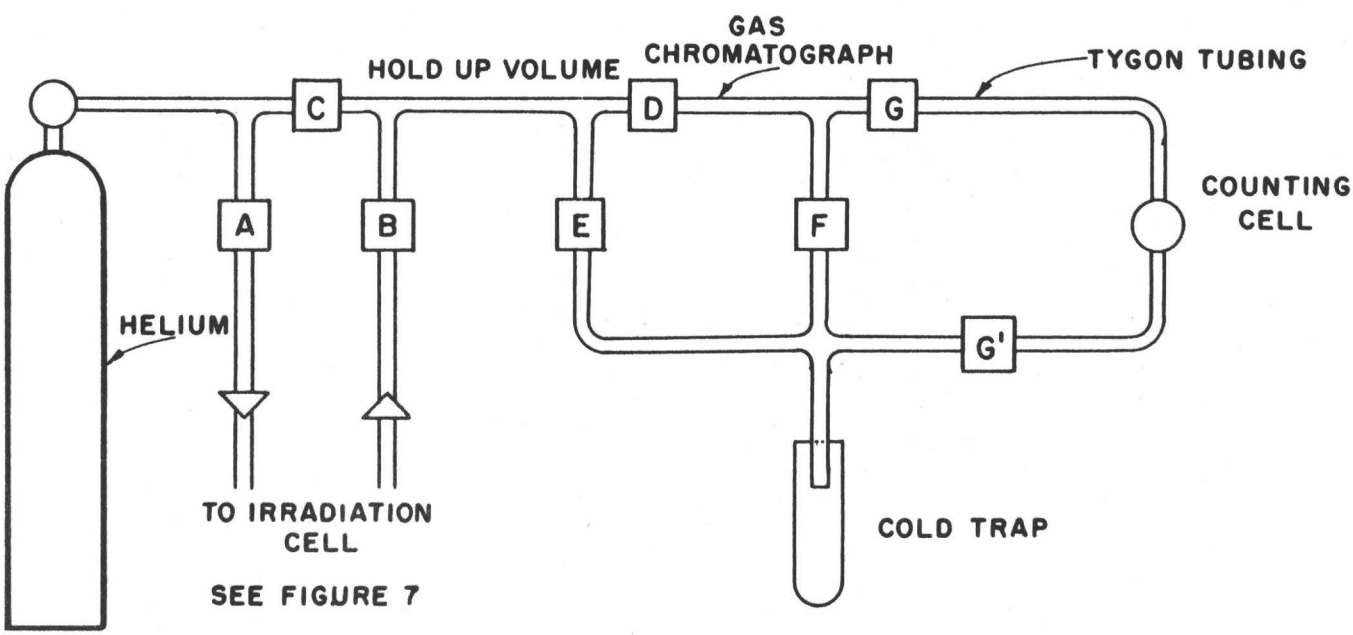
GAS
CHROMATOGRAPH
HOLD UP VOLUME
TYGON TUBING
C
D
G
A
B
E
F
COUNTING
CELL
HELIUM
G'
TO IRRADIATION
CELL
SEE FIGURE 7
COLD TRAP

In order to maximize the amount of Kr^{90}, relative to the other isotopes, the following time sequence was followed: 4 sec. for irradiation, 20 sec. for cooling and chromatography, and 30 sec. for counting the sample. The notation for this sequence, which will be used subsequently, is 4-20-30.

The counting cell used for these experiments is shown in Fig. 9. The cell is a cylinder of copper tubing 1" long and 3/4" in diameter with its open ends covered by Saran wrap. The radioactive gases were admitted into the counting chamber through a 1/8" diameter copper pipe soldered into one side of the cell, and an outlet pipe of similar material was fitted at an angle of 60° to the inlet. A lucite or aluminum beta stopper was placed between the cell and the gamma detector. In addition, the detectors were shielded from the inlet and outlet lines, which gradually built up residual activity.

The counting cell was replaced after every source, and a run involved about twenty to fifty sources depending on the intensity of the transitions under study. The total cycle time for a source was about 2.5 min.

B) Half-Life Measurements

In previous studies of its decay the half-life of Kr^{90} was found to be about 33 seconds (Dillard 1951, Kofoed-Hansen and Nielson, 1951, Wahlgren 1961, and Ockenden and Tomlison 1962). In order to identify which gamma rays were associated with this activity, a series of half-life measurements were performed. Since the samples at the start of the counting interval contained only radioactive krypton, the activities present were Kr^{88} ($T_{\frac{1}{2}}$ = 10,000 seconds), Kr^{89} ($T_{\frac{1}{2}}$ = 192 seconds), Kr^{90} ($T_{\frac{1}{2}}$ = 33 seconds) and Kr^{91} ($T_{\frac{1}{2}}$ = 10 seconds) and over the counting interval the rubidium daughters of these isotopes would have grown in.

Figure 9

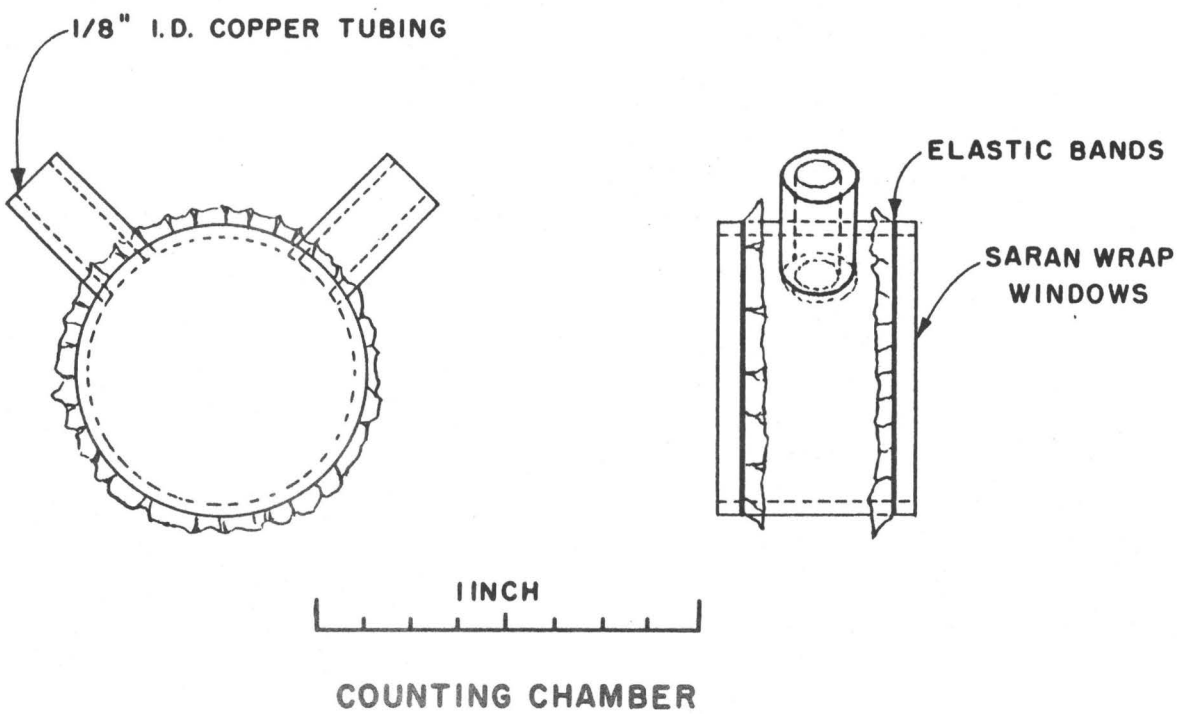
1/8" I.D. COPPER TUBING
ELASTIC BANDS
SARAN WRAP
WINDOWS
1 INCH
COUNTING CHAMBER

The main gamma rays associated with the 33 second activity were identified by observing the change of the spectrum with time. The gamma spectrum was observed with a 3" x 3" NaI(Tl) detector and the electronics shown in Fig. 11. The multi-channel analyser was operated as four 128 channel units. The radioactive gas was passed into the counting chamber and the spectrum was recorded for 15 seconds in the first quadrant of the analyser. The spectrum was reexamined at 30 second intervals, counting for 15 seconds each time and using the other three quadrants of the analyser.

These spectra thus represent four points on the decay curve and were used to identify the prominant features of the 33 second activity. Gamma rays of energies 0.12, 0.54, 1.12, 1.54 and 1.79 MeV were identified as belonging to Kr^{90}. This is in agreement with the previous work on this isotope.

After these prominent features had been established, an attempt was made to obtain a better value for the half-life of Kr^{90}. For this purpose, the multi-channel analyser was operated as a multi-channel scaler (MCS). A block diagram of the electronics used is shown in Fig. 10. Pulses from the detector were amplified in a preamplifier and double-delay line amplifier (DD2) and the photopeak whose half-life was to be measured was selected by the pulse height selector (PHS). The output of the PHS was shaped (S) and fed into the MCS. The scaler accepted counts in one channel for a time Δt, and then the input pulses were routed into the next channel and the cycle repeated. The channel advance was initiated by a shaped output pulse which was derived from the sweep circuit of a Tektronix oscilloscope. The time Δt was determined by the 10 kilocycle crystal oscillator of an EPUT (Events per Unit Time) meter.

The selection of the time Δt is influenced by two contradictory criteria. In order to study details of the decay, a short time Δt should be used, but in order to obtain adequate statistics per channel a long time is required. A suitable compromise was found to be a Δt of two seconds, and thus a total counting time of 1024 seconds was used. This total time is more than two half-lives of the long lived Kr^{89} isotope.

A simple plot of the counting rate versus time on semi-log graph paper showed that all the prominent peaks decayed with a half-life of about 30 seconds. This is in agreement with the 'four spectra' experiment discussed earlier. However the graphical analysis was complicated by the presence of the 162-second Rb^{90}, which was growing in at the same time as the Kr^{90} and 192-second Kr^{89} were decaying. The process of subtracting these activities was quite subjective and led to variations of up to 20% in the half-life of the Kr^{90} component.

In an attempt to improve on this measurement, a computer program was written to fit the data to an equation of the form

$$N(t) = A e^{-\lambda_1 t} + B\frac{\lambda_1}{\lambda_1-\lambda_2}\left(e^{-\lambda_2 t} - e^{-\lambda_1 t}\right) + C e^{-\lambda_3 t} + D \qquad (3\text{-}1a)$$

where λ_2 and λ_3 were taken as the known half-lives of Rb^{90} and Kr^{89}, and λ_1 was used as a parameter to obtain the best fit. The constants A, B, C, and D were allowed to be variables. The constant D represents the background, while A, B, and C are proportional to the Kr^{90}, Rb^{90} and Kr^{89} activities in the sample. The computer fitted the data to a curve of the shape of eq. (3-1), using given values of λ_1, λ_2 and λ_3, and thus values for A, B, C and D were obtained. The weighing factor used was the errors on the points, $\frac{1}{\sqrt{N}}$, and the goodness of fit was measured as the sum of the squares of the deviations between the experimental numbers and the calculated points. This sum was minimized for a value of λ_1 and then λ_1 was changed by $\Delta\lambda_1$ and the process

Figure 10

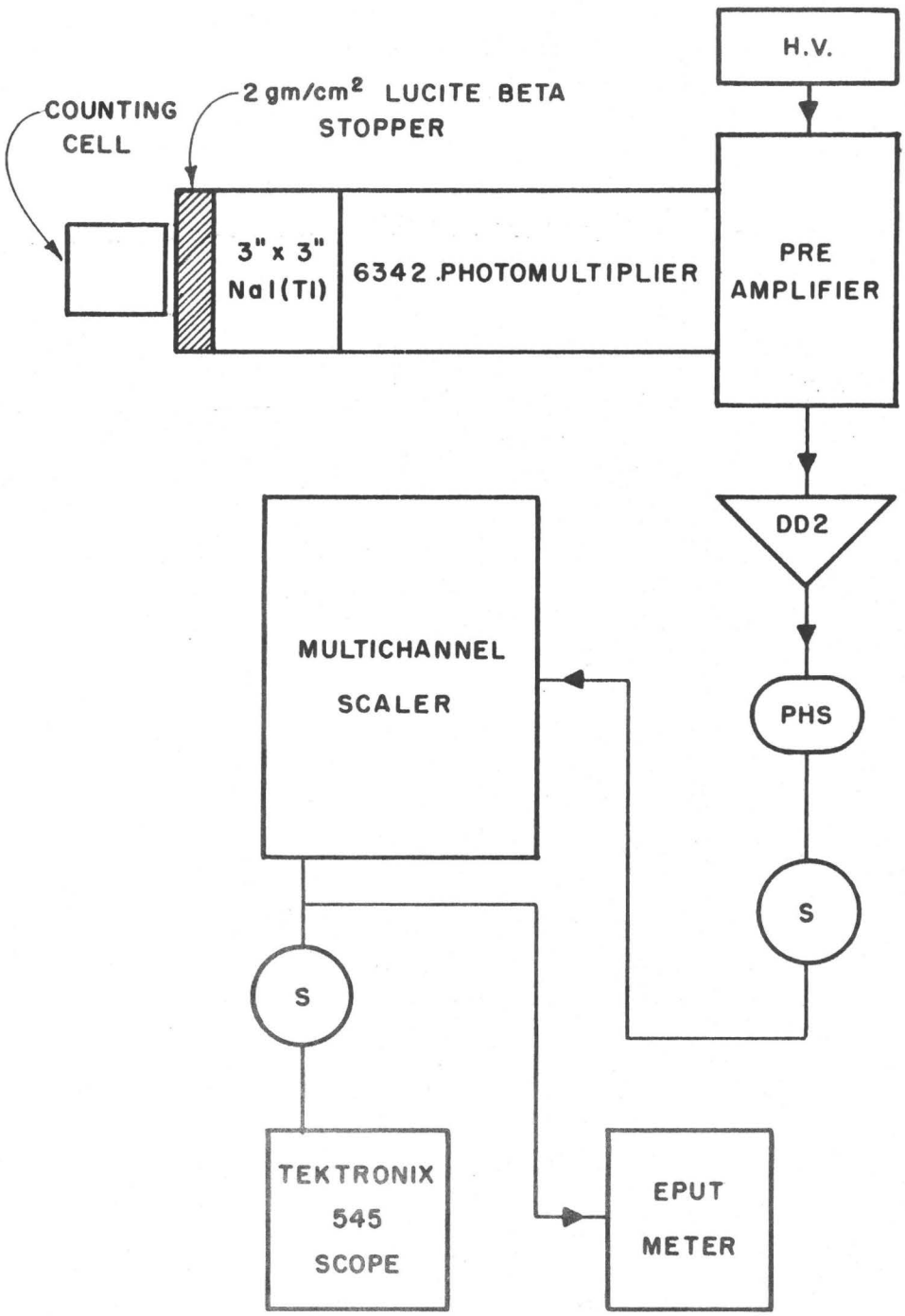
H.V.
COUNTING CELL
2 gm/cm² LUCITE BETA STOPPER
3" x 3" NaI(Tl)
6342 PHOTOMULTIPLIER
PRE AMPLIFIER
DD2
MULTICHANNEL SCALER
PHS
S
S
TEKTRONIX 545 SCOPE
EPUT METER

repeated until a minimum was found in the residual. This was taken as the best fit value for λ_1. The counting rate was initially about 8,000 counts per channel and after 1000 seconds it decreased to about 300 counts per channel.

The fitting process was not very satisfactory and there was not a marked dependance of the residual with λ_1. The values of B and C tended to be erratic and in general one or the other became negative for the best fit situation. While this is physically absurd, the situation is not surprising since λ_2 and λ_3 are near the same value. This may be seen if equation 3-1 is rewritten with $\lambda_3 = \lambda_2 + \Delta$, where Δ is the difference in the mean-lives of the two isotopes, Kr^{89} and Rb^{90}.

$$N(t) = \left\{ A - B\frac{\lambda_1}{\lambda_1 - \lambda_2} \right\} e^{-\lambda_1 t} + \left\{ B\frac{\lambda_1}{\lambda_1 - \lambda_2} + C \right\} e^{-\lambda_2 t} + e^{-\Delta t} + D \qquad (3\text{-}1b)$$

Thus if Δ is small, it is only at long times t, that the coefficients B and C can be evaluated. However for large values of t, the counting rate is low and there is a large statistical error in each point. The situation for Kr^{89} and Rb^{90} was such that no unique solution of 3-1 was possible and this is indicated by the negative values of either B or C. With this inherent problem of analyzing the data, it was felt that no reliable half-life measurement could be made with the present apparatus. The half-life of Kr^{90} was determined to be 33 seconds with an error of about 2 seconds, but this error is difficult to estimate.

C) The Gamma Rays of Kr^{90}

The gamma-ray spectrum was studied with NaI(Tl) detectors of dimensions 3" x 3" and 2" x 2". The latter was chiefly useful for the coincidence measurements, and the former was used to establish the intensities and energies of the gamma transitions in the decay. The experimental arrangement for the 3" x 3" crystal is shown in Fig. 11.

Figure 11

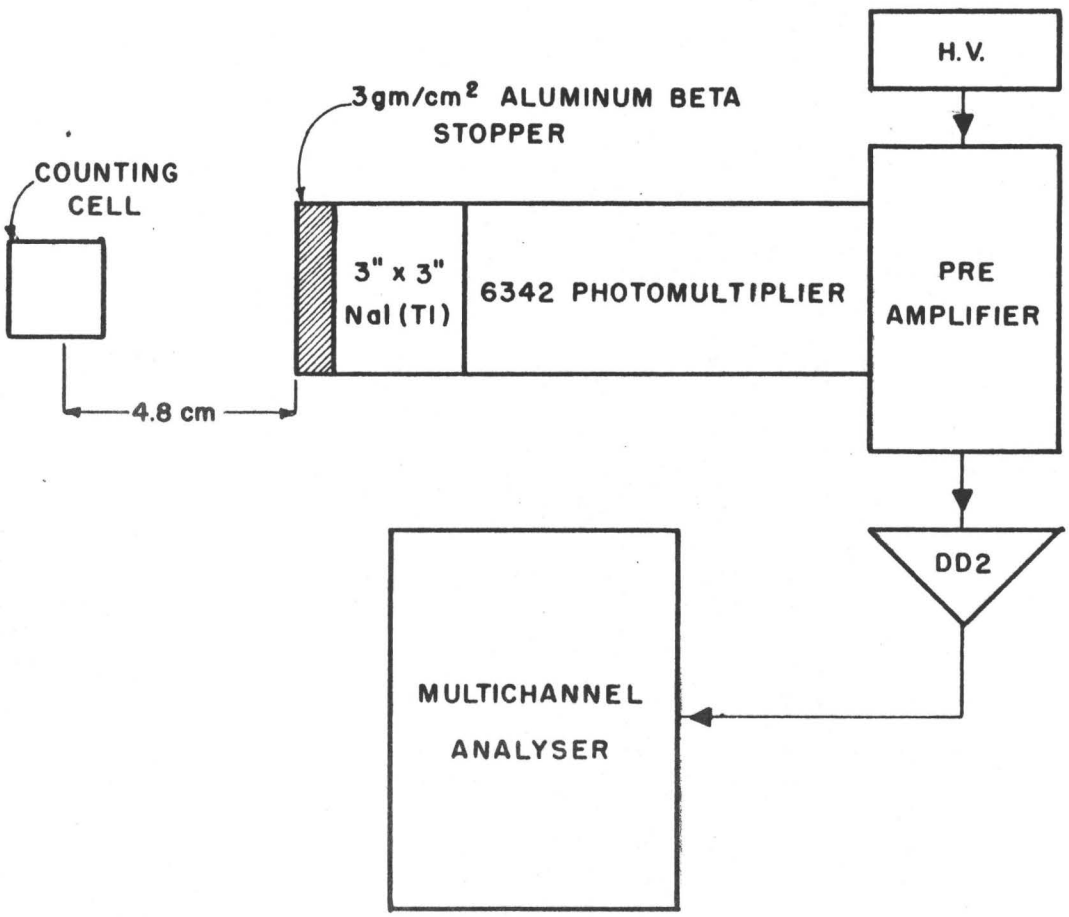
H.V.
3gm/cm² ALUMINUM BETA STOPPER
COUNTING CELL
3" x 3" NaI (Tl)
6342 PHOTOMULTIPLIER
PRE AMPLIFIER
4.8 cm
DD2
MULTICHANNEL ANALYSER

The gas chromatograph allowed only krypton isotopes to reach the counting chamber, and the half-lives of those produced in fission were Kr^{88} (10,000 sec.) Kr^{89}, (192 sec.), Kr^{90} (33 sec.) and Kr^{91} (10 sec.). Thus, by choosing a suitable irradiation procedure, one could effectively eliminate all but the 192-second Kr^{89} from the Kr^{90} samples. In addition to the Kr^{89} contaminant, there were also the contributions due to the Rb^{90} daughter, the reactor background and the Bremsstrahlung produced in the beta stopper, which was negligible.

The reactor background was small for the coincidence experiments; for single crystal measurements it could be simply removed by setting the multi-channel analyser to the subtract mode after the sample had been removed from in front of the detector.

The number of atoms decaying in a sample of isotope of mean life λ^{-1}, produced by an irradiation of R seconds, held before counting for C seconds, and then counted for t seconds is given by

$$N = P(1 - e^{-\lambda R}) e^{-\lambda C} (1 - e^{-\lambda t}) \qquad (3\text{-}2)$$

where P is the production rate and depends on the cross-section for production, the neutron flux, the number of atoms in the U^{235} target and the efficiency of the delivery system. It was constant for any given experimental situation.

In order to determine experimentally the contribution of Kr^{89} in the Kr^{90} samples, sources were alternately studied with the operating sequences 4-20-30 and 4-200-60. Such operating sequences should both contain the same

amount of Kr^{89} activity. The latter are essentially pure Kr^{89} while the former are mainly Kr^{90}. Since sample sizes were not very reproducible, it was necessary to average the results of many pairs of sources to obtain a reliable Kr^{89}/Kr^{90} ratio for the operating sequence used. After this ratio had been measured, it was possible to correct for the Kr^{89} contribution in the Kr^{90} samples, by taking a Kr^{89} spectrum, normalizing it to the appropriate value, and then subtracting it, point by point, from the Kr^{90} spectrum.

The contribution of the 162-second Rb^{90} daughter to the Kr^{90} samples depended only on the sample counting time and the half-lives of the parent and daughter. The number of Kr^{90} atoms decaying in a t-second counting interval is

$$K(t) = K^{o} \left(1 - e^{-\lambda_K t}\right) \tag{3-3}$$

and for the same period, the number of Rb^{90} atoms decaying is

$$R(t) = K^{o}\left[1 - e^{-\lambda_K t} - \frac{\lambda_K}{\lambda_K - \lambda_R}\left\{e^{-\lambda_R t} - e^{-\lambda_K t}\right\}\right] \tag{3-4}$$

where the subscripts refer to Kr^{90} (K) and Rb^{90} (R) respectively, and K^{o} is the number of Kr^{90} atoms present at the beginning of the counting interval, immediately after the krypton activities have been separated from the others by gas chromatography. For the standard 4-20-30 sequence R(30)/K(30) equalled 0.083. However, this was not the ratio of the gamma activities, because the Kr^{90} and Rb^{90} decay schemes are not the same. Since Rb^{90} is a solid, which adheres to the walls of the counting chamber, the Kr^{89} and Kr^{90} activities could be removed from the cell, by flushing with helium

immediately after the 30-second counting period, to leave an essentially pure Rb^{90} sample behind. (Most of the active deposits of the other krypton isotopes would either have been removed by the gas chromatograph or would not have yet had time to grow into the sample.) By counting the Rb^{90} sample for 162 seconds, immediately following the flushing operation, one would expect to obtain 5.46 times as many Rb^{90} decays as were in the original Kr^{90} sample. With the use of the Rb^{90} spectrum obtained in this manner and the normalization factor given above, it was possible, in principle, to correct the Kr^{90} spectrum for Rb^{90}.

In practice, the procedure outlined above always gave too small a correction for the Rb^{90} activity, because some of the active deposit was carried away in the flushing procedure. However, it was found that the spectra from the Kr^{90} and Rb^{90} samples were identical above 4.1 MeV, (the very small Kr^{89} contribution in this region had been previously subtracted) and so one could use this fact to subtract the appropriate contamination over the entire spectrum. This procedure could not be followed for the coincidence experiments and was replaced by a more involved method which will be discussed later.

The spectrum of Kr^{90}, as observed in a typical experiment, (see experiment C below) is shown in Fig. 12. After appropriate corrections for the Kr^{89} (lower solid curve) and Rb^{90} (dotted curve) contaminations had been subtracted, the spectrum was analysed using a library of standard line profiles and the stripping procedure previously described. The standard line shapes were obtained with the same beta stopper and the same source-

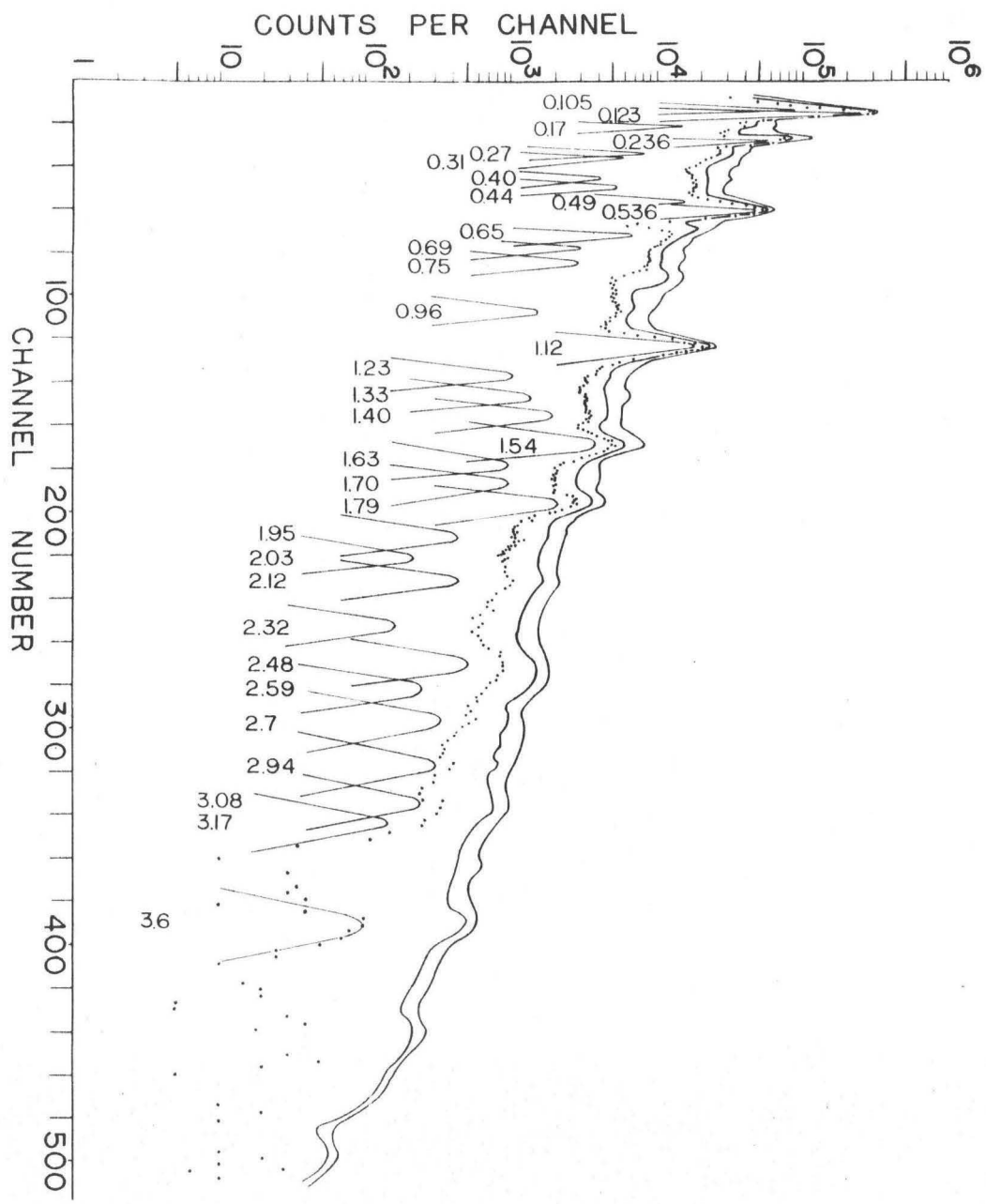
COUNTS PER CHANNEL
1
10
10²
10³
10⁴
10⁵
10⁶
CHANNEL NUMBER
100
200
300
400
500
0.105
0.123
0.17
0.236
0.31
0.27
0.40
0.44
0.49
0.536
0.65
0.69
0.75
0.96
1.12
1.23
1.33
1.40
1.54
1.63
1.70
1.79
1.95
2.03
2.12
2.32
2.48
2.59
2.7
2.94
3.08
3.17
3.6

Figure 12

detector distance as were used for the Kr^{90} sources. The standards used, were all essentially point sources, while the Kr^{90} samples occupied a volume of about 4 cc. Such Kr^{90} sources gave the same quality of spectra as those obtained by trapping the krypton on a speck of activated charcoal, cooled to liquid air temperature. These cooled sources were used in some of the preliminary gamma-ray work, but were abandoned because of the fact that they were inconvenient to use, and they were useless for beta-ray experiments.

Table I presents the results of the analysis of two different Kr^{90} spectra. The data for experiment A were obtained using a 3" x 3" NaI(Tl) detector with a resolution of 8% on the 0.661 MeV line of Cs^{137}. The source-crystal distance was 2.8 cm, and 1.46 gms/cm^2 of aluminum were used as a beta stopper. The three most prominent photopeaks of the spectrum (0.120, 0.536 and 1.12 MeV) were used as internal energy calibrations. These energies had been measured in preliminary experiments, in which a Kr^{90} source and standard sources were simultaneously viewed by the crystal. The standards, which were used to bracket the three Kr^{90} lines, were Ho^{166m}, In^{114}, Au^{198}, Cs^{137}, Mn^{54} and Na^{22}. The Rb^{90} and Kr^{89} contaminations were corrected for by counting the Kr^{90} sources for 30 seconds, allowing the activity to stay in the source chamber for a further 200 seconds, and then counting for 60 seconds. The activity recorded in the second counting period contained the same Kr^{89} activity, and considerably more Rb^{90} activity than that obtained in the 30-second period. In fact, the number of counts recorded in the spectrum beyond 3 MeV for the 60-second counting period was found to be 24% larger than in the 30-second period. The contamination correction

was then made by normalizing the 60-second spectrum to the 30-second spectrum beyond 3 MeV. This procedure undercorrects for Kr^{89}.

Columns B and C of Table I show the results of two independent analyses of the raw data using different corrections for the Kr^{89} and Rb^{90}. The sources were placed 4.8 cm from a Harshaw 3" x 3" NaI(Tl) crystal, integrally mounted on a 6363 photomultiplier, which was selected for stability of gain with counting rate changes (less than 1% gain shift for a factor of 20 changes in counting rate) and which had a resolution of 7.4% at 0.661 MeV. A 3 gm/cm^2 aluminum beta stopper was used. Experimentally it was found that the total Kr^{89} contribution to the Kr^{90} samples was $21 \pm 1\%$. Analyses B and C were made with Kr^{89} corrections of 11% and 21% respectively; a comparison of the two gives some indication of the sensitivity of the method to the amount of Kr^{89} present. In both analyses, the Rb^{90} correction was obtained by normalizing the spectra above 4 MeV in the manner already discussed.

There are inherent upper limits to the corrections that can be applied for either Rb^{90} or Kr^{89}. Too large a correction, for either isotope, will create negative peaks in the stripping process, at a position of the prominent contamination lines (0.836 MeV for Rb^{90} and 0.2 and 1.5 MeV for Kr^{89}). In analysis C, the Rb^{90} corrections exceeded this limit.

Evidence from Table I supports the predictions concerning the uncertainties in subtracting the contamination background. The intensities of the lines about 0.2 MeV in A and B are indicative of the presence of Kr^{89}

in the analysed spectra. Some of the weak lines in this region disappear in analysis C. An examination of the stripped spectra shows that the strong 0.836 MeV Rb^{90} transition is still present in A, while in C a slight negative peak appears in this region. Analysis C provides the most reliable approximation to the spectrum of Kr^{90} and ought to be weighted most heavily in assessing the data (except around 0.8 MeV).

It can be clearly seen from the table, that all three analyses give good agreement as to energy and intensity for the stronger peaks, but the values for the weaker peaks are very uncertain. The last two columns of Table I give the adopted values of the energies and intensities of all the lines. These are not simple averages of the three runs, but have been weighted by the experimenter in the light of considerations regarding contamination already discussed. Some of these factors are presented in the form of foot-notes.

The measurement of the energy and intensity of the 0.105 MeV line in Kr^{90}, was complicated by the fact, that a gamma ray of about this energy appeared when a 5-3-5 second time scale was used. This line had an intensity roughly equal to the intensity of the 0.12 MeV transition of Kr^{90} and it is believed that this gamma ray represents the most prominent transition in the decay of 10-sec Kr^{91}. No serious attempt to study this activity has been made up to the present.

TABLE I

ENERGIES AND INTENSITIES OF GAMMA-RAYS OF Kr^{90}

Energy (MeV)			Intensity			Adopted Values	
A	B	C	A	B	C	Energy(MeV)	Intensity
		0.105			30	0.105	30[a]
0.119[a]	0.120	0.120	164[a]	129	134	0.120	130
0.162	0.162	0.172	17	7.5	8.5	0.17	9[b]
	0.185[b]			4.7[b]		[b]	
0.214[b]			23				
0.239	0.236	0.236	50	29	36	0.236	32
0.264	0.264	0.288	15	8.6	7.2	0.27	6
0.317	0.298	0.311	13	9.2	5.5	0.31	6
0.381	0.401	0.396	11	5.7	5.3	0.40	6
0.423	0.436	0.436	11	8.6	7.7	0.44	8
0.501	0.495	0.495	16	25	26	0.50	25
0.536	0.542	0.537	98	98	98	0.536	98[c]
0.620	0.630	0.649	12.5	14.4	16	0.64	16[d]
0.678	0.662	.....	6.1	11.5	.....	[e]	
.....	.....	0.692			9.2		
0.726	0.718	.....	10.8	9.2	.....	0.72[f]	8[f]
0.782	0.760	0.754	7.0	7.3	9.1	0.77	6[f]
0.84	.....	.....	6.0	.....	.....	0.836 (Rb^{90})	
0.886	0.877	.....	8.5	3.5	.....	0.89[f]	4[f]
0.944	0.968	0.964	6.3	7.4	8.3	0.97[g]	8[g]
1.120	1.122	1.123	99.5	102	102	1.122	102[c]
.....	1.224	1.249	.....	7.4	6.3	[e]	
1.300[h]	1.323	1.1346	8.6	9.8	9.6	1.34[h]	10[h]
1.460	1.461	.....	10	11.4	.....	[i]	
1.545	1.541	1.540	37	35	33	1.54	35
1.635	1.618	1.64	8.6	9.8	9.6	1.63	9
1.70	1.69	1.71	9.5	12.8	10	1.7	10
1.792	1.783	1.795	19	25	23	1.79	23
1.95	1.93	1.94	3.5	5.1	5.0	1.94	5

(continued 66a)

2.06	2.00	2.05	3.0	2.4	2.6	2.03	2.5
2.14	2.12	2.12	4.5	4.7	5.7	2.12	5.7
2.28	2.29	2.32	2.2	1.6	2.3	2.3	2[j]
2.42	2.38	.....	2	2.6	.....	2.4	2[j]
2.48	2.49	2.48	8.0	8.2	8.8	2.48	8
2.60	2.57	2.59	2.4	5.8	4.4	2.58	4
2.69	2.69	2.72	4.0	6.2	5.7	2.70	6
2.80	2.80	.....	4.2	5.9	.....	2.8	4[j]
2.94	2.92	2.94	4.2	10	7.4	2.94	7
3.06	3.10	3.08	5.1	9.3	5.5	3.08	5
3.18	k	3.17	2.5	k	3.0	3.17	3
k	k	3.60	k	k	2.7	3.6	3

Footnotes

a) The high intensity of the 0.119 MeV peak in A is due to a contribution from the 0.105 MeV radiation, since these two could not be resolved.

b) The intense Kr^{89} spectrum in the 0.2 MeV region makes the search for weak peaks in Kr^{90} very difficult. The 0.17 MeV transition is the only one that has sufficient intensity to be identifiable with Kr^{90}.

c) The mean intensity of the 0.536 and 1.122 MeV lines has been used for normalization.

d) The intensity and energy of this peak are difficult to determine because of a strong Kr^{89} peak at 0.595 MeV.

e) These peaks are attributed to summing with the 0.12 MeV radiation.

f) Measurements in this entire region are confused by the strong 0.836 MeV radiation in Rb^{90}.

g) The intensity of these peaks is very sensitive to the shape of the 1.122 MeV profile.

h) The A^{41} gamma-ray at 1.29 MeV is the most prominent feature of the reactor background. Errors in subtracting this background may make the energy and intensity of this line somewhat less certain than the analysis would indicate.

i) The 1.46 MeV peak is in Kr^{89} and probably not in Kr^{90}.

j) The existence of these three lines is in doubt.

k) Analysis not performed for these energies.

D) The Gamma-Gamma Coincidence Experiments

The gamma-gamma coincidence experiments were carried out with a fast-slow coincidence circuit using, as detectors, two 2" x 2" NaI(Tl) crystals coupled to 56AVP photomultipliers. A block diagram of the electronics is shown in Fig. 13. Output pulses from each detector were limited, and then applied to the two control grids of a 6BN6 tube. The integrated anode current of this tube was proportional to the degree of overlap of the two limited pulses and thus the circuit functioned as a time-to-amplitude converter, (Green and Bell, 1958). The output of the time-to-amplitude converter was amplified and this pulse was passed into a pulse height selector circuit (PHS). This circuit was used to select that portion of the time spectrum which would be used to determine the coincidence condition. The output of this PHS (T) was shaped, and applied to the routing circuit to be described later. A pulse from the time channel pulse height selector could be used to gate the coincidence circuit of the multi-channel analyser (MCA) if desired. If this was done, then the only events from detector A that were analysed were those in coincidence with some other gamma ray detected in B. We shall use the term "pseudo singles" in referring to these events. This auxiliary gating circuit could be used to greatly reduce the dead time of the analyser, and permitted a much more efficient use of the short-lived sources.

Pulses from the tenth dynode of each photomultiplier were fed into double delay line amplifiers (DD2). The output of channel A (the analysing channel) was fed directly into the input of the MCA. The output of the

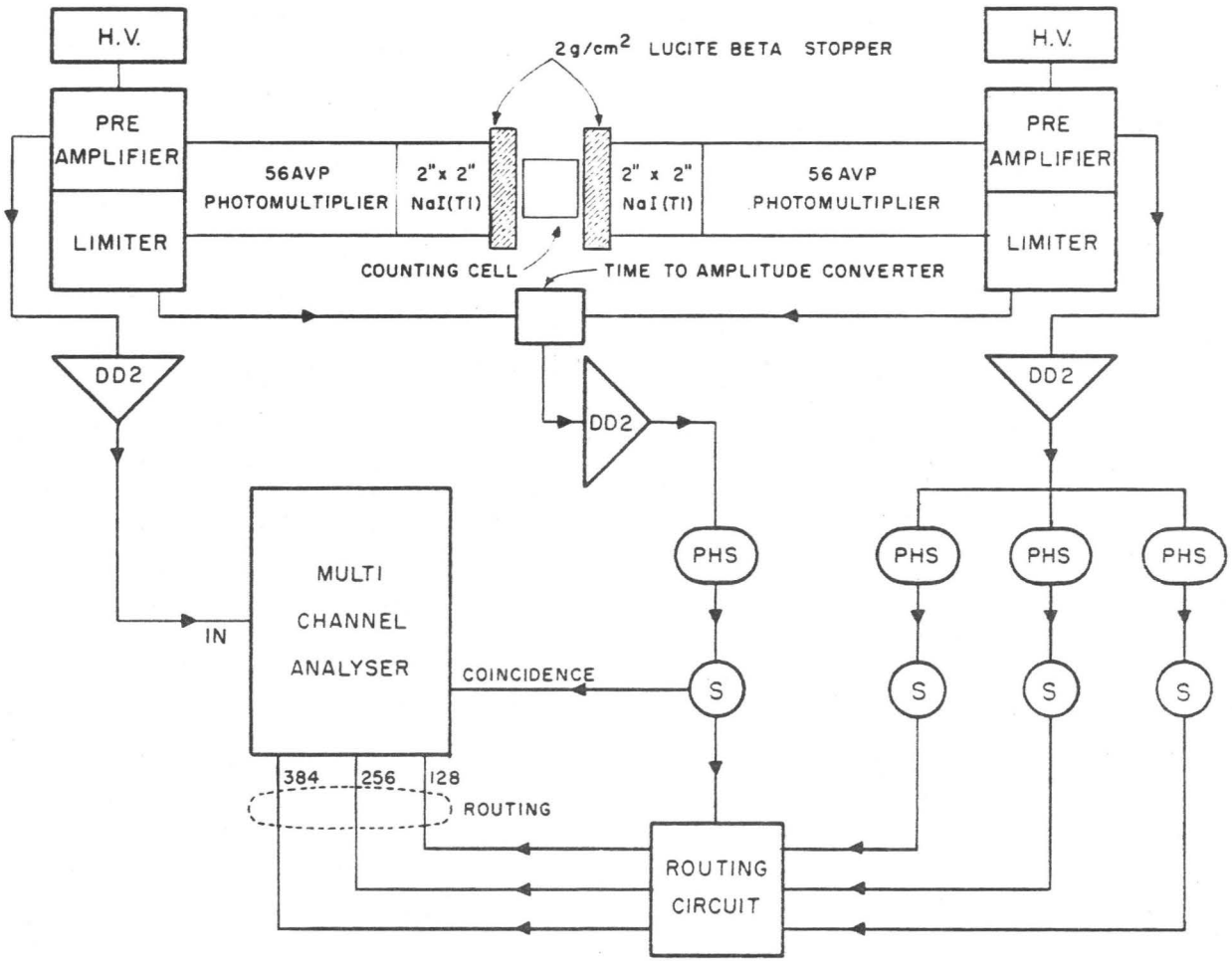
H.V.
2g/cm² LUCITE BETA STOPPER
H.V.
PRE AMPLIFIER
56AVP PHOTOMULTIPLIER
2" x 2" NaI(Tl)
2" x 2" NaI(Tl)
56 AVP PHOTOMULTIPLIER
PRE AMPLIFIER
LIMITER
COUNTING CELL
TIME TO AMPLITUDE CONVERTER
LIMITER
DD2
DD2
DD2
PHS
PHS
PHS
PHS
MULTI CHANNEL ANALYSER
IN
COINCIDENCE
S
S
S
S
384
256
128
ROUTING
ROUTING CIRCUIT

Figure 13

channel B amplifier (the gating channel) was fed into the inputs of three pulse height selectors, which were used to select three portions of the gating spectrum. The outputs of the three PHS (1, 2, 3) were shaped and applied to the routing circuit. The routing circuit consisted of three two-input AND gates whose output after being shaped was fed into a low impedance driving circuit. The AND gate inputs T and 1, T and 2 and T and 3 lead to three output circuits, which were connected to the three routing jacks of the MCA: T and 1 to 128, T and 2 to 256 and T and 3 to 384. The 512 channel analyser was thus converted into a 4 x 128 channel unit, the first quadrant of which stored either "singles" or "pseudo singles" and the other quadrants stored events coincident with pulses selected by the three pulse height selectors.

The relationship between the "singles" spectrum and the "pseudo singles" is dependent on the nature of the decay scheme. A gamma transition to the ground state, from a level which is fed only by direct beta decay, would not appear in the "pseudo singles", while the intensities of those gamma rays, which do appear, are related to the strength of the cascades to which they belong. Since the "pseudo singles" spectrum was independent of the gating channel, it could be used to normalize between different experiments. This normalization could also have been determined by connecting a scaler to either side channel; however, it was found that the "pseudo singles" spectrum for these isotopes with their high-Q values were very similar to the "singles" spectrum up to an energy of about 1.5 MeV.

Thus the "pseudo singles" could be used to monitor the behaviour of the whole coincidence circuit and still maintain the live time of the MCA at a value close to 100%. The live time would have been about 50% had the true "singles" been recorded in the first quadrant.

In order to measure the portions of channel B, selected by the three PHS units, for the short half-life Kr^{90} sources, it was necessary to use the MCA as shown in Fig. 14. Two outputs from the same detector were fed into two different amplifiers, A and B. The output of A was fed into the MCA, while the output of B was fed into the three PHS units. The shaped outputs of the PHS were applied to the routing jacks of the MCA, and thus any event which passed through a given PHS was transferred from the first quadrant into the one corresponding to that of PHS. The oscilloscope display of the gamma spectrum in the first quadrant showed gaps corresponding to the gates; these gaps appeared as spikes in the other three quadrants. A plot of a typical gating spectrum is shown in Fig. 15. The solid points represent the "singles less gates" spectrum while the addition of the counts stored in the gate channel to this spectrum yields the "singles" spectrum, shown by the open circles. This method of setting up the gates made it very easy to adjust the gating channel for the experiments with short half-lives.

The time-to-amplitude converter was aligned by using a Sc^{46} or Co^{60} source, and observing its output spectrum with the MCA. The PHS of the time channel was then set to include most of the observed coincidence

Figure 14

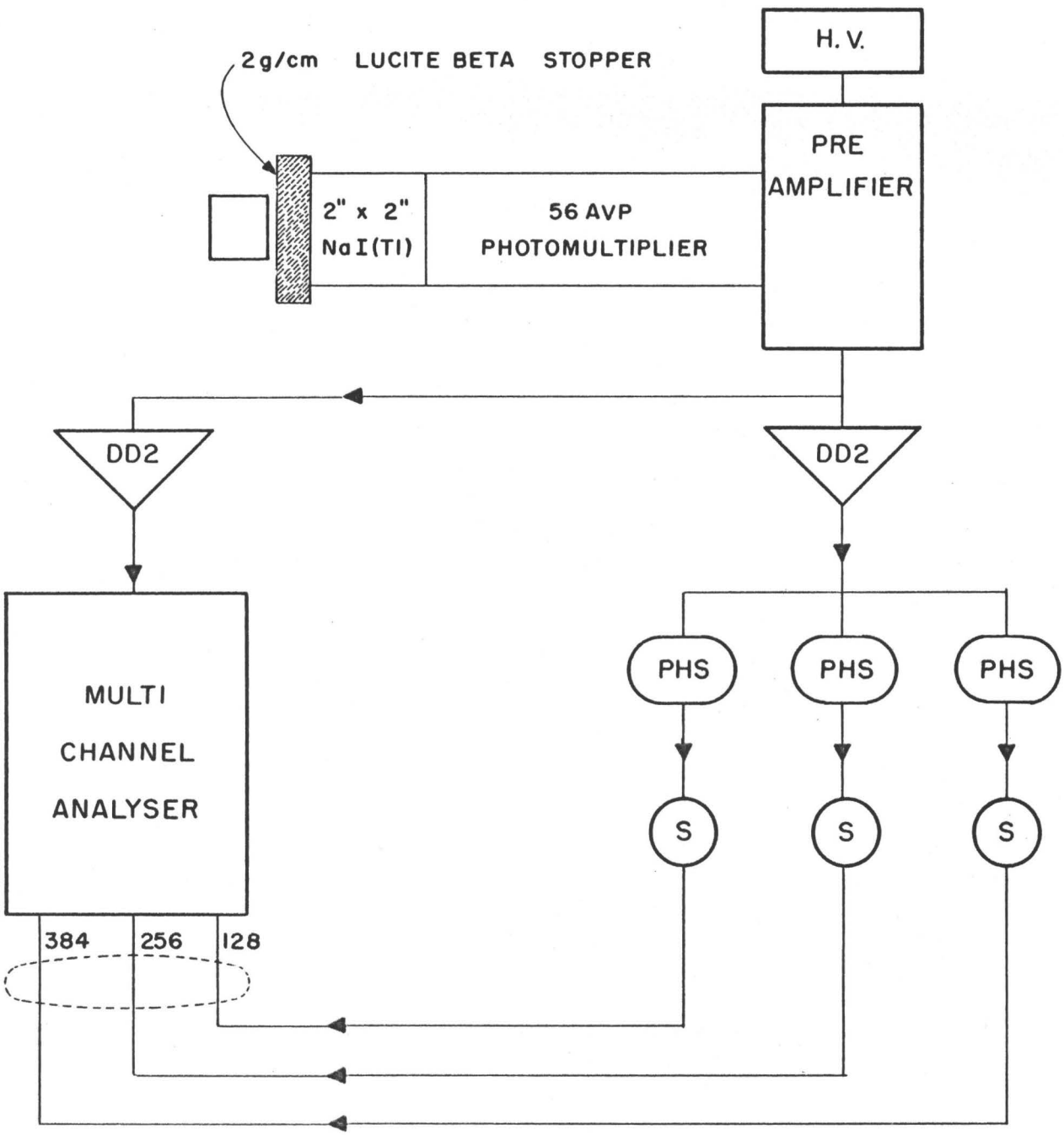
2g/cm LUCITE BETA STOPPER
H. V.
PRE AMPLIFIER
2" x 2" NaI(Tl)
56 AVP PHOTOMULTIPLIER
DD2
DD2
MULTI CHANNEL ANALYSER
PHS
PHS
PHS
S
S
S
384
256
128

Figure 15

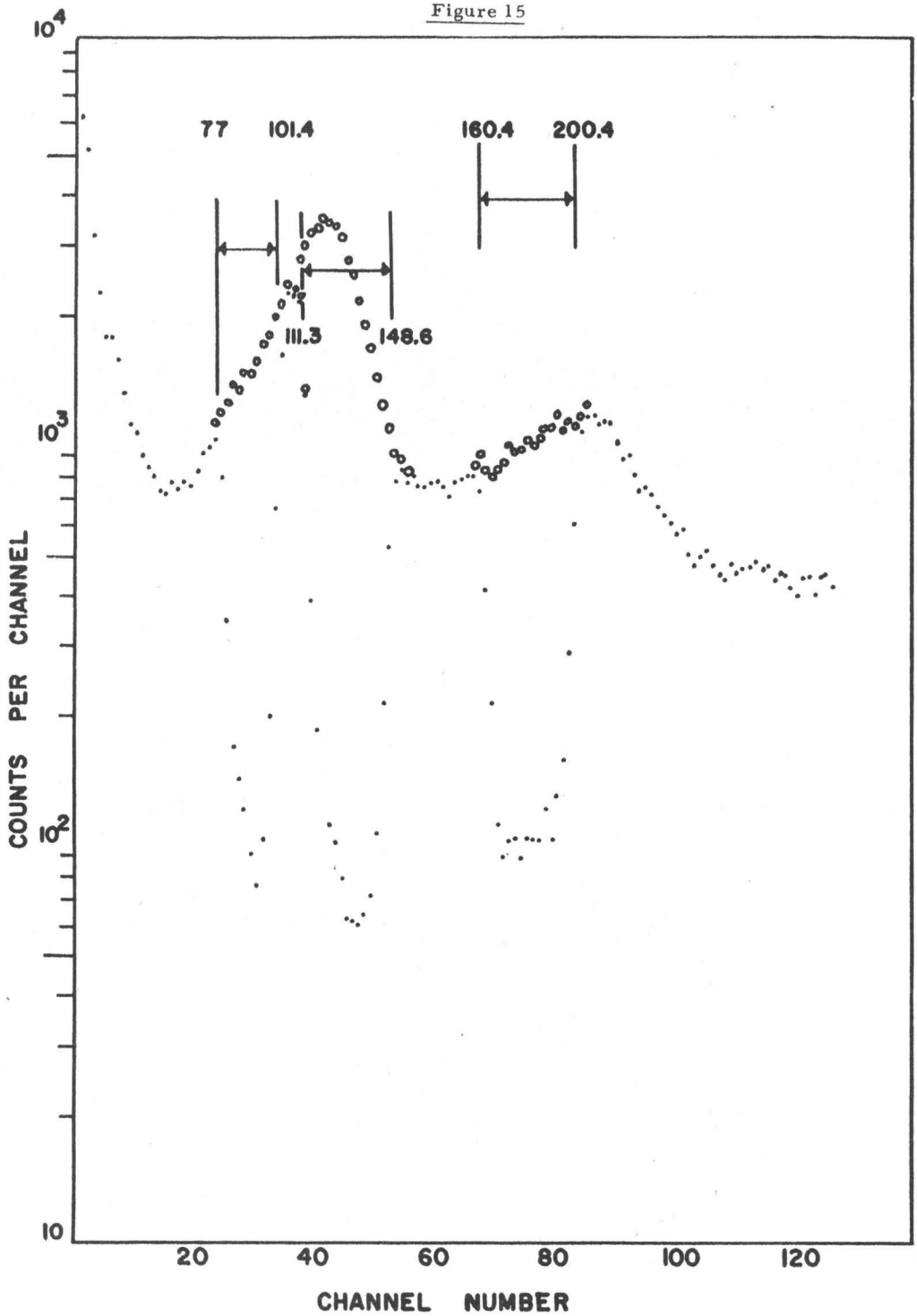
77
101.4
160.4
200.4
111.3
148.6
COUNTS PER CHANNEL
CHANNEL NUMBER
10
10²
10³
10⁴
20
40
60
80
100
120

peak. Since the width of this peak was dependent on the energy being detected, the same setting of the PHS could not be used for all experiments. The width of this peak for coincidences between photopeaks in the 1 MeV region was about 5 ns. Above 0.3 MeV, the position and width of the peak was relatively insensitive to the gating energy, whereas below this energy, the position of the window of the PHS had to be lowered and broadened to maintain the coincidence efficiency (e_{12}) of the circuit. The variation of e_{12} with energy was determined for the conditions of the experiments, by using a source of Co^{60}, setting the gate from 0.2 to 0.3 MeV, and recording the coincidence spectrum. The ratio of the counts in each channel of this spectrum to the corresponding counts in the "singles" spectrum, taken under the same conditions, was proportional to the coincidence efficiency at that channel. It was found that e_{12} remained constant above 0.15 MeV, and dropped sharply to a quarter of this value at an energy of 0.090 MeV. To establish the value of e_{12} for energies around 1 MeV a comparison was made between the coincidence and single channel rates of a calibrated Co^{60} source, when the gating channel was set on the 1.3 MeV photopeak. The measured coincidence efficiency was 100% at these energies and decreased to about 75% at 0.12 MeV. It would have been preferrable to maintain the full efficiency to a lower energy,

but the properties of the 56 AVP photomultiplier made this undesirable[1].

With the gates set on three prominent photopeaks in the Kr^{90} spectrum, twenty to fifty sources of Kr^{90} (about 70 microcuries each) were accumulated, to give a statistically significant coincidence spectrum. Spectra of Kr^{89} and Rb^{90} were obtained for the same gates. After normalization of the two contaminating spectra, they were subtracted from the coincident spectra obtained with Kr^{90} sources. The normalization procedure adopted for the Kr^{89} contaminant was the same as for the "singles" case previously discussed. The procedure for Rb^{90} had to be modified, because essentially no "pseudo singles" were observed at gamma energies greater than 3 MeV.

It is known that, in the decay of Rb^{90} (Johnson et al, 1958), there are a large number of gamma rays of energies greater than 3 MeV in coincidence with the 0.836 MeV transition from the first excited state to the ground state. This transition showed very strongly in the Rb^{90} spectra, in coincidence with the 3.08 MeV gate, and was also present in the Kr^{90}

---

1) As the voltage on the 56 AVP was increased, a region of non-linear response appeared at high photon energies. The break in the linear region moved down to about 0.4 MeV, if the high voltage was increased to the 1950 volts required for 100% coincidence efficiency at 0.1 MeV. The cause of this effect was not known, but it was sufficiently serious to render the analysis of the data very uncertain.

spectrum coincident with the same gate. Since, in the present work, the total decay energy of Kr^{90} was found to be only 4.5 MeV, it seemed unlikely that many of these coincidences could be due to this isotope. Therefore, all the 3.08-0.836 MeV coincidences were attributed to Rb^{90}, and this rate was used to establish in the Kr^{90} samples the fraction of the "pseudo singles" rate, which was due to Rb^{90}. After subtraction of the contributions from the two contaminants, the residual coincidence spectra were analysed by the stripping process using a library of line profiles obtained for the 2" x 2" crystals in the same geometry. Some allowance had to be made for the broadening of the Kr^{90} peaks, due to the shift of peak position with the changes in counting rate. Chance coincidences were recorded by inserting 80 ns of delay line in one of the fast channels. With the sources used for these experiments, the chance contribution was almost too small to be detected.

E) Analysis of Gamma-Gamma Coincidence Experiments

Figures 16 to 22 present the results of the coincidence experiments together with an analysis of the spectra. In each figure, the solid curve presents the uncorrected data and the dots show the spectrum, after the subtraction of the contaminants. The Gaussian peaks below this spectrum are the photopeaks resulting from the stripping process.

Figures 16 and 17 display the "pseudo singles" and the coincidence spectra, simultaneously recorded with the 1.79, 2.48 and 3.08 MeV gates. Because there were no prominent peaks in the Kr^{90} spectrum in this region,

the gates were established by using the 2.76 MeV gamma ray in Na^{24} for the two higher gates, and the 1.78 MeV transition in Al^{28} for the lower gate.

The 3.08 MeV gate extended from 2.92 to 3.30 MeV, and therefore included the entire photopeaks of the 3.08 and 3.17 MeV transitions, and half of that of the 2.94 MeV transition. The coincidence spectrum beyond channel 40, assumed to be due to Rb^{90}, was used for estimating the effect of this contamination for all coincidence runs. The Kr^{89} contribution in the gate was about 10% of the total in channels 8-10 and negligible elsewhere. The only prominent coincidence peaks in the Kr^{90} spectrum were those at 0.12 and 0.536 MeV.

The 2.48 MeV gate extended from 2.28 to 2.56 MeV. It included roughly 50% of the 2.48 MeV photopeak, and about as many counts from the spectrum of the gamma rays in the 3.08 MeV gate, as are in that gate itself. Therefore, the coincidence spectrum recorded, had to be corrected, by subtracting the spectrum associated with the 3.08 MeV gate, to obtain the true 2.48 MeV-gamma coincidence spectrum. The residue, resulting from this subtraction, was statistically zero and it was concluded that there were very few 2.48 MeV-gamma coincidences. This strongly indicated that the 2.48 MeV transition feeds the ground state.

The 1.79 MeV gate covered the energy range from 1.60 to 1.91 MeV. It included the entire photopeaks of the 1.63, 1.70 and 1.79 MeV transitions as well as 10% of the 1.54 MeV photopeak. The coincidences, due to the underlying background, arose from the gamma rays in the 3.08 MeV gate,

Figure 16

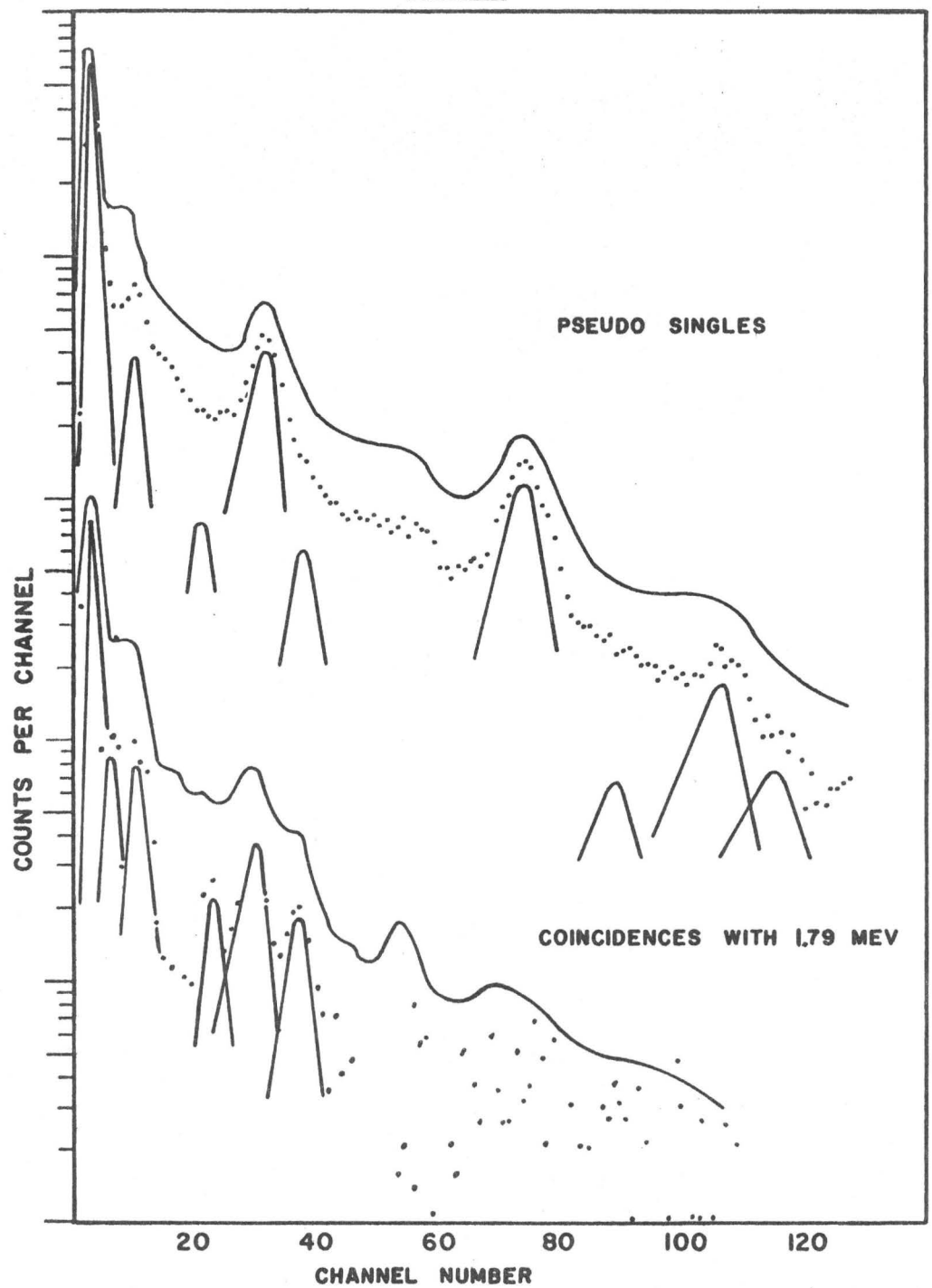
PSEUDO SINGLES
COINCIDENCES WITH 1.79 MEV
COUNTS PER CHANNEL
20
40
60
80
100
120
CHANNEL NUMBER

Figure 17

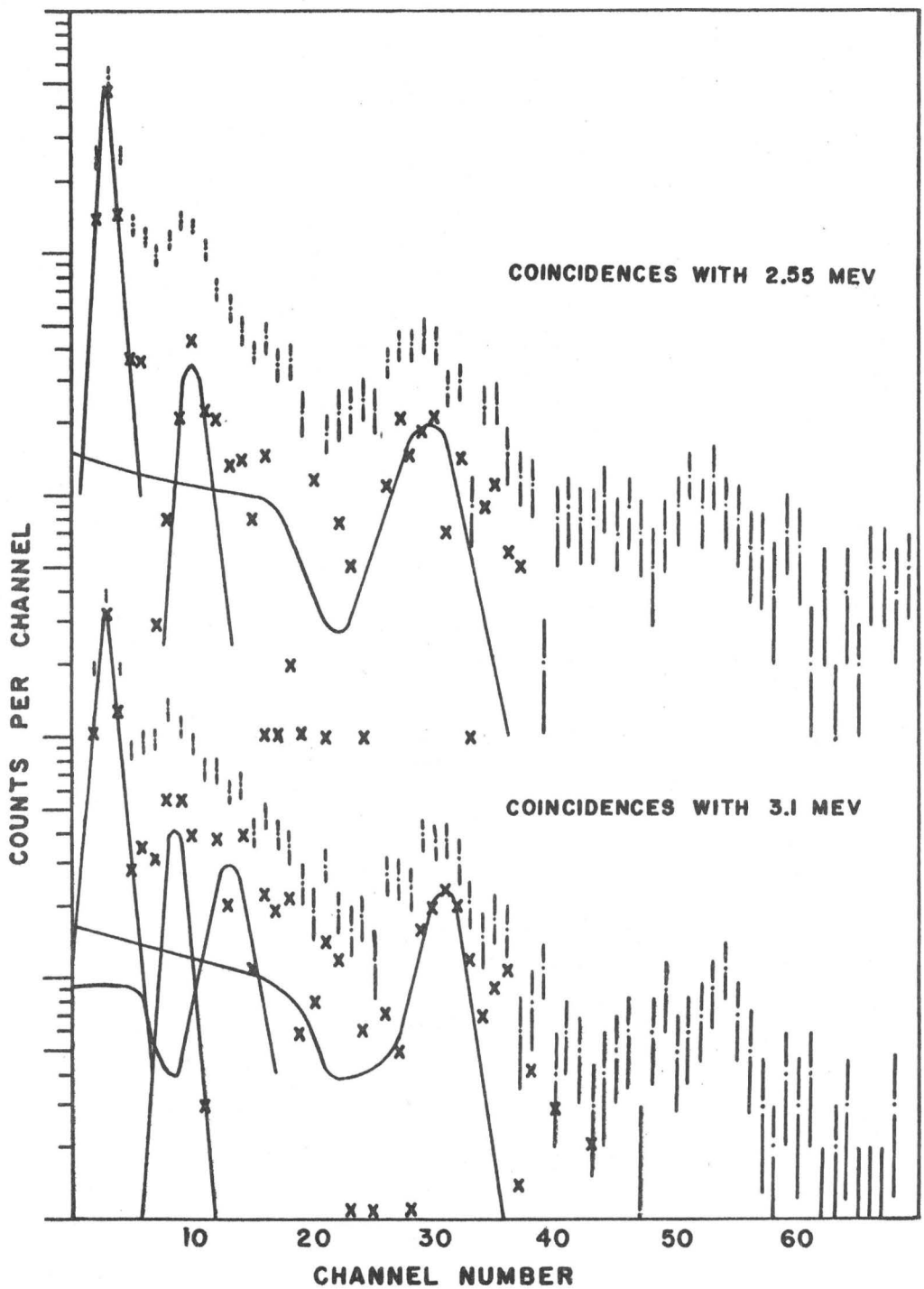
COINCIDENCES WITH 2.55 MEV
COINCIDENCES WITH 3.1 MEV
COUNTS PER CHANNEL
10
20
30
40
50
60
CHANNEL NUMBER

Figure 18

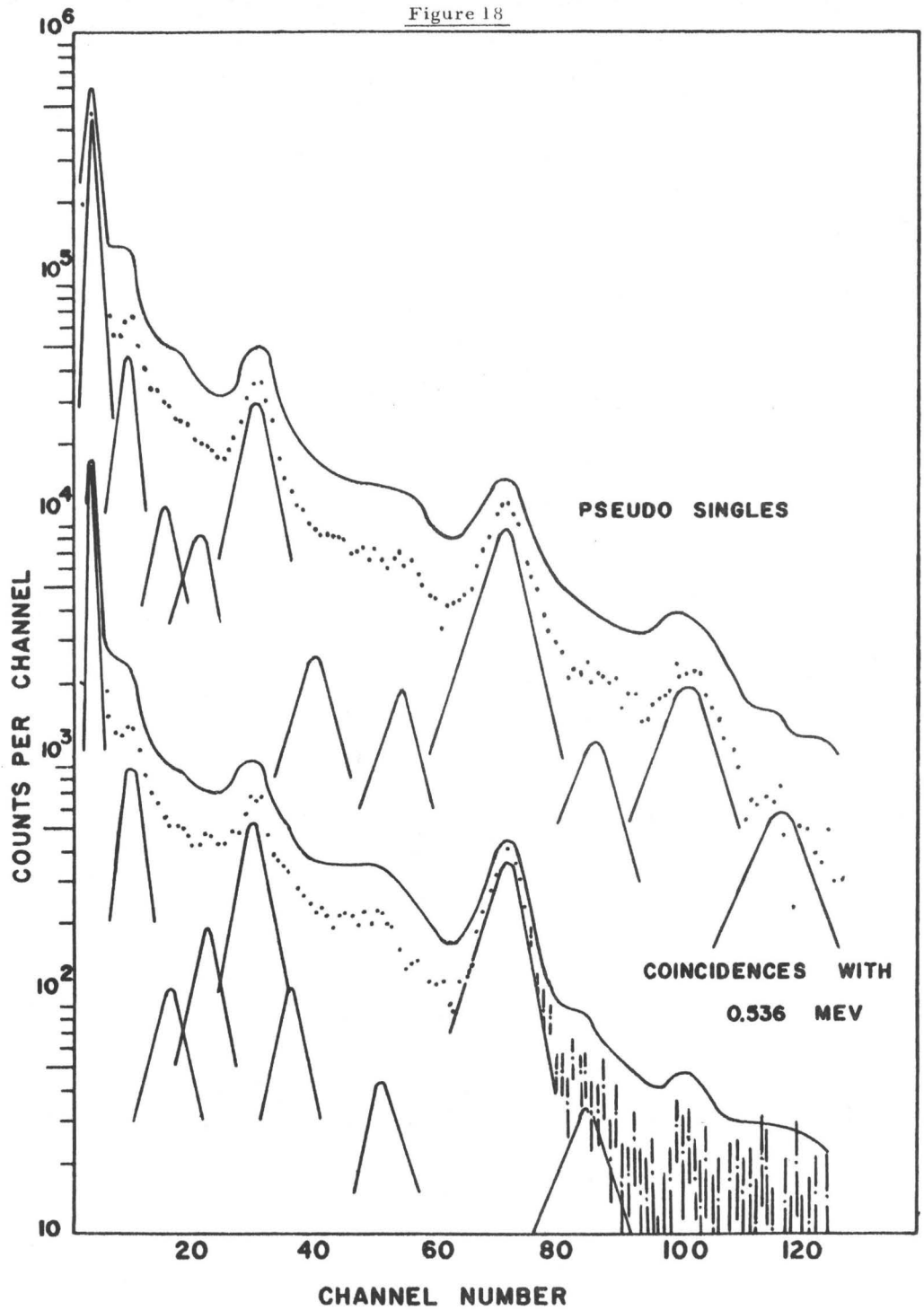
COUNTS PER CHANNEL
CHANNEL NUMBER
PSEUDO SINGLES
COINCIDENCES WITH
0.536 MEV
10
10²
10³
10⁴
10⁵
10⁶
20
40
60
80
100
120

Figure 19

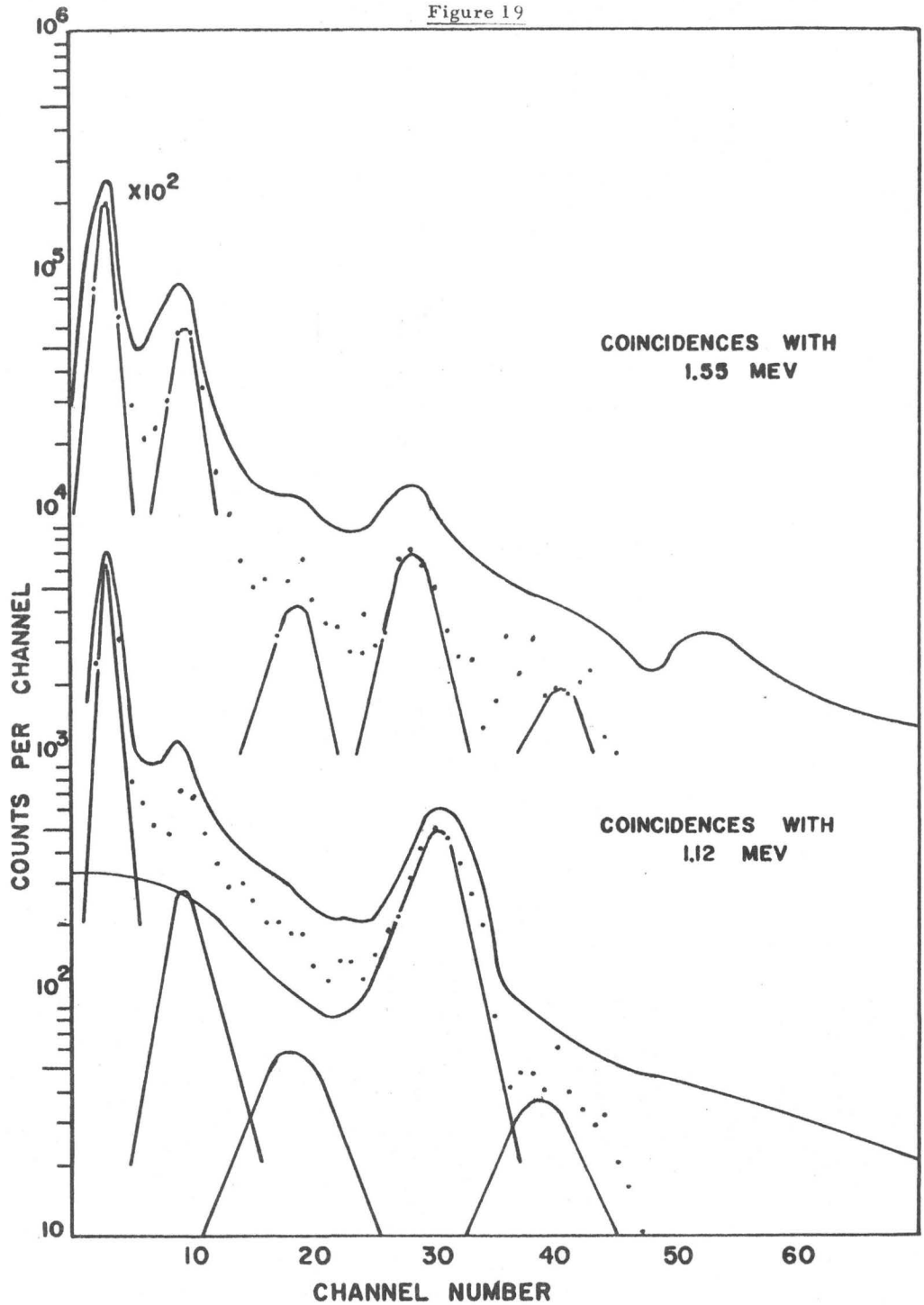
COUNTS PER CHANNEL
CHANNEL NUMBER
X10²
COINCIDENCES WITH
1.55 MEV
COINCIDENCES WITH
1.12 MEV
10⁶
10⁵
10⁴
10³
10²
10
10
20
30
40
50
60

Figure 20

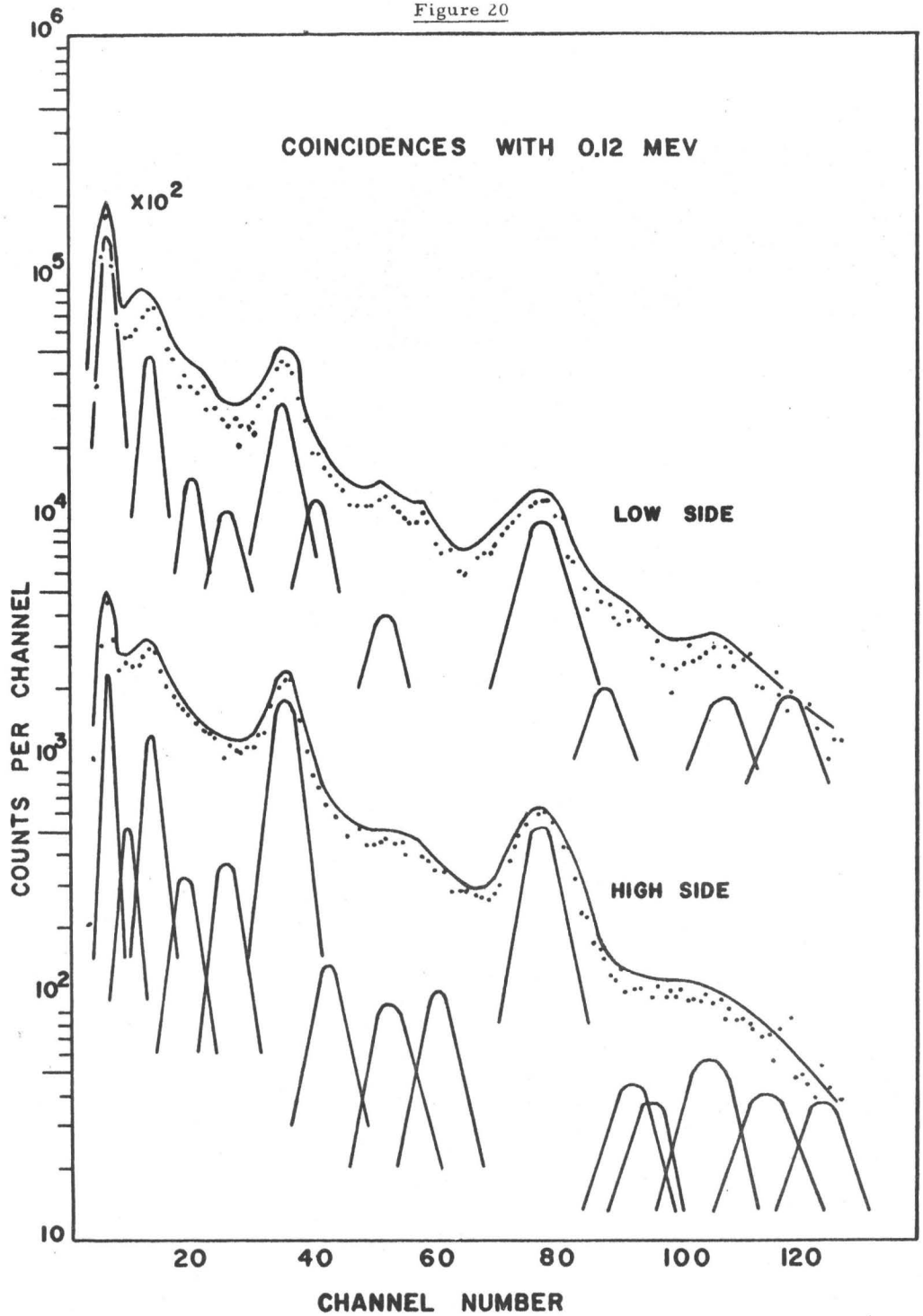
COINCIDENCES WITH 0.12 MEV
X10²
LOW SIDE
HIGH SIDE
COUNTS PER CHANNEL
CHANNEL NUMBER
10⁶
10⁵
10⁴
10³
10²
10
20
40
60
80
100
120

Figure 21

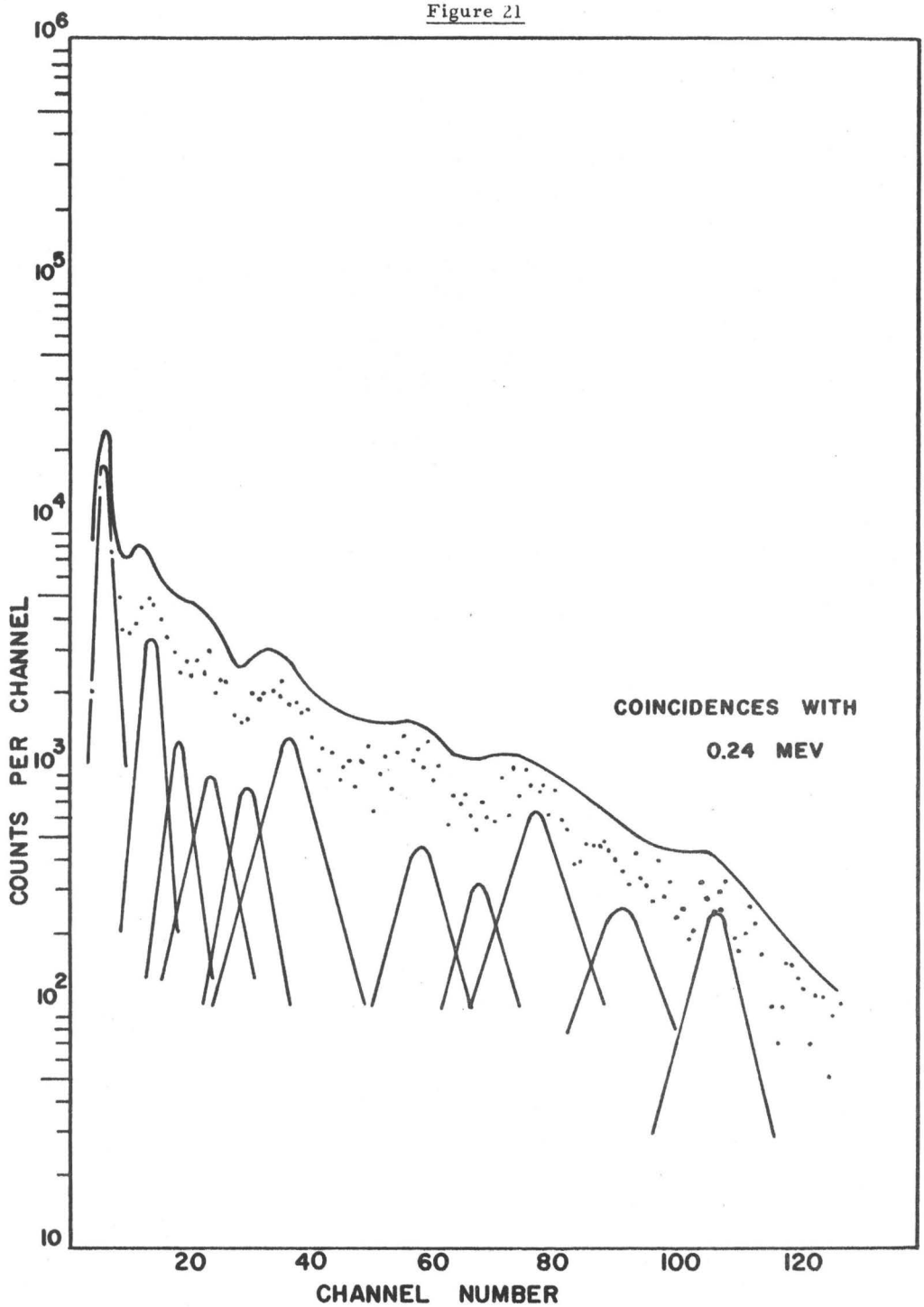
COUNTS PER CHANNEL
CHANNEL NUMBER
COINCIDENCES WITH
0.24 MEV
10
10²
10³
10⁴
10⁵
10⁶
20
40
60
80
100
120

Figure 22

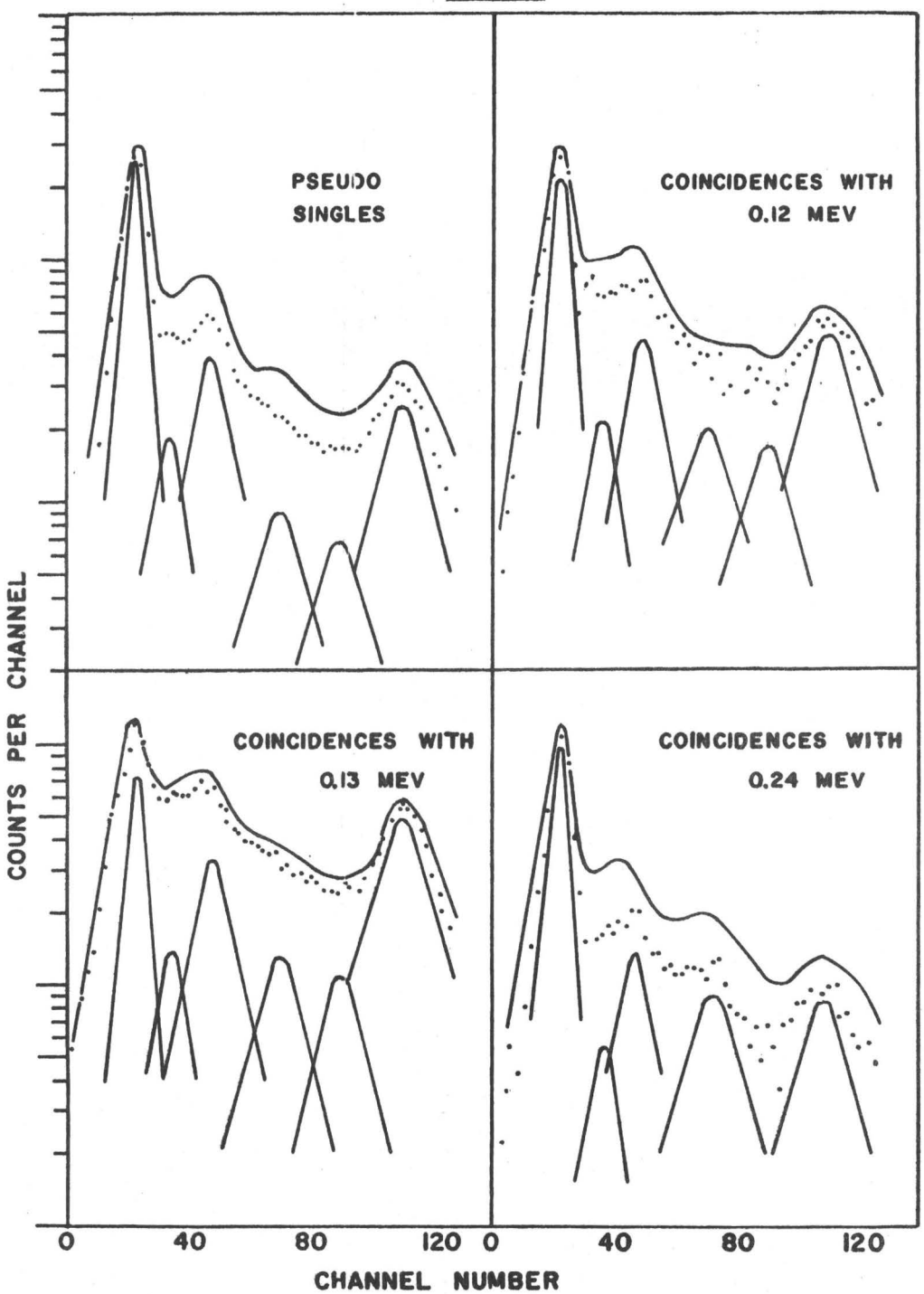
PSEUDO
SINGLES
COINCIDENCES WITH
0.12 MEV
COINCIDENCES WITH
0.13 MEV
COINCIDENCES WITH
0.24 MEV
COUNTS PER CHANNEL
0
40
80
120
0
40
80
120
CHANNEL NUMBER

and contributed 20% of the coincidence spectrum, associated with that gate, to the recorded 1.79 MeV-gamma coincidence spectrum. The most striking feature of this spectrum was the presence of a 0.50 MeV peak, which was 2 channels lower than the strong 0.536 MeV peak in the "pseudo singles" spectrum.

Figures 18 and 19 show the results of the experiments carried out with the 0.536, 1.12 and 1.54 MeV gates and the simultaneously recorded "pseudo singles" spectrum. These gates were set by using the Kr^{90} spectrum and covered the ranges of 0.478-0.690, 1.08-1.29 and 1.40-1.75 MeV respectively.

The 1.54 MeV gate somewhat overlapped the 1.79 MeV gate, and contained the equivalent of 108% of the 1.54, 30% of the 1.79 and 20% of the 1.33 MeV photopeaks, as well as a background of 20% of the gamma rays contributing to the 3.08 MeV gate. The spectrum again revealed a strong 0.50 MeV peak, as well as the two strong low energy peaks at 0.12 and 0.24 MeV.

The 1.12 MeV gate contained the equivalent of 70% of the 1.12, 25% of the 1.33, 70% of the 1.54 and 100% of the 1.79 MeV photopeaks. The background due to the 3 MeV complex was negligible. The coincidence spectrum showed very prominent peaks at 0.12, 0.24 and 0.536 MeV.

The 0.536 MeV gate included the equivalent of 75% of the 0.536, 50% of the 0.50, 58% of the 1.12, 55% of the 1.33, 65% of the 1.54 and 80% of the 1.79 MeV photopeaks. The coincidence spectrum was dominated by strong peaks at 0.12, 0.24 and 1.12 MeV. The apparent coincidences

of the 0.536 MeV peak with itself, were accounted for by coincidences with the underlying Compton of the 1.12 MeV transition, in the gate, and by coincidence between 0.50-0.536 MeV transitions.

Figures 20 to 22 show two sets of coincidence experiments with the 0.10, 0.12 and 0.24 MeV gates (see Fig. 15 for a detailed presentation of this gating spectrum). In the first experiment, (Figs. 20 and 21), the analysing channel was set to collect the spectrum to 1.8 MeV; in the second experiment, (Fig. 22), the gain was increased to show details of the spectrum to 0.6 MeV. The two lower energy gates were designed to "split" the 0.12 MeV peak, and covered the energy regions from 0.077 to 0.101 and 0.111 to 0.148 MeV. The third gate extended from 0.160 to 0.200 MeV and was meant to cover the 0.236 MeV photopeak. This was a very difficult gate to set, as the "singles" spectrum in this region contained a prominent Kr^{89} peak at about 0.2 MeV. These narrow gates were all somewhat sensitive to gain shifts.

It was estimated, that the 0.24 MeV gate contained the equivalent of 33% of the 0.236, 7% of the 0.536, 6% of the 1.12, 7% of the 1.54 and 10% of the 1.79 MeV photopeaks. The coincidence spectrum was quite complex and appeared to contain most of the peaks of the "pseudo singles" spectrum. The only prominent feature was the 0.12 MeV photopeak, which was stronger with this gate than it was in the "pseudo singles" spectrum. The two experiments with different gains agreed very well in the regions of overlap.

The 0.12 MeV gate contained the equivalent of 70% of the 0.12 MeV photopeak and roughly 3% of each of the 0.536, 1.12, 1.33, 1.54 and 1.79 MeV

photopeaks. The coincidences from photopeaks with energies greater than 1.79 MeV, made a negligible contribution to the coincidence spectrum. This spectrum was again very complex, containing all the lines of the "pseudo singles" spectrum.

The 0.10 MeV gate contained the equivalent of about 50% of the 0.105 MeV photopeak, 25% of the 0.12 and about 1.5% of each of the 0.536 MeV and higher energy photopeaks. The coincidence spectrum was again very complex and was similar to that obtained with the 0.12 MeV gate, except for the strong enhancement of the 0.12 MeV contribution.

All the coincidence experiments were normalized to the same number of total coincidence counts ("pseudo singles" plus coincidence spectra). The normalized areas and energies, resulting from the analysis, are presented in Table II. The left hand column of the table presents the energies of the more prominent Kr^{90} gamma rays, as found in the analysis of Table I. The headings, across the top of Table II, indicate the gates used, and the heavy vertical lines mark off the four experiments analysed. The number of counts ($\times 10^{-3}$), in the respective photopeaks, are recorded in columns below each gate. The number in parenthesis is the gamma energy determined in the coincidence experiments. The energy agreement for the stronger peaks is excellent, while for the weaker ones, the statistics are often poor and the energies vary considerably from run to run.

By applying the percentage figures, given for the content of each gate, the areas in Table II may be corrected for the contributions of the higher-energy gamma rays, and for the effective gate width, to give a

photopeak area which is associated with a single gamma ray or a group of unresolved gamma rays. These areas may be converted to relative coincidence probabilities by dividing each by the product $(YP)_1 (YP)_2 e_{12}$ as previously described. The values of YP were taken from Fig. 3a of Chapter II. The value of e_{12} was assumed to be unity for all transitions except for the 0.10 and 0.12 MeV radiations. For these, values of 0.75 and 0.40 MeV, respectively, were used on the basis of the experimental determination of e_{12} already described.

In order to compare these relative coincidence probabilities with the gamma-ray intensity scale of Table I, it was convenient to normalize the 0.536-1.12 MeV value to 100. The results of these procedures led to the normalized f_{ij} values tabulated in Table III. Each value includes an estimate of uncertainty, based on an examination of the corresponding peak in the stripped spectrum and an evaluation of the errors introduced by the subtraction of the underlying Compton. There was no allowance made for systematic errors, caused by uncertainties in the values of YP or e_{12}, or in the analysis of the gate widths and positions. The bracketed numbers, following each f_{ij} value, indicate the energies found in the analysis.

In such a coincidence matrix, one would expect to find $f_{ij} = f_{ji}$. This appeared to be true within the limits of error, except for the runs involving the 0.10 and 0.12 MeV gates. For these, the numbers appeared to be roughly half of the values given by the complimentary experiment. This suggested that either the coincidence efficiency for these low energy gates was overestimated, or that drifts occurred in these narrow gating

channels which were significant. Because of these possibilities, one ought not to take too seriously the f_{ij} values in the four columns involving the 0.10 and 0.12 MeV gates. The situation was further complicated by the fact that both the 0.10 and 0.12 MeV gamma rays were partially included in each gate. In spite of these difficulties, it was clear that the pulses in the 0.10 MeV gate were much more strongly in coincidence with the 0.12 MeV gamma ray than those in the 0.12 MeV gate. The reverse was true for both the 0.536 and 1.12 MeV transitions. This indicated, that there are indeed two low energy radiations in this decay, and that the higher energy of these is in coincidence with both the 0.536 and 1.12 MeV transitions while the lower one is not. The lower energy gamma ray appeared in strong coincidence with the 0.12 MeV radiation, and slightly in coincidence with a number of other lines.

The coincidence experiment involving the 0.536 MeV gate was very sensitive to the large correction for the Compton of the 1.12 MeV gamma, which was included in the gate. To analyse this spectrum, the Compton contribution was removed, point by point, and the residual spectrum was analysed by the stripping process. When this was done, the 0.50 MeV peak appeared with the intensity as shown in Table III. A peak of this energy also appeared in coincidence with the 1.54 and 1.79 MeV gamma rays where the interference due to the 0.536 MeV radiation was not present.

TABLE II

UNCORRECTED COINCIDENCE INTENSITIES

E Gamma \ E Gate	0.10	0.12	0.24	0.10	0.12	0.24	0.536	1.12	1.54	1.79	2.48	3.08
0.12[a]	4.1 ± 0.5[b] (0.12)[c]	5.3 ± 0.1 (0.12)	4.7 ± 0.5 (0.12)	3.8 ± 0.4 (0.12)	6.8 ± 0.7 (0.12)	4.9 ± 0.5 (0.12)	32.3 ± 3 (0.12)	11.6 ± 1 (0.12)	3.7 ± 0.4 (0.12)	1.25 ± 0.2 (0.12)	0.26 ± 0.2 (0.12)	0.24 ± 0.04 (0.12)
0.17	0.76 ± 0.3 (0.17)	2.1 ± 0.4 (0.16)	1.5 ± 0.5 (0.17)	0.65 ± 0.2 (0.17)	2.1 ± 0.4 (0.17)	0.45 ± 0.2 (0.18)	←-------some evidence --------→			0.26 ± 0.05 (0.18)	0.04 ± 0.04 (0.24)	0.05 ± 0.02 (0.23)
0.236	2.5 ± 0.3 (0.24)	6.0 ± 1.2 (0.236)	1.7 ± 0.3 (0.236)	1.5 ± 0.3 (0.28)	5.8 ± 0.7 (0.236)	1.3 ± 0.2 (0.23)	4.45 ± 0.6 (0.24)	2.22 ± 0.3 (0.24)	1.7 ± 0.2 (0.24)	0.26 ± 0.05 (0.24)		0.04 ± 0.02 (0.23)
0.27	0.8 ± 0.2 (0.28)	-----	-----	-----	-----	-----	-----	-----	-----	-----		
0.31	6.7 ± 0.2 (0.35)	2.3 ± 1 (0.30)	0.7 ± 0.4 (0.29)	0.9 ± 0.4 (0.34)	3.5 ± 0.8 (0.34)	1.3 ± 0.5 (0.34)	0.75 ± 0.4 (0.35)	-----	-----	-----		
0.40	-----	0.2 ± 0.1 (0.41)	0.6 ± 0.3 (0.36)	-----	-----	-----	-----	0.54 ± 0.2 (0.36)	0.22 ± 0.1 (0.36)	-----		
0.44	0.5 ± 0.2 (0.44)	-----	0.6 ± 0.3 (0.45)	0.8 ± 0.4 (0.43)	2.8 ± 0.5 (0.44)	-----	1.2 ± 0.3 (0.44)	-----	-----	0.077 ± 0.03 (0.42)		
0.495	-----	-----	-----	-----	-----	-----	0.7 ± 0.4 (0.49)	-----	0.52 ± 0.8 (0.49)	0.19 ± 0.04 (0.50)		
0.536	2.9 ± 0.3 (0.536)	14.2 ± 2 (0.536)	1.3 ± 0.3 (0.536)	2.3 ± 0.2 (0.536)	1.2 ± 1 (0.536)	1.15 ± 0.2 (0.536)	3.5 ± 0.5 (0.536)	4 ± 0.5 (0.536)	-----	-----	0.055 ± 0.05 (0.52)	0.06 ± 0.01 (0.536)
0.64	0.6 ± 0.2 (0.62)	1.2 ± 0.4 (0.63)	-----	-----	-----	-----	0.7 ± 0.2 (0.63)	-----	0.21 ± 0.1 (0.65)	0.10 ± 0.02 (0.62)		
0.67	0.35 ± 0.1 (0.74)	-----	-----	Beyond Range of Scan			-----	0.34 ± 0.1 (0.66)	-----	-----		
0.89	0.35 ± 0.1 (0.85)	1.1 ± 0.5 (0.78) 1.1 ± 0.8 (0.80)	0.44 ± 0.2 (0.85)				0.39 ± 0.3 (0.83)	-----	-----	-----	No significant counts beyond 0.600 MeV.	
0.97	0.16 ± 0.05 (1.00)	-----	0.3 ± 0.1 (0.99)				-----	-----	-----	-----		
1.12	1.07 ± 0.2 (1.12)	5.6 ± 0.1 (1.12)	0.75 ± 0.1 (1.12)				3.42 ± 0.3 (1.12)	less than 0.08				
1.33	0.3 ± 0.1 (1.34)	0.7 ± 0.2 (1.33)	0.3 ± 0.1 (1.32)				0.36 ± 0.1 (1.32)					
1.54	0.24 ± .1 (1.55)	0.9 ± 0.3 (1.54)	0.28 ± 0.1 (1.54)				0.4 ± 0.2 (1.56)					
1.67	-----	0.95 ± 0.3	-----				-----					
1.79	0.3 ± 0.1	0.9 ± 0.3	-----				-----					

a) Energies in MeV from single crystal spectrum.
b) Errors are statistical errors.
c) Bracket numbers are gamma energies from coincidence spectra.

TABLE III

COINCIDENCE PROBABILITIES FOR VARIOUS GAMMA RAY GATES

E_γ \ E_{Gate}	Int.	Gating Gamma Energy in MeV							
		0.10+ 0.12	0.12+ 0.10	0.24	0.495+ 0.536	1.12	1.54+ 33% 1.33	1.79+ 1.63+1.70	2.48	2.94+3.08+ 3.17
0.12 (a)	80	$6^{+}_{-}1$(0.12) (b)	$2^{+}_{-}1$(0.12)	$3^{+}_{-}1$(0.12)	$41^{+}_{-}7$(0.12)	$40^{+}_{-}7$(0.12)	$14^{+}_{-}2$(0.12)	$4^{+}_{-}1$ (0.12)	No coincidences observed	$2^{+}_{-}1$(0.12)
0.17	5	$1^{+}_{-}0.4$(0.17)	$1^{+}_{-}0.04$(0.17)	$0.6^{+}_{-}0.3$(0.17)				$1^{+}_{-}0.2$(0.18)		
0.236	16	$4^{+}_{-}1$ (0.236)	$4^{+}_{-}1$ (0.236)	$2^{+}_{-}0.5$(0.21)	$5^{+}_{-}1$(0.24)	$5^{+}_{-}1$(0.24)	$7^{+}_{-}1$(0.24)	$0.5^{+}_{-}0.3$(0.24)		$0.5^{+}_{-}0.2$(0.21)
0.27	3									$0.5^{+}_{-}0.2$(0.28)
0.31	3	$3^{+}_{-}1$ (0.31)	$3^{+}_{-}1$ (0.32)	$2^{+}_{-}1$(0.31)	$2^{+}_{-}1$(0.31)					
0.40	3	$2^{+}_{-}1$(0.42)	$4^{+}_{-}2$(0.42)	$2^{+}_{-}1$(0.36)	$4^{+}_{-}2$(0.42)	$3^{+}_{-}1$(0.36)	$1^{+}_{-}0.5$(0.36)	$0.5^{+}_{-}0.3$(0.42)		
0.44	4			$2^{+}_{-}1$(0.45)						
0.495	12				$3^{+}_{-}2$(0.495)		$5^{+}_{-}2$(0.495)	$2^{+}_{-}0.5$(0.50)		
0.536	48	$13^{+}_{-}2$(0.536)	$24^{+}_{-}3$(0.536)	$4^{+}_{-}1$(0.536)		$51^{+}_{-}6$(0.536)				$2^{+}_{-}0.3$ (0.536)
0.64	7	$4^{+}_{-}1$(0.62)	$3^{+}_{-}1$(0.63)		$3^{+}_{-}1$(0.62)			$1^{+}_{-}0.5$(0.62)		
0.67	4					$3^{+}_{-}1$(0.66)	3^{+}_{-}(0.65)			
0.72	4	$2^{+}_{-}1$(0.74)								
0.77	3		$3^{+}_{-}2$(0.78)							
0.89	2	$3^{+}_{-}2$(0.85)		$4^{+}_{-}2$(0.85)	$3^{+}_{-}2$(0.83					
0.97	4	$2^{+}_{-}1$(1.00)	$5^{+}_{-}3$(0.90)	$3^{+}_{-}1$(0.99)						
1.112	48	$13^{+}_{-}3$(1.12)	$29^{+}_{-}4$(1.12)	$5^{+}_{-}2$(1.12)	$46^{+}_{-}5$(1.12)					
1.34	4	$5^{+}_{-}2$(1.34)	$5^{+}_{-}1$(1.34)	$5^{+}_{-}1$(1.32)	$4^{+}_{-}2$(1.32)					
1.54	17	$4^{+}_{-}2$(1.54)	$5^{+}_{-}2$(1.54)	$5^{+}_{-}1$(1.54)	$3^{+}_{-}1$(1.54)					
1.63	4		$7^{+}_{-}3$(1.67)							
1.70	5	$6^{+}_{-}3$(1.70		$4^{+}_{-}2$						
1.79			$7^{+}_{-}3$(1.78)							

(a) Energies in MeV measured in singles spectrum.

(b) Entries in brackets are gamma energies from coincidence spectra.

F) Beta and Beta-Gamma Coincidence Experiments

The arrangement of the apparatus for the beta and beta-gamma coincidence experiments is shown in Fig. 23. The beta rays entered the detector, after passing through the 1 mg/cm^2 walls of the source holder and the 2.5 mg/cm^2 aluminized Mylar covering of the detector. The gamma rays reached the 2" x 2" NaI(Tl) detector through a 2 gm/cm^2 lucite beta stopper. The gamma-gating channel B and the time channel T' were identical to those previously described for the gamma-gamma coincidence experiments. The beta detector was coupled to a 56 AVP photomultiplier, the output of which was fed into the input of the MCA, through suitable amplifiers. The guard detector was viewed by a 6292 photomultiplier, the amplified output of which was fed into a shaping circuit. The shaped pulses from this circuit activated the anti-coincidence mode of the MCA to reject all pulses from the beta detector which were in coincidence with a pulse from the guard. With this arrangement, the recording of "pseudo singles" was not possible.

Each experiment thus resulted in the simultaneous recording of the "singles" beta spectrum as well as the beta spectra coincident with three gates on the gamma spectrum, which were set as described earlier. About twenty sources were required for each experiment, to obtain usable statistics on the higher energy portion of the spectrum, which could be used in the Fermi analysis.

Figure 23

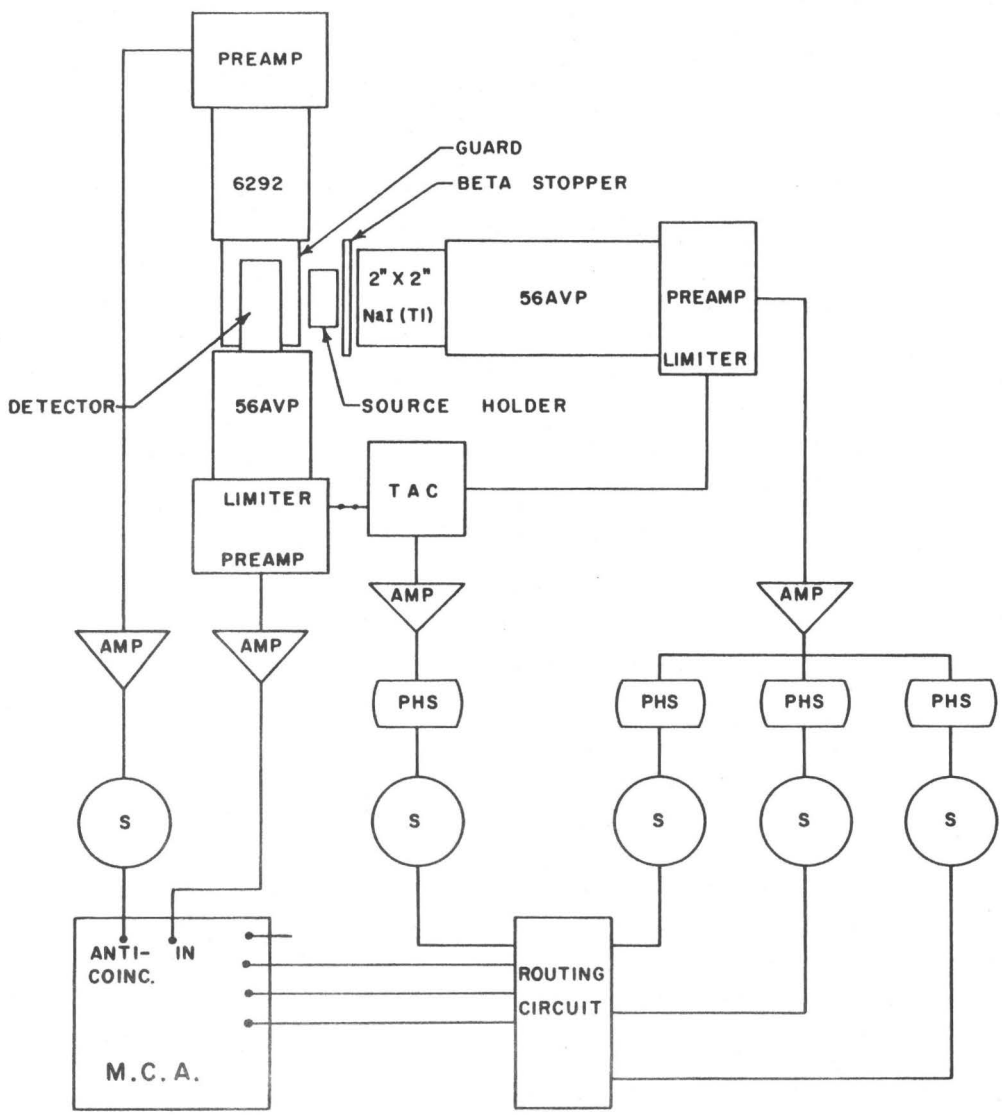
PREAMP
6292
GUARD
BETA STOPPER
2" X 2"
NaI (Tl)
56AVP
PREAMP
LIMITER
DETECTOR
56AVP
SOURCE HOLDER
LIMITER
PREAMP
TAC
AMP
AMP
AMP
AMP
PHS
PHS
PHS
PHS
S
S
S
S
S
ANTI-
COINC.
IN
M.C.A.
ROUTING
CIRCUIT

An examination of the sensitivity of the beta detector to gamma rays was made, by covering it with a 2 gm/cm^2 absorber and recording the resultant spectrum from a Kr^{90} source. This gamma spectrum in the beta detector was much less intense than the beta spectrum, and was essentially cut off at about 1 MeV. This result was consistent with the data already presented, and with the experience gained from the Al^{28} calibration sources. Inasmuch as the Kr^{90} beta spectra of interest had end-points above 2 MeV, no attempt was made to correct for this effect.

The Kr^{89} contamination was determined in the manner described for the gamma-ray experiments and was found to be about 21% in the "singles" spectrum. It was much less in the coincidence experiments. Because a beta spectrum is a continuous distribution, and because the Kr^{89} beta end-point was not markedly different from that of Kr^{90}, the subtraction of Kr^{89} led to no noticeable differences in the results of the analysis.

The Rb^{90} contamination was not measured experimentally, partly because of the difficulties of obtaining Rb^{90} sources dispersed over the same source volume as the gaseous Kr^{90} sources, and partly because there appeared to be no satisfactory way of determining a normalization factor. Experience with the Rb^{90} contamination in the gamma-gamma experiments indicated that it could only make an appreciable contribution to the beta-gamma spectra with the 2.48 and 3.08 MeV gates. For the latter gate, the Rb^{90} contribution to the spectrum masked the few 3.08 MeV-beta coincidences of Kr^{90}.

G) The Results of the Beta and Beta-Gamma Coincidence Experiments

Figure 24 presents Fermi plots for some typical beta-gamma coincidence spectra, obtained by gating on the more prominent photopeaks of the Kr^{90} gamma spectrum. All but one of these spectra were strikingly similar, with a high energy tail, a strong component with an end-point near 2.8 MeV, and a departure from linearity which began just above 1 MeV. The beta-2.48 MeV gamma-ray experiment had a lower end-point and followed the linear spectrum back to about 0.5 MeV, which was the limit of validity of the efficiency factors used. This difference might have been expected, since the 2.48 MeV gamma ray was the only one of those in Fig. 24 which was not in cascade with another gamma ray.

The reason for the high energy tail has been a cause of some concern. The situation is revealed in Fig. 25, which presents the Fermi plots of an Al^{28} calibration spectrum (end-point, 2.87 MeV), a "singles" Kr^{90} spectrum without correction for Kr^{89} or Rb^{90}, and a beta-0.12 MeV coincidence spectrum. The three spectra were normalized at 1.8 MeV. It is clear that the tail was smallest in the calibration spectrum and largest in the "singles" spectrum. This latter situation was to be expected since a considerable amount of Kr^{89} and Rb^{90} were present. However, the beta-0.12 MeV spectrum ought to have been quite free of both these contaminants. The difference between the Al^{28} and the beta-0.12 MeV spectra could be interpreted as being due to a high energy group in Kr^{90}, with an energy of about 4.5 MeV and an intensity in the order of 15% of the 2.8 MeV group. However, this solution was too simple. These experiments employed

Figure 24

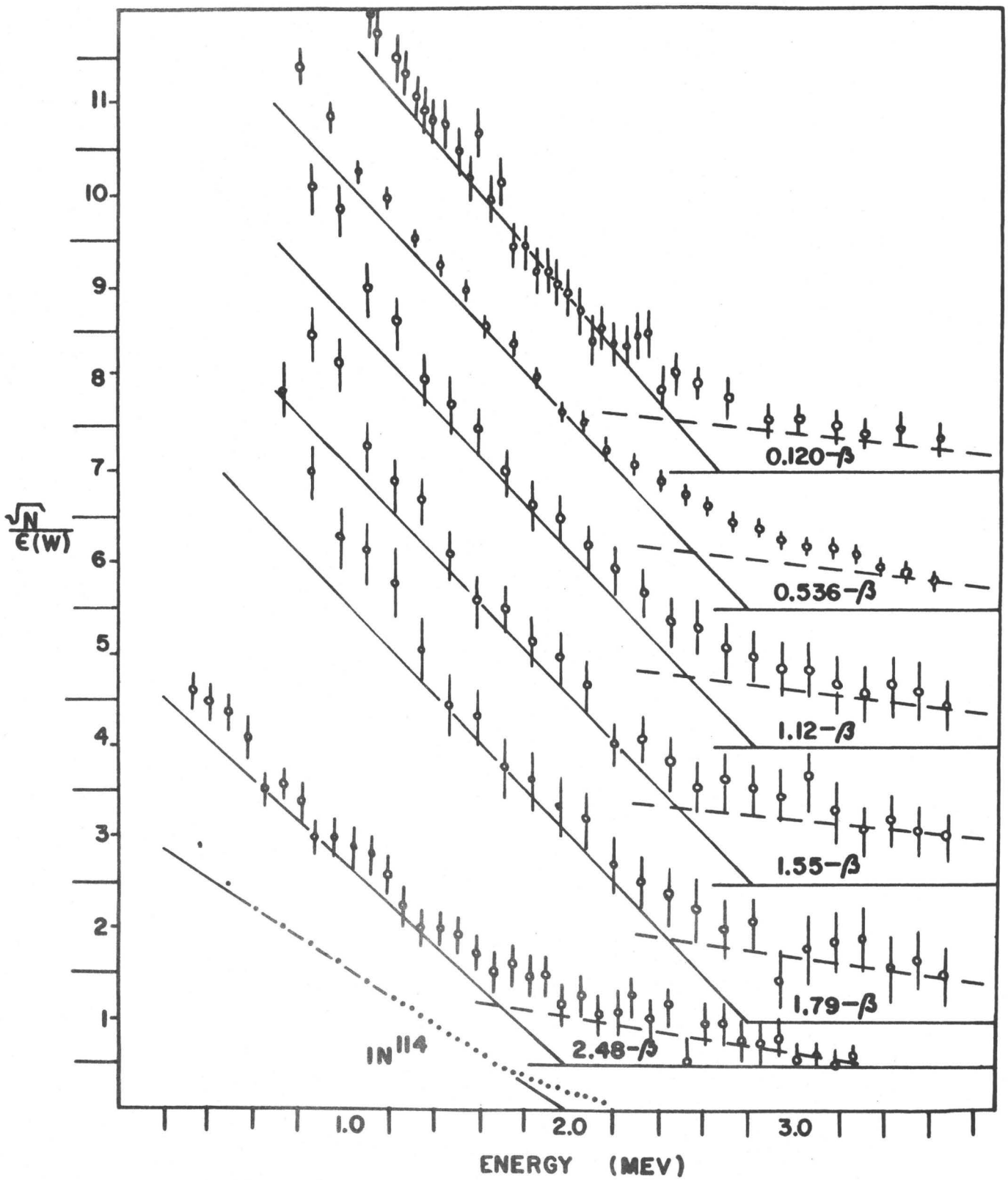
$\frac{\sqrt{N}}{\epsilon(W)}$
11
10
9
8
7
6
5
4
3
2
1
0.120-β
0.536-β
1.12-β
1.55-β
1.79-β
2.48-β
IN^{114}
1.0
2.0
3.0
ENERGY (MEV)

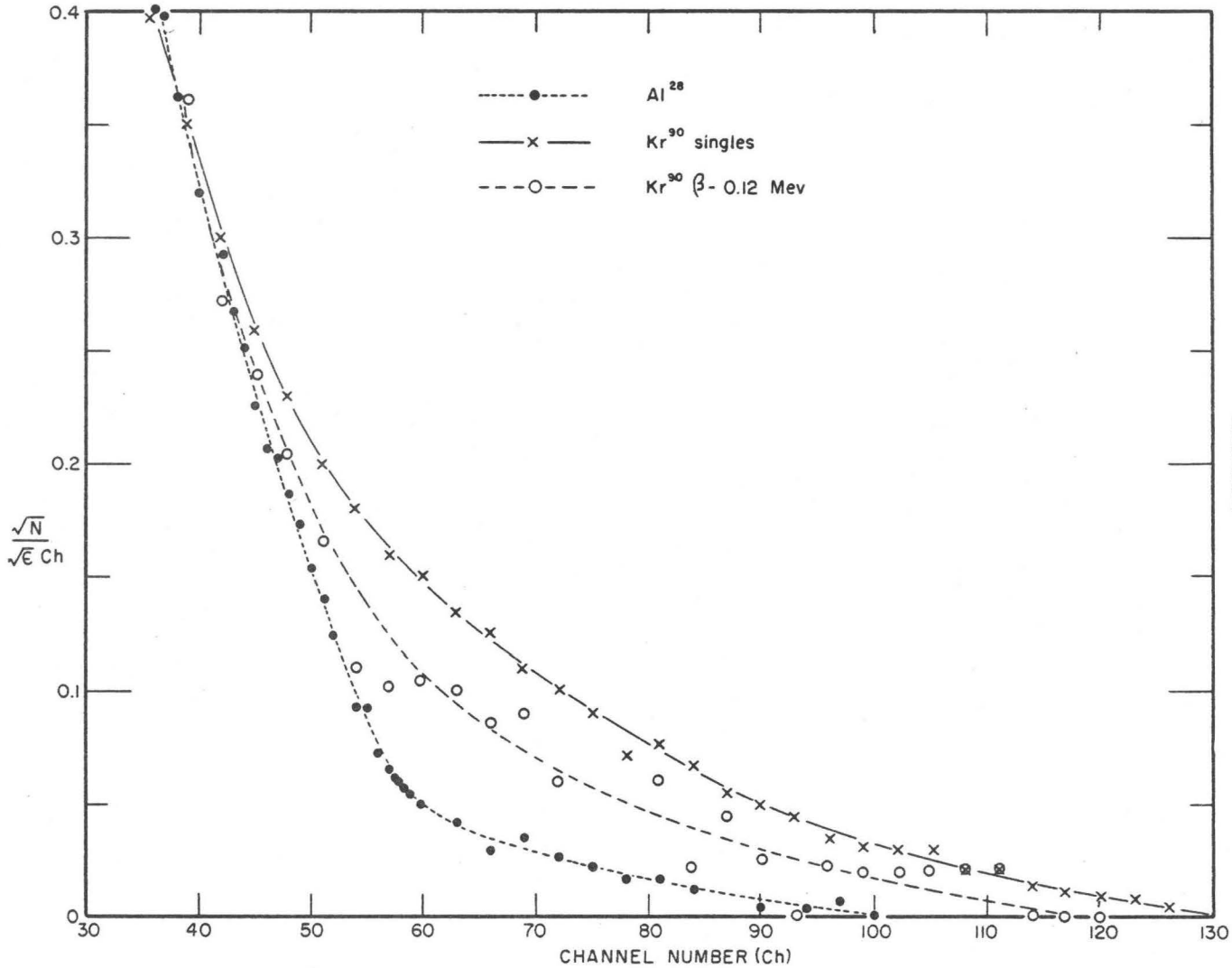
0.4
0.3
0.2
0.1
0
30
40
50
60
70
80
90
100
110
120
130
CHANNEL NUMBER (Ch)
$\frac{\sqrt{N}}{\sqrt{\epsilon}\,Ch}$
Al^{28}
Kr^{90} singles
Kr^{90} β- 0.12 Mev

Figure 25

multiple sources, which varied considerably in size and which decayed by a factor of two during the counting period. Pulses were received from the beta detector at an average rate of 10,000/sec. This meant that for about 1% of the events recorded, an overlap of two pulses would occur in the amplifier. This degree of electronic summing did not significantly effect the data except beyond the end of the true spectrum, where each event recorded was greatly magnified in the process of making a Fermi plot. A small amount of beta-gamma summing may also have occurred in the beta detector, which would have contributed a few counts to the high energy tail. It was not expected that this effect would be as important as "electronic summing", since the detection efficiency for gamma rays in the beta detector was small.

In the "singles" spectrum and in the coincidence spectra with the higher energy gates, the presence of the Rb^{90} spectrum was shown by the fact that a few events were recorded with energies up to 6 MeV. It was impossible with these data to disentangle these various contributions to the high energy tail, and hence there was no secure experimental evidence for beta rays of energy greater than 2.8 MeV, in the decay of Kr^{90}.

In the analysis of the beta spectra, the high energy component was simply stripped off as if it were a real beta group. The end-point of the strong 2.8 MeV spectrum was very insensitive as to how this was done.

Table IV presents the end-points of the beta-gamma coincidence spectra with the 0.12, 0.536, 1.12, 1.54, 1.79 and 2.48 MeV gates. Other

gates such as 0.24, 0.35 and 0.80 were also used. These and the "singles" gave very similar spectra but were certainly not as free of potential contaminants as the ones mentioned previously and have therefore been neglected in the determination of end-points. The evidence of Table IV suggests that most of the beta decays in Kr^{90} feed either a single high-lying level, or a cluster of such levels, from which de-excitation proceeds through cascading gamma rays. The mean value of the beta group in coincidence with the 0.12, 0.536, 1.12, 1.54 and 1.79 MeV transitions was 2.80 ± 0.02 MeV. The end-point of the beta group in coincidence with the 2.48 MeV radiation was 2.00 ± 0.07 MeV.

H) Construction of the Decay Scheme

The most striking feature in Table III is the evidence for an intense 0.12-0.536-1.12 MeV triple cascade. If it is assumed that one of these radiations is a ground state transition, this cascade defines a level at 1.78 MeV. Support for such a level is also provided by the strong 0.24-1.54 MeV cascade. The presence of a strong 1.79 MeV transition in Table I, and the relatively weak coincidence probabilities recorded with the 1.79 MeV gate further support this level. The fact that the beta spectra, in coincidence with all the above-mentioned transitions, have the same end-point, indicates that a large fraction of the beta transitions proceed to this level. In turn, this establishes the energy release in the decay of Kr^{90} as 4.58 MeV.

Nothing that has been said in the last paragraph indicates the order of the gamma rays in the 0.12-0.536-1.12 MeV and 0.24-1.54 MeV cascades. The spectrum in coincidence with the 3.08 MeV gate showed coincidences

TABLE IV

END POINTS OF BETA SPECTRA FROM β-γ COINCIDENCE EXPERIMENTS

Experiment Number	Energy Calibration keV/ch.		Gamma Ray Gates (MeV)					
			0.12	0.536	1.12	1.54	1.79	2.48
1	Al^{28} Rh^{106}	36.3 35.7		2.79	2.82			
2	Al^{28} Rh^{106}	38.9 38.9		2.82				
3	In^{114}	46.5	2.87					
4	In^{114}	37.7		2.78	2.72			
5	In^{114}	40.7		2.83		2.79	2.79	
6	Al^{28} Rh^{106}	50.3 49.9	2.69					
7	In^{114} Au^{198}	39.3 39.9					2.82	2.00
Estimated error on each end-point 0.07 MeV.								

with the 0.12 and 0.536 MeV transitions and not with the 1.12 MeV gamma ray. Since there is not enough energy available to provide for a 3.08 MeV radiation to feed the 1.78 MeV level, the 3.08 MeV-gamma experiments could pick out only the lower lying transitions in the strong triple cascade. This experiment, therefore, indicated that a level exists at 0.656 MeV, which is fed from the 1.78 MeV level by the strong 1.12 MeV transition.

The 0.12 MeV transition was the strongest gamma ray in the spectrum. Its coincidence probability with the 0.536 or 1.12 MeV gamma rays was not large enough to support all this intensity in the triple cascade, and this suggests that the first excited state of Rb^{90} is at 0.12 MeV. This level is fed by other transitions as well as by the 0.536 MeV radiation.

The coincidence experiments with the 0.10 and 0.12 MeV gates indicated that there are two gamma rays of energy near 0.12 MeV, with the lower energy component not strongly in coincidence with either the 0.536 or 1.12 MeV transition. It was, however, relatively strong in coincidence with the 1.54 MeV gamma ray. These facts, together with the previously noted 0.24-1.54 MeV coincidences, establish a level at 0.24 MeV.

The levels at 0, 0.12, 0.24, 0.66 and 1.78 MeV are responsible for about 85% of the total gamma ray intensity in Kr^{90}. In addition, the level at 1.78 MeV accounts for most of the beta transitions. The weaker gamma rays must be fitted into the framework of these five levels.

The 0.236 MeV gamma ray had an intensity of 32%, and its combined coincidence probability with the 1.12, 1.54 and 1.79 MeV gamma rays was about the same amount. Thus this gamma transition must feed the 0.12-0.536-1.12 MeV cascade. This requires the presence of a level at 2.02 MeV, which feeds the 1.78 MeV level by means of a 0.24 MeV radiation. The coincidence data suggests, that the intensity is divided about evenly between the two 0.24 MeV transitions. This level arrangement accounts for the 0.24-0.24 MeV coincidences, which are created via the 1.54 MeV radiation. This is also consistent with the fact that gamma rays of this energy were in coincidence with both the 0.10 and 0.12 MeV gates.

The existence of two other higher energy levels, is well supported by energy and coincidence information. A level of 3.60 MeV accounts for the observed coincidences with the 3.08 MeV gate, and permits the inclusion of the 2.94 and 3.60 MeV gamma rays in the decay scheme. The absence of any coincidences with the 2.48 MeV gamma ray establishes it as a ground state transition and defines a level at 2.48 MeV. The beta-gamma coincidence experiments support this assignment.

A decay scheme embodying these eight levels is shown on the left hand side of Fig. 26. The total decay energy of Kr^{90}, as determined from the beta-gamma experiments with gamma rays of energy up to 1.78 MeV, is

$$(1.78 \pm 0.01) + (2.80 \pm 0.02) = 4.58 \pm 0.022 \text{ MeV}$$

whereas, the value found from the 2.48 MeV-beta experiment is

$$(2.48 \pm 0.02) + (2.00 \pm 0.07) = 4.48 \pm 0.07 \text{ MeV}.$$

The best value, from these experiments for the Kr^{90}-Rb^{90} energy difference, is 4.56 ± 0.02 MeV. The beta intensities, shown in brackets in Fig. 27, have been normalized, on the basis of the gamma-ray intensities, to 100% for the total decay.

Any gamma ray, feeding the 1.78 MeV level, should have coincidence probabilities with the 1.79 MeV, 1.54 MeV, and the "0.12-0.536-1.12 MeV triplet" in the ratio of 0.23:0.35:1.0 respectively. An examination of Table III shows that several gamma rays reveal this pattern, within the limits of error of the measurements.

The 0.50 MeV gamma ray had an intensity of 25%, and appeared in coincidence with the 0.536, 1.54 and 1.79 MeV transitions. It would have been masked by the 0.536 MeV peak in the 1.12 MeV-gamma experiment. The intensity of the 0.50 MeV gamma ray in the 0.536 MeV-gamma experiment was hard to determine, because of the presence of a much stronger 0.536 MeV peak in coincidence with the 1.12 MeV Compton in the 0.536 MeV gate. These coincidence data are all accounted for by postulating a level at 2.28 MeV, which is deexcited to the 1.78 MeV level by a 0.50 MeV transition. The weak 2.03 MeV, and the even weaker 2.29 MeV gamma rays may represent transitions from this level to the 0 and 0.24 MeV states, however the real evidence for the existence of the 2.28 MeV level must come from the coincidence results. The relatively strong 1.63 MeV line, whose energy fits the 2.28-0.656 MeV gap is not in coincidence with

Figure 26

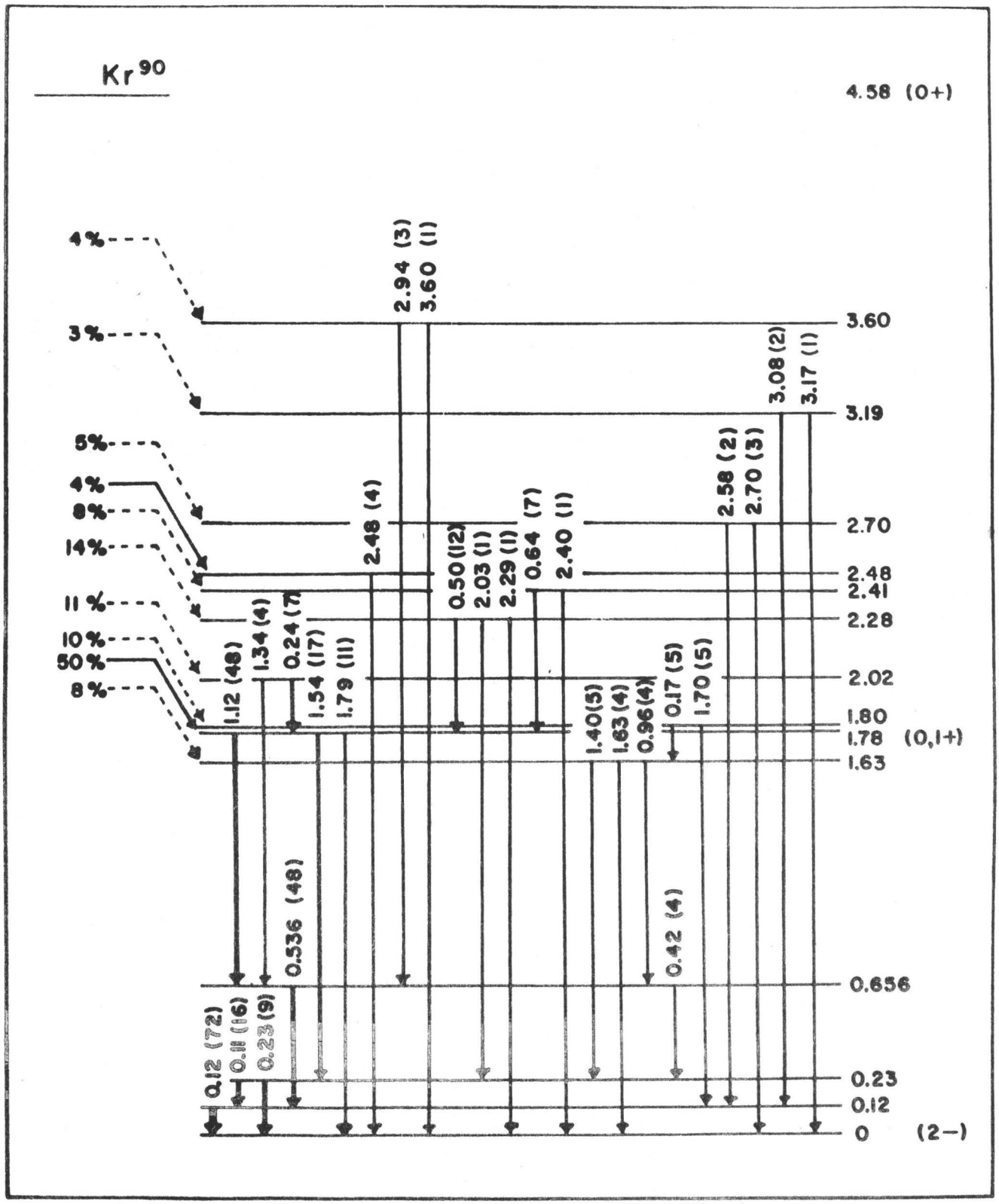
Kr 90
4.58 (0+)
4%
3%
5%
4%
8%
14%
11%
10%
50%
8%
2.94 (3)
3.60 (1)
3.08 (2)
3.17 (1)
2.58 (2)
2.70 (3)
2.48 (4)
0.50 (12)
2.03 (1)
2.29 (1)
0.64 (7)
2.40 (1)
1.12 (48)
1.34 (4)
0.24 (7)
1.54 (17)
1.79 (11)
1.40 (5)
1.63 (4)
0.96 (4)
0.17 (5)
1.70 (5)
0.42 (4)
0.536 (48)
0.12 (72)
0.11 (16)
0.23 (9)
3.60
3.19
2.70
2.48
2.41
2.28
2.02
1.80
1.78 (0,1+)
1.63
0.656
0.23
0.12
0 (2−)

the 0.536 MeV gate, and therefore can not be placed at this position in the decay scheme.

Similar arguments apply to the pattern of 0.63 MeV coincidences. There is a gamma ray of energy, with an intensity of 16% in Table I, which might well be this line. Both the energy and intensity of this peak were difficult to determine in the singles spectrum, because of the strong 0.595 MeV Kr^{89} radiation. The situation was more favourable in the coincidence spectrum. The 0.63 MeV transition was in coincidence with both the 1.54 and 1.79 MeV gates, and had the expected intensities. It was also in coincidence with the 0.536 MeV radiation, although this peak was riding on a large background, due to the Compton of the 1.12 MeV radiation in the gate. This made it difficult, to define precisely the energy and intensity of the 0.63 MeV for this gate. Possible coincidences with the 1.12 MeV radiation would have been masked by the strong 0.536 MeV photo-peak. These coincidence data require a level at 2.41 MeV. The ground state transition from this level may also be present, and has been shown in the decay scheme.

In the spectrum of coincidences with the 1.12 MeV gate, there was a reasonably prominent peak at 0.66 MeV, which has the appropriate energy to represent a transition from the 0.656 MeV level to the ground state. However, its energy and intensity are also appropriate for its interpretation as a sum peak, accompanying the 0.12-0.536-1.12 MeV triple cascade. The corresponding sum peak has already been commented on in the singles spectrum.

The spectrum in coincidence with the 0.536 MeV gate, was originally analysed to show a peak at 1.32 MeV. In the expectation of a sum peak at 1.24 MeV, the data may be reinterpreted as supporting a 1.24 MeV sum peak with an intensity of 8% of the strong 1.12 MeV peak, and a 1.34 MeV photopeak with an intensity of about 70% of the 1.32 MeV peak given by the previous analysis. The change in this part of the spectrum, from one to two peaks, is indicative of the subjectivity inherent in the stripping procedure.

It is believed that the 1.34 MeV radiation represents the transition between the 2.02 MeV level, and the 0.656 MeV level. It was found in coincidence with both the 0.12 and 0.536 MeV radiations and was not in coincidence with the 1.12 MeV gamma ray.

The gamma rays of energies 1.40, 1.63 and 1.70 MeV are the three strongest lines which have not yet been classified. They are all too strong to feed the 1.78 MeV or any higher level, since any inclusion of these radiations in the high energy part of the decay scheme, creates serious problems with ft values to the high lying states. At the same time, they are too weak to give definite coincidence information of their position in the decay scheme. The inclusion of two levels, at 1.64 and 1.81 MeV respectively, makes the assignment of the 0.17, 0.97, 1.40, 1.63 and 1.70 MeV gamma rays in the decay scheme possible. The energy fit is not perfect, but is reasonable for peaks of this intensity. The presence of strong 0.12 coincidences with the 1.79 MeV gate, is accounted for by the 1.70-0.12 MeV cascade. Moreover, the pattern of coincidences with the

0.17 MeV transition, is consistent with this arrangement of levels.

There are several unresolved peaks, in most of the coincidence spectra, in the energy range between 0.236 and 0.536 MeV. The analysis of these, is complicated by the Compton of the 0.536 MeV transition, and the data are inadequate to draw unique conclusions about these events. It does seem reasonable that some of these are due to a 0.42 MeV transition between the 0.656 MeV and the 0.24 MeV levels, and this transition has therefore been included in the decay scheme.

The gamma rays above 2 MeV must feed low lying levels, and some of them are almost certainly ground state transitions. The two pairs of gamma rays at 2.70 and 2.58 MeV, and at 3.08 and 3.17 MeV appear to define levels at 2.70 and 3.19 MeV, although this assignment must be regarded as very tentative.

It is thus possible, with a total of 14 levels, to place 28 of the 35 lines of Table I. The only two transitions of appreciable strength, which remain unclassified are those at 1.94 and 2.12 MeV. It is believed that the seven levels on the left side of the decay scheme are firmly established; while those on the right, while consistent with the present data, require more refined experiments to establish their validity.

I) Discussion

As has already been pointed out, the Kr^{90}-Rb^{90} energy difference is 4.56 ± 0.02 MeV. This is about 0.2 MeV larger than the predictions by Everling et al (1961). A portion of Everling's disintegration-energy vs. mass number chart is presented in Fig. 27. The measured disintegration-energy for the Kr^{90}-Rb^{90} pair falls nicely on the straight line for the neutron number 54. The chart also suggests that the Kr^{88}, which differs only in possessing two less neutrons than Kr^{90}, should have a somewhat similar decay pattern. A decay scheme for Kr^{88} has been proposed by Thulin (1955). No information is available on the decay of other even-mass krypton nuclei.

The spin of Kr^{90}, an even-even nucleus, is presumably zero with positive parity. None of the spins of the other levels, involved in this decay, are securely known. Experiments on Rb^{90} (Johnson et al, 1958), indicated that the ground state transition to Sr^{90} had an intensity between 7% and 39%. The log ft value for this transition must therefore lie between 7.0 and 7.7, characteristic of a first forbidden transition. In the decay of Rb^{88}, a corresponding first forbidden unique transition has a log ft value of 7.25, (Nuclear Data) and therefore the mass-90 transition may also fall in the same category. If this is so, the spin of the ground state of Rb^{90} is 2-. Even if the first forbidden unique designation does not hold, the ground state spin is limited to the values 0-, 1-, 2-, according to Johnson's experiment.

Figure 27

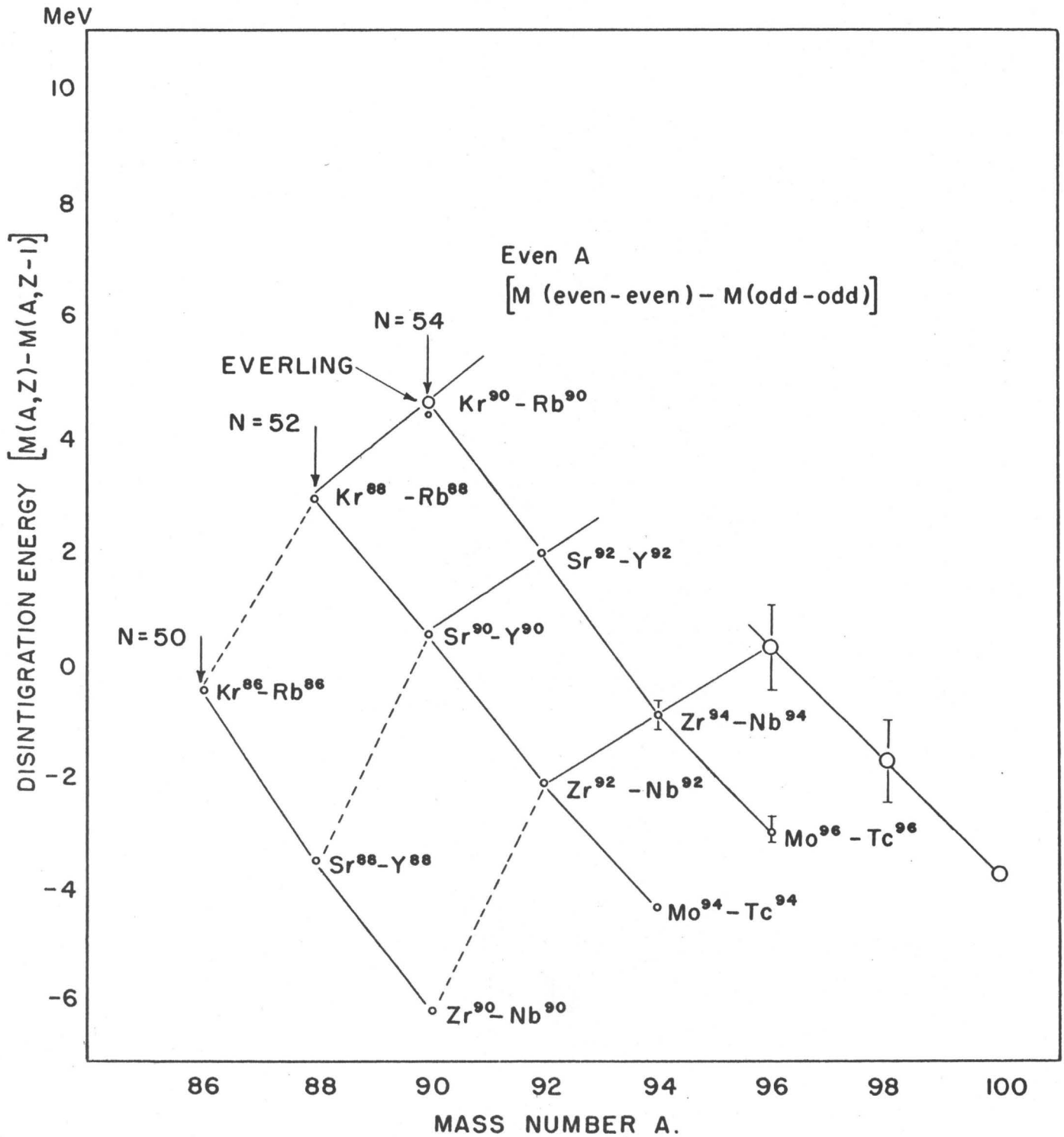
MeV
10
8
6
4
2
0
-2
-4
-6
DISINTIGRATION ENERGY [M(A,Z)-M(A,Z-1)]
Even A
[M (even-even) – M(odd-odd)]
N=54
EVERLING
N=52
N=50
Kr90 - Rb90
Kr88 - Rb88
Sr92 - Y92
Sr90 - Y90
Kr86 - Rb86
Zr94 - Nb94
Zr92 - Nb92
Mo96 - Tc96
Sr88 - Y88
Mo94 - Tc94
Zr90 - Nb90
86
88
90
92
94
96
98
100
MASS NUMBER A.

Rb^{90} has 37 protons and 53 neutrons. The shell model predicts that the 37^{th} proton is in a $p_{3/2}$ state (eg. $_{37}Rb^{87}_{50}$, $_{35}Br^{81}_{46}$) and that the 53^{rd} neutron is in a $d_{5/2}$ state (eg. $_{38}Sr^{91}_{53}$, $_{42}Mo^{95}_{53}$). According to Nordheim's rule, the coupling of a $p_{3/2}$ proton and a $d_{5/2}$ neutron ought to give a 4- or 3-ground state, but 2- and 1- assignments are allowed. In any case, one could expect a group of negative parity states with these spins, to occur near the ground state.

Studies of the decay of Kr^{88} have led to a unique 2- assignment to the ground state. Since Rb^{90} differs from Rb^{88} only in the addition of two neutrons, the 2- assignment for this latter nucleus is made attractive.

Thus all the available evidence points to a 2- assignment for the ground state of Rb^{90}, even though it does not follow Nordheim's rule.

The beta transitions to the 1.78, 2.48 and 3.60 MeV levels have log ft values of 4.7, 5.3 and 4.0 respectively. All these values are consistent with allowed transitions, and thus the spins of these three states must be 0 or 1, with positive parity. Lower limits can be set on the log ft values of beta transitions to the 0, 0.12, 0.23 and 0.656 MeV levels, from the absence of observed beta transitions with total intensity greater than 15%. These lower limits are 6.2, 6.1, 6.0 and 5.9 respectively. All these values are consistent with first forbidden decays, and suggest that these levels must have negative parity and/or a high spin value.

Since only relative intensities of the gamma transitions are known, it has been impossible to make spin assignments to any of the remaining states in the decay scheme. It would appear that the strong transitions,

depopulating the 1.78 MeV state, must be E1 in character, but this does not really help in the assignment of spins to the various levels.

It is interesting to note that the 1.78 MeV level in Rb^{90} and the 2.40 MeV level in Rb^{88} seem to have a similar character. In both cases, three strong transitions lead from these states to a triplet of levels between 0 and 0.25 MeV. The very strong 1.12-0.536 MeV cascade in Rb^{90} is paralleled by a strong 1.55-0.845 MeV cascade in Kr^{88}. When more information about spins is available, a comparison of this type may prove more valuable.

A number of further experiments would seem to be feasible with present techniques. By taking more elaborate precautions, one ought to be able to reduce the uncertainty of the intensity of the beta-transitions to the low lying levels. To do this, it would be desirable to remove the Rb^{90} daughter as it grew into the samples, either by electrostatic or by chemical means. If a good method could be devised for removing Rb^{90}, the need for changing sample holders would disappear. The coincidence equipment could be used quite satisfactorily, to determine the lifetimes of the low energy transitions. Also with slight modifications in the physical arrangement, it should be possible to carry out sufficient angular correlation measurements on the strong transitions, to obtain the anisotropy. All of this information would be useful in any serious attempt to make spin assignments.

REFERENCES

1. Ajzenberg-Selove, F. 1960. Nuclear Spectroscopy (Academic Press, New York)

2. Barnes, C.A., Fowler, W.A., Greenstein, H.B., Lauritsen, C.C., and Nordberg, M.E. 1958. Phys. Rev. Let. 1, 328

3. Becquerel, H. 1896. Comp. Rend. 122, 1

4. Berger, M.J. and Dogget, J. 1956. J. Res. Nat. Bur. of Standards, 56, 355

5. Bethe, H.A. and Bacher, R.F. 1936. Rev. Mod. Phys. 8, 82

6. Brennan, M.H. and Bernstein, A.M. 1960. Phys. Rev. 120, 927

7. Cohen, B.L. and Pric, R.E. 1960. Phys. Rev. 118, 1582

8. Davisson, C.M. 1955. See Siegbahn 1955. p 857

9. Dillard, C.R., Adams, R.M., Finson, H., and Turkevitch, A. 1951. The Fission Products, edited by Coryell, C.D. and Sugarman, N. (McGraw-Hill, New York)

10. Eichholz, G.G. 1954. Cdn. Patent No. 503, 906

11. Everling, F., Gove, N.B., and VanLieshout, R. 1961. Nuclear Data Charts. (National Academy of Sciences, National Research Council, Washington, USA)

12. Feenberg, E. and Trigg, G. 1950. Rev. Mod. Phys. 22, 399

13. Fermi, E. 1934. Physik, 88, 161

14. Fleming, W.H. 1962. Research Reactor J. 2, No. 4, 1

15. Ford, K.W. 1955. Phys. Rev. 98, 1516

16. Freedman, M.S., Novey, T.B., Porter, F.T., and Wagner, F. 1956. Rev. Sci. Inst. 127, 716

17. Green, R.E. and Bell, R.E. 1958. Nucl. Inst. 3 (1956), 127

18. Haxel, O., Jensen, J.H.D., and Suess, H.E. 1949. Phys. Rev. 75, 1766

19. Heath, R.L. 1957. USAEC Report No. IDO-16408

20. Johnson, N.R., O'Kelley, G.D., and Eichler, E. 1958. Bull. Am. Phys. Soc. 3 No. 3, 207

21. Ketelle, B.H. 1950. Phys. Rev. 80, 758

22. Kisslinger, L.S. and Sorenson, R.A. 1960. Dan. Mat. Fys. Selkb. 32 No. 9, 1

23. Kofoed-Hansen, O. and Nielsen, K.O. 1951. Phys. Rev. 82, 96

24. Lauritsen, T., Barnes, C.A., Fowler, W.A., and Lauritsen, C.C. 1958. Phys. Rev. Let. 1, 326

25. Lauterjung, K.H., Schimmer, B., and Maier-Leibnitz, H. 1958. Z. Physik, 150, 657

26. Mayer, M. 1949. Phys. Rev. 75, 1969

27. Nilsson, S.V. 1955. Dan. Mat. Fys. Medd. 29 No. 16, 1

28. Nordheim, L.W. 1950. Rev. Mod. Phys. 23, 322

29. Ockenden, D.W. and Tomlinson, R.H. 1962. Can. J. Chem. 40, 1594

30. Pauli, W. 1933. Noyaux Atomique, Proc. of Solvay Congress, Brussels

31. Preston, M.A. 1962. Physics of the Nucleus (Addison Wesley Publishing Co., Reading, Mass)

32. Rose, M.E., Dismuke, N.M., Perry, C.L., and Bell, P.R. 1955a. See Siegbahn 1955. p 875

33. Rose, M.E. 1955b. See Siegbahn 1955. p 884

34. Rose, M.E. 1955c. See Siegbahn 1955. p 905

35. Schiff, L.I. 1955. Quantum Mechanics (McGraw-Hill, London)

36. Siegbahn, K. 1955. Beta- and Gamma-Ray Spectroscopy (North Holland, Amsterdam)

37. Sliv, L.A. and Band, I.M. 1957. Univ. of Illinois 571CCK1

38. Stanford, A.L. and Rivers, W.K. 1958. Rev. Sci. Inst. 29, 406

39. Thulin, S. 1955. Ark. för Fys. 9, 137

40. Wahlgren, M.A. and Meinke, M.R. 1961. USAEC Report TID-11807

41. Wu, C.S., Ambler, E., Hayward, R.W., Hoppes, D.D., and Hudson, R.P. 1957. Phys. Rev. 105, 1413

42. Weisskopf, W.F. 1951. Phys. Rev. 83, 1073

- - - - -